

Research Process on Photodetectors Based on Group-10 Transition Metal Dichalcogenides

*Waqas Ahmad, Jiang Wu, Qiandong Zhuang, Arup Neogi, Zhiming Wang**

W. Ahmad, J. Wu, A. Neogi, Z. Wang

Institute of Fundamental and Frontier Sciences, University of Electronic Science and Technology of China, Chengdu 610054 China

Email: zhmwang@uestc.edu.cn

Q. Zhuang

Physics Department, Lancaster University, Lancaster LA14YB, UK

Z. Wang

Institute for Advanced Study, Chengdu University, Chengdu 610106, China

Keywords: two dimensional materials, group-10 transition metal dichalcogenides, optoelectronic devices, broadband photodetectors

Rapidly evolving group-10 transition metal dichalcogenides (TMDCs) offer remarkable electronic, optical, and mechanical properties, making them promising candidates for advanced optoelectronic applications. Compared to most transition metal dichalcogenides semiconductors, group-10-TMDCs possess unique structures, narrow bandgap, and influential physical properties that motivate the development of broadband photodetectors, specifically infrared photodetectors. This review presents the latest developments in the fabrication of broadband photodetectors based on conventional 2D TMDCs. It mainly focuses on the recent developments in group-10 TMDCs from the perspective of the lattice structure and synthesis techniques. Recent progress in group-10 TMDCs and their heterostructures with different dimensionality of materials-based broadband photodetectors is provided. Moreover, this review accounts for the latest applications of group-10 TMDCs in the fields of nanoelectronics and optoelectronics. Finally, conclusions and outlooks are summarized to provide perspectives for next-generation broadband photodetectors based on group-10 TMDCs.

1. Introduction

Photodetector is an optoelectronic device which converts light into electrical signals. Photodetector is one of the core technologies of many applications such as optical communications, missile guide systems, bio-imaging, and biological sensing systems.^[1] Generally, when the photodetector is irradiated by the light, charge carriers (electrons and holes) are generated, resulting in a change in conductance or photovoltage. This phenomenon facilitates the holes and electrons moving toward the anode and cathode. Traditional photodetectors composed of conventional semiconducting materials such as Si, InGaAs, HgCdTe, GaSb, and InAs, exhibit higher detectivity (D^*), making it useful for infrared (IR) optical devices with a spectral range of up to 15000 nm and D^* as high as $\sim 10^{14}$ Jones. However, employing these conventional photodetectors in commercial applications is challenging due to several factors, including narrow bandgap, complex and expensive fabrication process, and low-temperature operation mode.^[2]

Usually, conventional bulk semiconductor materials, even in the form of thin films, cannot be tempered. Using these materials to develop transparent, flexible, and bendable devices is challenging. Si possesses an indirect energy bandgap (1.12 eV) that is suitable for visible to near-infrared (NIR) spectrum but is significantly limited beyond the NIR spectrum. Therefore, there is an increased need for novel materials that can overcome the limitations of bulk Si for broadband photodetection and can be suitable for developing advanced electronic and optoelectronic devices at low cost. Compared with conventional materials-based photodetectors, two-dimensional (2D) materials-based photodetectors are very sensitive to broadband spectrum owing to their tunable bandgap, which varies from 0 to 3 eV, as shown in **Figure 1**.^[3] 2D materials-based photodetectors show a broad spectrum and excellent stability and thus can operate at room temperature.^[4] 2D materials based photodetectors not only shows broaden spectrum but also shows excellent stability and thus can operate at room temperature.

[1b, 5]

The discovery of 2D transition metal dichalcogenides (TMDCs) materials has invoked great research interests in nanoelectronic and optoelectronic devices owing to their fascinating electronic and optoelectronic properties. In 2004, A. K. Geim and K. Novoselov assembled the graphene in the laboratory by mechanical exfoliation at room temperature.^[6] According to the crystalline structure, 2D TMDCs layered materials can be divided into different prismatic phases such as hexagonal, octahedral, and tetragonal. In 2D TMDCs, each unit (MX_2) is composed of a transition metal (M) layer sandwiched between two chalcogens (X) atomic layers.^[3e, 7]

The 2D TMDCs materials family is a continuously emerging class of material systems with more than 150 different types of layered materials that can easily be exfoliated from the bulk crystals and possess distinctive features.^[8] For instance, graphene with zero bandgap shows linear depression near the Dirac point, which allows broadband photodetection.^[9] Black phosphorus (BP) based photodetector also exhibits spectrally broadened photodetection from the ultra-violet (UV) to the NIR regime.^[10] Likewise, 2D TMDCs semiconductors such as molybdenum disulfide (MoS_2), molybdenum diselenide (MoSe_2), tungsten disulfide (WS_2), tungsten diselenide (WSe_2), and indium selenide (InSe) based photodetectors show excellent performance by offering fast photoresponse, high responsivity, low dark current and excellent D^* .^[11] The atomically layered structure of 2D TMDCs allows it to be integrated with state-of-the-art semiconductors like GaN and Si for enhancing its functionality for a wider range of practical electronic and optoelectronic applications.^[12] Apart from the unique benefits of 2D materials-based photodetectors, some downsides limit their practical applications in commercial industries: For instance: graphene-based photodetectors show a low ON/OFF ratio and limit their photoresponse; photodetectors based on BP show wide spectrum regime as well as excellent optical response but have poor environmental stability. The high-quality synthesis of 2D materials is still challenging as a large-area synthesis of 2D materials along with its high

crystallinity, are essential parameters to meet the requirements of practical applications. The realization of a rapid photoresponse with a high responsivity rate is currently a major bottleneck for 2D materials-based photodetectors.

Emerging **group-10 TMDCs** emerged as new 2D materials. Compared to the conventional 2D materials family, **group-10 TMDCs** exhibit numerous fruitful properties, such as strongly layer-dependent tunable bandgap (0 to 1.6 eV), higher carrier mobility, anisotropic behaviour, and excellent air stability.^[3c] **Group-10 TMDCs** have unique atomic structure characteristics in which d-orbitals are fully occupied and offer tunable electronic structures with highly hybridized p_z orbitals of interlayer chalcogen atoms. These features cause higher interlayer interaction among these materials and make their properties tunable with a change in the number of layers. To date, various **group-10 TMDCs** materials have been discovered, including platinum diselenide (PtSe_2), palladium diselenide (PdSe_2), platinum disulfide (PtS_2), palladium disulfide (PdS_2), platinum ditelluride (PtTe_2) and palladium ditelluride (PdTe_2). Among **group-10 TMDCs**, PtS_2 , PtSe_2 , and PdSe_2 -based optoelectronic devices show outstanding carrier mobility up to $40,000 \text{ cm}^2 \text{ V}^{-1} \text{ s}^{-1}$ and exceptional stability in the air for up to 5 months.^[13] PdS_2 and PdSe_2 show anisotropic behavior due to puckered pentagonal structures like black phosphorus (BP), which makes them suitable candidates for IR photodetection. These deliver far better air stability as compared to BP. PtTe_2 and PdTe_2 possess type-II fermions that have many applications in the field of chiral anomaly and topological phase transition. These outstanding properties of **group-10 TMDCs** make them a worthy choice for constructing next-generation optoelectronic devices.^[3c, 14]

This review presents a detailed summary of the current progress of broadband photodetectors based on **group-10 TMDCs**, along with their latest applications in optoelectronics. There is a brief introduction to the photodetection mechanism and recent progress of broadband photodetectors based on conventional **TMDCs and their heterostructures**. It is followed by an

overview of the structural characteristics and synthesis of **group-10 TMDCs** used in realizing their heterostructures aimed at broadband photodetectors. Subsequently, the potential applications of **group-10 TMDCs** in electronics and optoelectronics have been discussed. In the end, the results and discussions are concluded, and prospects are presented for the emerging **group-10 TMDCs** based broadband photodetectors.

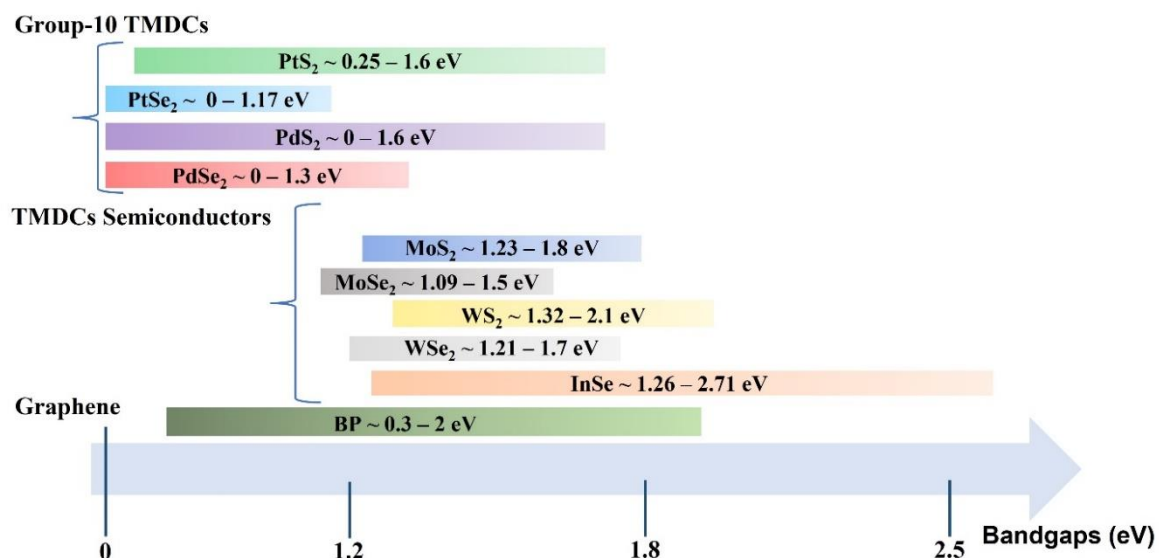


Figure 1. Energy Bandgap of conventional 2D materials (graphene, BP, TMDCs) and **group-10 TMDCs** at ambient temperature.

2. Fundamentals of Photodetectors

A photodetector converts the light into electrical signals through optical absorption, during which extra charge-carriers are produced. In this section, the various mechanisms of photodetection and the key figures of merits affecting the performance of a photodetector are summarized.

2.1. Photodetection Mechanism

Normally, two types of photodetection mechanisms are considered: (1) light is incident on an active channel of the device, which excites the free charge carriers. This phenomenon is associated with the photovoltaic effect (PVE), photoconductive effect (PCE), and photogating effect (PGE). (2) Thermal effect associated with photo-thermoelectric effect (PTE) and photo-

bolometric effect (PBE) produces/excites free charge carriers and causes light detection.^[15]

These mechanisms have been depicted in **Figure 2**.

2.1.1. Photoconductive Effect (PCE)

PCE embraces a process wherein a semiconductor absorbs the photons and produces extensive free carriers, increasing its conductivity. Without light irradiation (dark current), the semiconductor channel allows only a very small source-drain current to drive dark current (I_{ds}) by using the external bias between the electrodes (V_{ds}). When the light is incident on the semiconductor channel, it produces electron-hole pairs that mainly depend on the materials, as depicted in Figure 2a. As shown in Figure 2b, the typical output curve reflects increasing conductivity in the semiconductor under two opposite conditions. The charge carriers can be separated by applying the bias voltage V_{ds} . The charge carriers can be separated by applying the V_{ds} . This phenomenon is the reason for increased photocurrent (I_{ph}) in the channel.^[15a] **The relationship of the I_{ph} could be expressed as**

$$I_{ph} = I_{illumination} - I_{dark} = \frac{P_{in}}{h\nu} \frac{\eta\mu q E \tau_{photocarriers}}{L} \quad (1)$$

In the above relations, P_{in} defined as incident light power, h and ν knows as planks constant and frequency of light incident respectively. η and E is quantum efficiency and strength of electric field respectively and L is knowing as the distance of both electrodes (source and drain).^[16]

Usually, strong V_{ds} enable quick carrier transport and rapid separation of the electron-hole pair. The photocarrier lifetime greatly affects the response speed and photoconductive gain. Photodetector based on the PCE has a larger gain than unity. Under the normal V_{ds} , the majority carrier, such as electrons, shows high mobility and low transit time compared to the minority carrier, such as holes. More electrons from the external electrode are transported into the channel within the hole lifetimes of holes to sustain charge neutrality.^[17] **Photoconductive gain**

can be expressed as

$$G = \frac{\tau_{lifetime}}{\tau_{transit}} = \frac{\tau_{photocarriers} \cdot \mu \cdot V_{DS}}{L^2} \quad (2)$$

τ_{lifetime} denotes the lifetime of holes, and τ_{transit} is the electron transit time. Whereas transit time can be determined by the following relation $\tau_{\text{transit}} = L^2/\mu V_{\text{DS}}$, in which L is separate distance of electrodes (source and drain) and μ is known as carrier mobility.^[16] higher gain can be obtained by adjusting the electron transit time to be shorter and increasing it for the holes. However, response time also depends on the charge carrier, such as the electrons/holes recombination process. For example, rapid carrier recombination at the surface leads to more efficient photoresponse. Although, a higher gain will reduce the response time. Therefore, adequate engineering is required to maintain response time and gain to obtain the appropriate presentation of the photoconductor.

2.1.2. Photogating effect (PGE)

Another type of PCE that exists in photoconductive photodetectors and phototransistors is the photogating effect. Generally, PGE exist in hybrid structures or defective semiconductor devices.^[16] The light absorbed by these devices generates electron-hole pairs, as shown in Figure 2c. The trapping of particular species of charge carriers (either electrons or holes) in the localized states of the semiconductor can lead to a localized floating gate that can be used to tune the channel conductivity due to electrostatic interaction. A high gain can result from the enhanced transport of the mobile charges during the trapped lifetime of the other species of carriers within the semiconductor's localized states. The typical transfer curve of the PGE demonstrates horizontal (ΔV_g) control of the photogating effect, as shown in Figure 2d. In other words, in the PGE process, lifetime of excess charge carriers becomes longer due to capture of opposite charge carriers. As per equation (2), the large photoconductive gain can be realized.^[16] This phenomenon is mostly observed in nanostructured materials, for example, nanowires, colloidal quantum dots, and 2D nanoflakes, where the dimensions of the structures are significantly shorter than the mean free path of the carriers.^[16] Although photodetectors based on PGE show a higher gain compared to PCE-based photodetectors, but they suffer from a slower photo-response speed. PCE and PGE can be realized within the same device to simultaneously enhance the gain and photo-response speed.^[11a, 16]

2.1.3. Photovoltaic effect (PVE)

The photovoltaic effect (PVE) arises due to the rapid separation of photo-generated carriers due to the built-in electric field within a device. This effect can be attained by utilizing two different materials with different work functions, as shown in Figure 2e. This effect is mostly utilized in photodiodes. Usually, a photodiode is realized using a p-n junction made from semiconductors with two different doping polarities along with metal electrodes forming a Schottky barrier at the metals and semiconductor interface. In the PVE process, electrons/holes rapidly separate due to an internal electric field and are collected by electrodes in the presence of optical illumination. Photodetectors based on PVE usually do not need external bias voltage and are normally self-powered. The photodiode usually displays typical I-V characteristics, as shown in Figure 2f. Photogenerated current could be visualized under the illumination of the light at 0 bias voltage. Two important parameters, such as short circuit current (I_{sc}) and open circuit voltage (V_{oc}), express the self-powering capability of photovoltaic devices for photovoltaic photodetectors. Based on this mechanism of PVE, photodiodes such as PN photodiode, PIN photodiode can be constructed. Usually, the working mechanism of photodiodes based on the reverse biased such as avalanche breakdown voltage ($< V_{ds} < 0V$) which is beneficial to achieve the quick photoresponse as well as minimum capacitance rate. In the reverse bias condition, dark current can be achievable very low due to PN junction or Schottky junction and thus detectivity can be higher. However, mostly photodiodes show very low photo-gain due to fast sweep charge carriers in the space area. But, avalanche photodiode shows large photo-gain due to large reverse bias that provide extra space to charge carriers production through collisional ionization and thus can attain high photo-gain in the avalanche photodiode.^[3c, 16]

2.1.4. Photo-thermoelectric effect (PTE) and photo-bolometric effect (PBE)

PTE is associated with thermal (heat) effects observed upon light illumination on two different substances (semiconductors or conductors) that lead to a temperature gradient resulting in a temperature difference (ΔT) between the two materials. This temperature difference leads to a

voltage differential termed photo thermoelectric voltage (V_{PTE}). The ratio between voltage difference and V_{PTE} voltage is known as the Seebeck coefficient or PTE. The V_{PTE} can be measured as

$$V_{PTE} = (S_1 - S_2)\Delta T \tag{3}$$

S_1 and S_2 are the Seebeck coefficients of the two materials in the above equation. In PTE semiconductor devices, ΔT can be obtained by localized illuminations and under global illumination if optical absorption comes from different regions.^[3c, 16]

The PBE mechanism is related to the direct heat generated due to the incident light on the semiconductor materials leading to a change in the transport conductance produced by the incident photons. Usually, PBE can be found in sensitive detection such as IR and beyond.^{[3c,}

11a, 16]

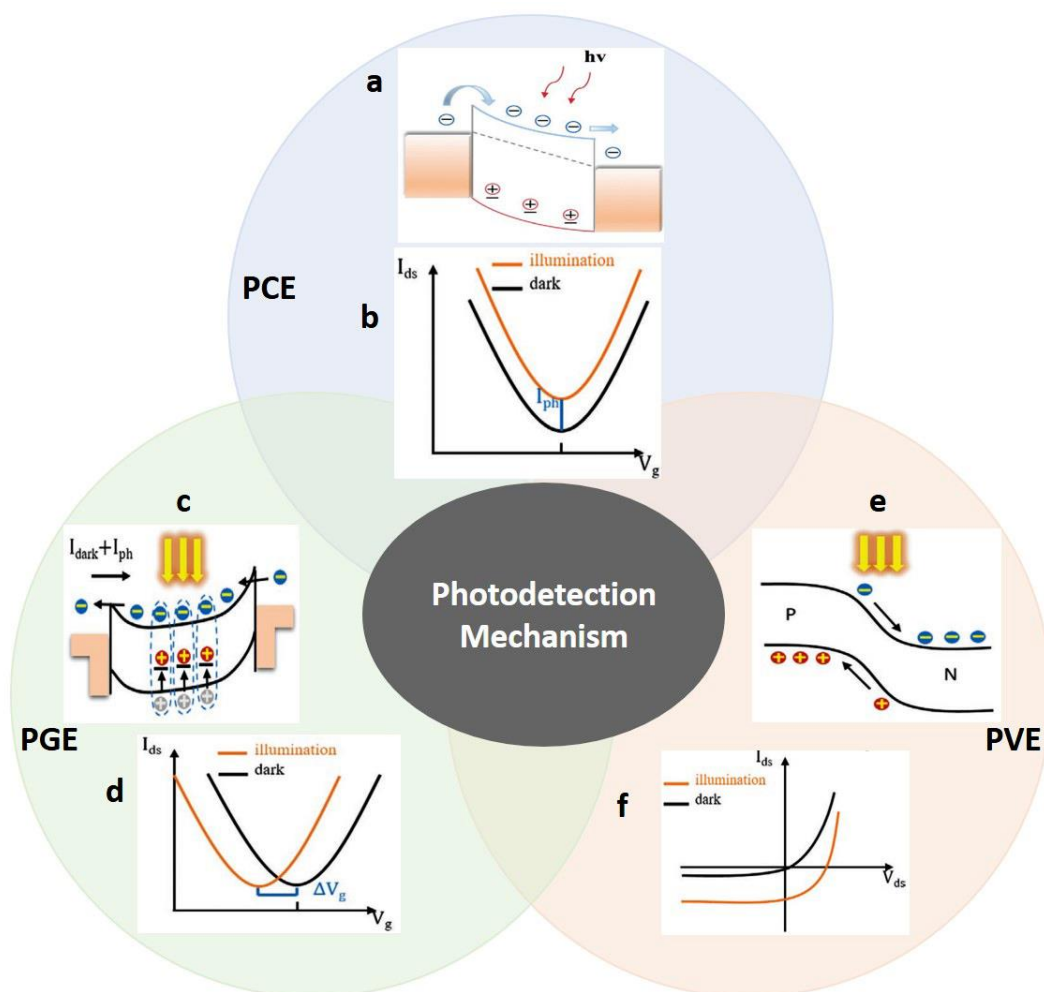


Figure 2. Schematic illustration for photodetection mechanisms: (a) Schematic diagram of PCE. Reprinted with permission from Ref.^[15a]. Copyright 2020 Wiley-VCH (b) typical transfer curve of the PCE. Reprinted with permission from Ref.^[11a]. Copyright 2021 Wiley-VCH. (c, d) Schematic diagram and typical transfer curve of PGE respectively. Reprinted with permission from Ref.^[11a]. Copyright 2021Wiley-VCH. (e, f) Schematic diagram and typical output curve of PVE respectively. Reprinted with permission from Ref.^[11a]. Copyright 2021Wiley-VCH.

2.2. Key Characteristics of Photodetectors

Key characteristics of effectual photodetectors are associated with output of a laser or light irradiation. In this sub-section, we present the various characteristics of photo-response of the medium and the device that are very important to measure the performance of the photodetector.^[18]

2.2.1. Responsivity (R)

It implies ratio of the photocurrent or photovoltage to the illuminated power density. It is evaluated as ampere/watt (AW^{-1}) or power/watt (VW^{-1}). The responsivity is denoted as R and can be calculated as follows.^[16]

$$R = \frac{I_{ph} \text{ or } V_{ph}}{P_{in}A} \quad (4)$$

Whereas P_{in} is incident optical power and A is the illuminated area. This property has an impact on light capability for photoelectric conversion in the photodetector.

2.2.2. Gain (G)

Gain is an important parameter to evaluate the performance of the photodetector in which detected charge carriers per single incident photons are known as gain. It can be expressed as^[16]

$$G = \frac{I_{ph}/q}{\eta P_{in}/h\nu} = R \frac{hc}{\eta q \lambda} \quad (5)$$

In this relation, h is known as Planck constant (6.63×10^{-34} Js), c is the velocity of light (3×10^8 m s⁻¹), η is quantum efficiency, λ is the excitation wavelength. Gain can be turned to external quantum efficiency as η is ignored.

2.2.3. External quantum efficiency (EQE)

The ratio of incident photons contributing to the photocurrent is named EQE and is related to R through the following relation.^[16]

$$EQE = \frac{I_{ph}/q}{P_{in}/h\nu} = R \frac{hc}{q\lambda} \quad (6)$$

Normally, the value of G and EQE are greater than 1, because two or more than two charge carriers induced by one incident photons.

2.2.4. Internal Quantum Efficiency (IQE)

IQE is defined as the ratio of the number charge carrier (electrons or holes) generating photocurrent and number of the absorbed photons by photodetector.^[16]

$$IQE = \frac{I_{ph}/q}{A_{ab}P_{in}/hc} \quad (7)$$

Where A_{ab} is the absorbed fraction, unlike EQE equation, number of absorbed photons is vigorously considered in IQE equation. To precisely determine the IQE and number of photons absorption in the photodetector, optical interference effects on should be considered.

2.2.5. Signal to noise ratio (SNR)

The ratio of the signal power and the noise power is known as the SNR, and is measured in terms of decibel (db).^[16]

$$SNR = \frac{\text{signal power}}{\text{noise power}} \quad (8)$$

Higher values of SNR are very important to improve the performance-sensitivity of a photodetector because lower noise in the photodetectors enables the detection of weak signals.

2.2.6. Noise equivalent power (NEP)

NEP of a photodetector is defined as the minimum input optical power equivalent to the root mean square of noise current for a 1Hz bandwidth used for producing the photocurrent. It is calculated as^[16]

$$NEP = \frac{I_n \text{ or } V_n}{R} \quad (9)$$

whereas I_n or V_n is the mean-square noise current or mean square noise voltage and can be determined at the bandwidth of 1 Hz in darkness (in A Hz^{-1/2}) and in V Hz^{-1/2}, respectively. From this relation, it can be concluded that a low noise signal and larger R can be achieved through a smaller NEP. So, a smaller NEP is very important to enhance the performance of a photodetector.

2.2.7. Detectivity (D^*)

The ability to detect the lowest optical signals is known as detectivity and it is expressed as^[16]

$$D^* = \frac{\sqrt{AB}}{NEP} \quad (10)$$

Whereas A and B are the area and the bandwidth of the photodetector respectively and unit is Jones (cm Hz^{1/2} W⁻¹). If the total noise is assumed by the contributed of the shot noise from dark current. Then, D^* can be realized as^[16]

$$D^* = A^{1/2} \cdot R / (2 \cdot e \cdot I_d)^{1/2} \quad (11)$$

In this relation, I_d is the dark current. D^* can be enhanced for a lower dark current. It should be noted that the results based on these assumptions are usually one order of magnitude higher than the actual results calculated from the above expression (11).

2.2.8. Response time (rise time/fall time)

The ratio of response speed of the device for the appearing radiation signals is associated with response time. It is restricted by factors like trap states or defects in the 2D materials and the corresponding intrinsic RC constant of the device. The time taken by the output signal to

increase from 10% to 90% of the peak value at the onset of an input signal is considered to be the rise time, whereas the rate of drop in the output signal from 90% to 10% is termed as the fall time.^[16]

$$I = I_{pho} e^{-\left(\frac{t}{\tau}\right)^\beta} \quad (12)$$

In this relation, I_{pho} represents the current in device without light irradiation, β is the exponent co-efficient and τ is the response time. Normally, unit of the response time is expressed in ms or μ s.

3. Photodetectors based on TMDCs

2D layered materials has unique physical, electrical, and optical characteristics due to their layered nature characteristics than facilitates a tunable bandgap, higher carrier mobility, and larger optical absorption. For instance, the bandgap of WS₂, MoS₂, and WSe₂ can be shifted from indirect to direct bandgap when their bulk form is reduced to 2D layers. Additionally, 2D materials can be tailored through chemical doping and electrostatic gating. In the physical mechanism of 2D materials, each layer of 2D material is held due to covalent bonding, and each atom is bound to its neighbouring atom by weak vdWs forces. In this scenario, 2D materials can easily be exfoliated from bulk to few layers and monolayer. These can assemble vdWs heterostructures consisting of different layered materials without any lattice mismatch.^[18a, 19]

Most of the 2D vdWs heterostructures are functioned under extra applied voltage that consumes energy during light detection and causes the limitation of their practical applications. Self-powered photodetectors not required additional voltage bias to operate and thus consume less energy which makes them favorable for extreme conditions. Moreover, the p-n heterojunction photodetector offers a strong built-in electric field at the interface. It can show the ability of self-powered properties and rapid photoresponse owing to rapid charge separation at the surface.^[2c, 20] If a p-n junction consists of two different materials having different bandgaps, it will have the ability to break the limitation of the bandgap. Such photodetectors are ultra-

sensitive, self-powered, and broadband. Heterojunctions based on TMDCs are emerging as building blocks for promising semiconducting devices. For instance, WSe₂, GeSe, and BP behave as p-type, and InSe, WS₂, and MoS₂ act as n-type.^[21] Researchers have developed p-n and n-n heterojunctions based on WSe₂/WS₂/MoS₂, as shown in **Figure 3a**. The device can adjust the charge transport in heterojunction layers. A thin layer of h-BN was used in the heterostructure as a dielectric layer to reduce the defect/traps. It was revealed that the proposed structure offers ultra-high R (10⁶ AW⁻¹), notable D* (10¹⁵ cm Hz^{1/2} W⁻¹), and faster photoresponse <10 ms for wavelength 405 nm.^[22] Another report shows the fabrication of broadband self-powered photodetector based on p-n (GeSe/MoSe₂) heterojunction, as depicted in **Figure 3b**. This work achieved a higher rectification ratio of 1×10⁴, which is attributed to the interface between the metal and heterojunction. The device shows outstanding D* (7.3×10⁹ Jones), R (465 mAW⁻¹), EQE (670 %), and photoresponse (180/360 ms) in NIR spectral range (850 nm). These results evidence that 2D materials-based heterojunctions with sharp interfaces can develop novel electronic and optoelectronic devices owing to their various functionalities.^[23]

Heterojunctions based on low dimensional materials such as mixed dimensional heterostructures are effective strategy to bring the novelty in optical devices and enhance the broadband photoresponse, increase the sensitivity and reduce the dark current in photodetectors. Mixed-dimensional heterojunctions allow variety of materials to combine at one platform irrespective of degree of freedom. These offer a useful strategy to overcome the drawbacks of internist TMDCs 2D flakes to gain their full fledged performance.^[24] For instance, a broadband photodetector comprising of mixed dimensional materials such as Te (nanowire) and 2D MoTe₂ nanoflakes have been demonstrated which works for 520-1310 nm spectral range, as shown in **Figure 3c**. 2D MoTe₂ nanoflakes show strong ambipolar characteristics, which help these materials yield a high rectification ratio and remarkable D* (4.9×10¹¹ Jones) at 520 nm. At 1310 nm, the value of D* is reduced to 2.2×10⁵ Jones, and the photoresponse becomes faster (~4.8

ms). Moreover, the device shows the highest EQE ($7.16 \times 10^3\%$) based on the PGE. Heterojunctions based on low dimensional semiconductors can improve the device performance and bring uniqueness, which is essential to develop promising semiconducting devices.^[25]

Researchers have also demonstrated the vdWs heterostructure-based photodetector comprising of WSe₂ and Bi₂O₂Se, as illustrated in Figure 3d. The fabricated devices possessed a high rectification ratio (10^5), low dark current (10^{-11} A), and relatively fast photoresponse (2.6 μ s). Moreover, WSe₂/Bi₂O₂Se vdWs heterostructures-based broadband photodetector covers broadband spectral range (365 nm to 2000 nm) via strong interlayer coupling at the surface. Moreover, strong built-in potential brings a PVE mechanism that endows high R (285 mA W⁻¹) for 2000 nm. These results suggest that heterostructures of Bi₂O₂Se with other TMDCs can develop promising self-driven, highly sensitive, and high-performance electronic and optoelectronic devices.^[26] A report shows the plasma enhanced chemical vapour deposition (PECVD) synthesis of vdWs heterostructures comprising of MoS₂ and WS₂ at large scale (four-inch wafer scale), as shown in Figure 3e. These heterostructures were used for the fabrication of photodetector which showed R as 83.75 mA W⁻¹ and photoresponse as 60 ms for wavelength 660 nm. The results suggest that the PECVD synthesis can improve the crystallinity and layer arrangement during the synthesis of heterostructures and can produce high yield promising new generation electronic and optoelectronic devices.^[27] Several graphene's, BP, and TMDCs, and their heterostructures-based broadband photodetectors have offered a wide range of detection performances from VIS to IR, as tabulated in **Table 1**.

We may conclude from the afore-discussed literature that 2D materials and their homojunction or heterojunctions in the form of 2D p-n junctions, have the potential for the development of broadband and high-performance photodetectors. Table 1 summarizes various parameters of previously reported conventional 2D materials-based photodetectors. Aside from the benefits of 2D materials and 2D p-n junction-based photodetectors, 2D p-n heterojunctions suffer from

low carrier concentration. Preparation of 2D material flakes through conventional techniques such as CVD is not pretty controllable, which is very important to obtain the wide photodetection spectral range and fast photoresponse. In conventional 2D materials, charge transition between layers is usually an indirect transition that minimizes the photoresponse in the IR spectrum. In most cases, conventional 2D materials-based photodetectors have a trade-off between fast photoresponse and high R. This is depicted in **Figure 4**, showing the R versus response time plot for different scenarios. This analysis suggests that it is challenging to achieve a fast photoresponse along with a high R using 2D materials-based photodetectors. Therefore, there is much needed to develop such photoactive materials and unique detection mechanisms to utilize the broadband detection limits upto THz spectral range at room temperature and without compromising the photoresponse and R.

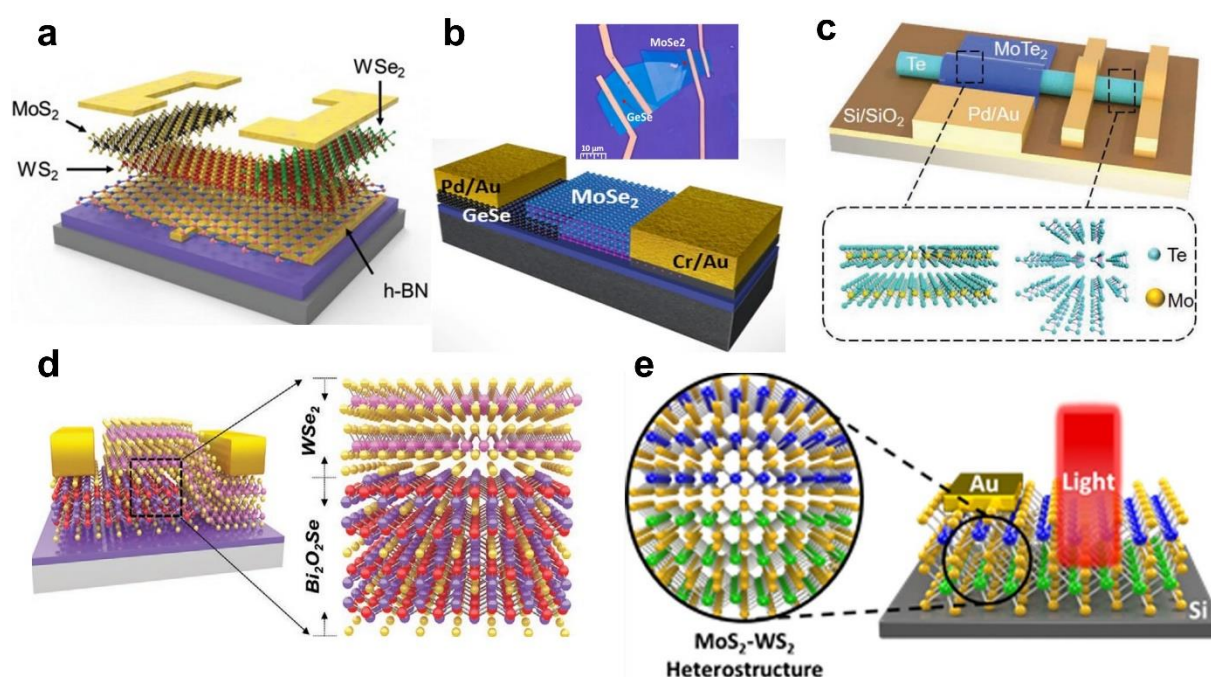


Figure 3. (a) Schematic design of TMDCs based heterojunction consisting of MoS₂-WS₂-WSe₂ with h-BN as a dielectric layer. Reprinted with the permission from Ref.^[22]. Copyright 2020 Wiley-VCH. (b) Schematic and optical image (inset) of GeSe (p-type)/MoSe₂ (n-type) based heterojunction; scale bar is 10 μm. Reprinted with the permission from Ref.^[23]. Copyright 2021 Springer Nature. (c) Schematic depiction of Te nanowire/MoTe₂ 2D flakes heterojunction.

Reprinted with the permission from Ref.^[25]. Copyright 2021 Wiley-VCH. (d) Schematic depiction of WSe₂/Bi₂O₂Se vdWs heterostructure based broadband photodetector. Reprinted with the permission from Ref.^[26]. Copyright 2020 Wiley-VCH. (e) Schematic diagram of MoS₂/WS₂ based vdWs heterostructure prepared at large scale (four-inch Si Wafer) through PECVD. Reprinted with the permission from Ref.^[27]. Copyright 2021 American Chemical Society.

Table 1: Summary of typical parameters of broadband photodetector based on graphene, BP and TMDCs including its heterostructures.

Device Structure	Wavelength Spectrum Range (nm)	Maximum R (AW ⁻¹)	Maximum D* (Jones)	Rise/Fall (ms)	References
Amorphous MoS ₂	473-2712	0.0475	1.26×10^7	10/16	[28]
MoS _{2.15}	445-9536	21.8	-	-	[29]
MoS ₂	405-650	164.3	5.01×10^{10}	-	[30]
WSe ₂	370-1064	0.92	-	900	[31]
WSe ₂	375-1064	8.573	1.2×10^{10}	120	[32]
Bi ₂ Te ₃	325-1550	74.32	3.8×10^9	420/444	[33]
Bi ₂ Se ₃	1456	2.74	3.3×10^{10}	540/470	[34]
SnSe ₂	400-1200	2×10^{-3}	2×10^{11}	380	[35]
InSe	370-980	27	-	0.5/1.7	[36]
HfS ₂	808	3.01×10^5	4.07×10^{12}	8	[37]

MoTe ₂	600-1550	0.024	1.3×10^9	1.6/1.3	[38]
MoS ₂	454-1550	2.3	-	50	[39]
GaTe	325-808	921	5×10^{10}	-	[40]
MoS ₂ /HfOx	550-800	10^4	7.7×10^{11}	10	[41]
MoS ₂ /CdTe	200-1700	0.036	6.1×10^{10}	0.043/0.082	[42]
MoS ₂ /Si	200-1100	11.9	2.1×10^{10}	0.03/0.071	[43]
MoS ₂ /Pattern Gallium Substrate	460	-	5.6×10^8	-	[44]
MoS ₂ /GaN/Si	300-1100	23.81	1.18×10^{12}	0.372/0.794	[45]
BP/WSe ₂	400-1550	10^3	10^{14}	0.8/0.8	[46]
MoS ₂ /MoTe ₂	800	0.038	-	-	[47]
WSe ₂ /SnSe ₂	532-1550	588	4.4×10^{10}	-	[48]
Gr/MoTe ₂ /Gr	473-1064	0.20	-	0.024/0.046	[49]
Gr/Bi ₂ Te ₃	532-1050	35	-	8.7/14.8	[50]
Gr/WS ₂ /Si	450-1050	54.5	-	0.045/0.0210	[51]
Germanium/Gr	350-1650	66.2	-	-	[52]
WSe ₂ /BP/MoS ₂	532-1550	6.32	1.25×10^{11}	-	[53]
ReS ₂ /Gr/WSe ₂	785	1.02	10^{10}	-	[54]

H-BN/b- As _{0.83} P _{0.17} /h-BN	3400-7700	0.9	-	-	[55]
Gr-MoS ₂ -WS ₂	400-1550	6.6×10^7	-	7	[56]
MoS ₂ /Porous Si	550-850	9	10^{14}	0.009	[57]
HfS _{2(1-x)} Te _{2x}	830-1310	2	-	8.8/75	[58]
MoO ₃ /MoS ₂	532	5.41×10^3	0.89×10^{10}	-	[59]
GaTe/HfSe ₂	532	10^3	-	0.018/0.024	[60]
GaSe/MoS ₂	375-633	0.9	-	5	[61]
BP/MoSe ₂	532	0.0032	-	-	[62]
GaTe/MoS ₂	532	0.145	-	< 10	[63]
Bi/WS ₂ /Si	370-1064	0.42	-	100	[64]
Si/NWs	300-1440	0.17	-	700	[65]
GQDs/ZnO/GaN	365	0.034	10^{12}	100/120	[66]
GaTe/InSe	405	0.0138	-	0.02	[67]
WS ₂ /Si	400-1100	1.1	-	42	[68]
WS ₂ /Bi ₂ Te ₃	370-1550	30.4	-	20	[69]
BP/InSe	633	0.0117	-	24	[70]
WSe ₂ /SnS ₂	550	244	1.29×10^{13}	13	[71]
MoTe ₂ /MoS ₂	637	0.046	-	0.06	[72]
Gr	532-10310	8.61	-	100	[73]
MoS ₂ /BP	532-1550	0.153	10^{11}	0.015	[74]
BP/InSe	532-1550	53.8	-	22	[75]
InSe/Gr	400-1000	60	-	1.2	[76]
GaTe/InSe	532-1550	1.5	10^{14}	360	[77]

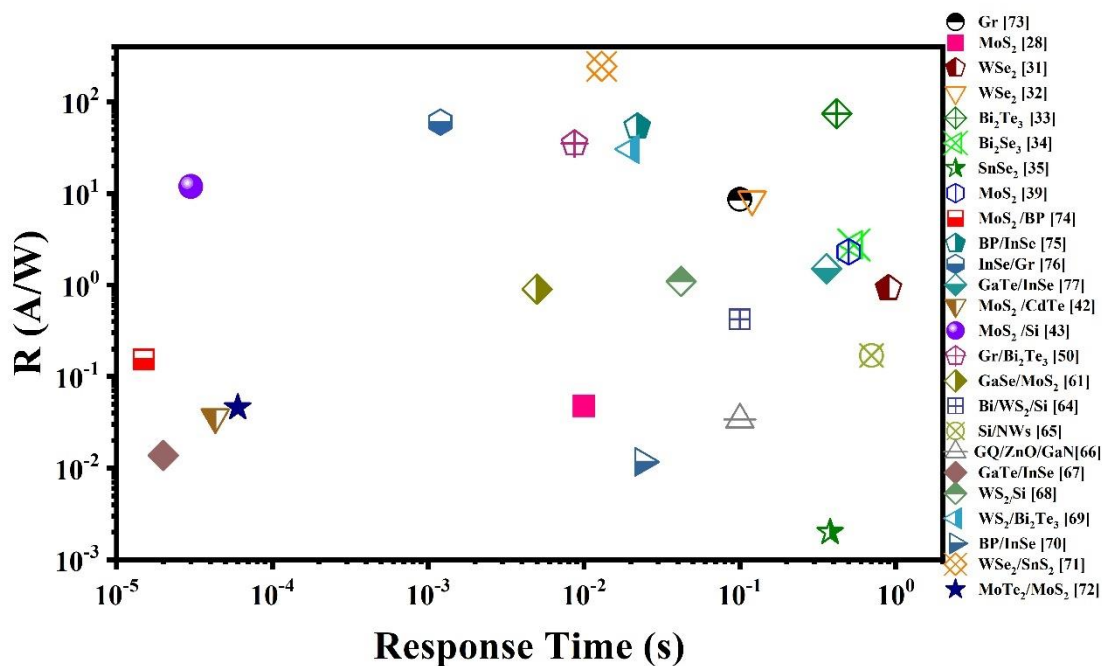


Figure 4. Comparison of photoresponsivity and response time of conventional 2D materials and their heterostructures based photodetectors.

4. Photodetectors based on **Group-10 TMDCs** Family

4.1 Lattice Structure

Recently, **group-10 TMDCs** emerged as interesting candidates for the fabrication of promising optoelectronic devices owing to their unique atomic structure. The typical structure of PtSe₂ is 1T-type hexagonal having space group $P-3m1$, as shown in **Figure 5a**. PtSe₂ has three atomic layers stacked in the order of Se-Pt-Se, which are held by weak vdWs forces. In the monolayer of PtSe₂, Se atoms are connected to Pt atoms and form the octahedral structure in which Pt atoms stay at the center of coordinates.^[78] PdSe₂ is an interesting 2D material in which Pd atoms bond with four Se atoms to form a basic tetragonal unit. These units are connected to the layers through Se-Se bonds and thus form a unique pentagonal structure, as illustrated in Figure 5b,c. This unique structure is responsible for strong interlayer transition, which leads to phase engineering. The vertical distance of each pentagonal structure is 1.6 Å which results in low

symmetry of puckered structure and endows anisotropic electrical and optical properties to PdSe₂. The introduction of Se vacancies to PdSe₂ can change its phase to Pd₁₇S₁₅ and Pd₂Se₃. Moreover, there are lots of functionalities in compounds of Pd and Se, which give them a variety of phases. Furthermore, the bandgap of PdSe₂ layers depends on the layers, such as 0 eV at bulk and 1.3 eV at monolayer.^[79]

Fascinatingly, Pd-based TMDCs offer unique geometric puckered pentagonal structures in PdS₄ and PdSe₄, which further link with S or Se atoms to assemble 2D layers. These materials show outstanding properties, including anisotropy and pentagonal structure, which are crucial to fabricate high-performance phototransistors, broadband photodetectors, and many other optoelectronic devices. Due to their increasingly remarkable optoelectronic properties, group-10 TMDCs are becoming an ideal choice in the 2D materials family. It has led to the discovery of new members of group-10 TMDCs and their physical and chemical properties. First principle calculations reveal that through lithiation and delithiation, phase transition of monolayer PdSe₂ can be achieved. In this mechanism, 8.33% of lithiation can change the transition of pentagonal PdSe₂ (P-PdSe₂) into T-PdSe₂, and it is found to be more energetic and favorable than P-PdSe₂.^[80]

T-PdSe₂ owns many interesting properties such as moderate and stable bandgap (1 eV), excellent photo-absorption co-efficient ($5 \times 10^5 \text{ cm}^{-1}$), notable carrier mobility ($2.3 \times 10^4 \text{ cm}^2 \text{V}^{-1} \text{s}^{-1}$), and anisotropic characteristics. These outstanding features reveal that the modified PdSe₂ monolayer combined with TMDCs monolayers such as T-PdSe₂/MoS₂ and T-PdSe₂/MoTe₂ can assemble type-II heterostructures which may offer potential applications in optoelectronic devices, for example, solar cells, light emitting diodes (LEDs), and other diversity of photoelectronic devices.^[80a] Ta₂PdS₆ is another emerging vdWs material derived from group-10 TMDCs, which possesses a layered structure with monoclinic space group *C2/m*. Its structure is approximately oriented parallel to plane (201) and forms PdS₄ quadrilaterals and TaS₇ polyhedral, as shown in Figure 5d.^[80b]

Introducing defects in 2D layered materials has great advantages for tunable electronic, optical, magnetic, and thermal properties, thereby adding to the functionality of the devices. It is also suitable to modify the structure (like chemical modification of Basal planes of 2D materials) and surface-to-volume ratio (by varying the lateral size of the sheets) of these materials. The defects can be introduced through various techniques, including post-growth annealing, plasma treatment, and laser irradiation. However, the practicality of these techniques for commercial application can be influenced by the requirement for high temperatures ($>500\text{ }^{\circ}\text{C}$) and unwanted damages that can affect the device's performance. Researchers have developed a unique technique for controllable/partial oxidization to overcome these issues by employing an ozone layer at the top of Se atoms in PdSe₂ layers. This technique involves fascinating features such as operating at low temperature ($60\text{ }^{\circ}\text{C}$), offering low disorders, endowing excellent air stability, and delivering atomic layer precision. Chemical doping of oxygen atoms at the surface of PdSe₂ has been investigated by state-of-the-art equipment, including scanning electron microscopy (SEM) and X-ray photoelectron spectroscopy (XPS). Density functional theory (DFT) has also been employed to perform the theoretical calculations for this purpose. It has been revealed that incorporating oxygen in a controlled manner is an effective strategy for engineering the physical and chemical properties of PdSe₂. Furthermore, it was observed that the partial oxidation at the atomic scale enhances the electronic, optical and catalytic activity of PdSe₂. The studies provide a fruitful pathway to understanding low-dimensional materials systems engineering and physical/chemical mechanisms.^[81]

Controlled doping has been an effective strategy to improve the wide range of electrical and optical properties of PdSe₂. Theoretical calculations (first principal study) reveal that the characteristics of PdSe₂ and others **group-10 TMDCs** can be improved through chemical doping. For instance, surface charge transfer doping is non-toxic, facile, and reliable. It can enhance the electrical properties of semiconductor materials. In this strategy, the desired doping molecules are adsorbed on the surface of the semiconductor material and interchange the charges with the

host material. This method is also effective for other 2D TMDCs to enhance their electro-optical properties.^[82]

Researchers have also studied the effect of charge transfer doping on PdSe₂-based FET. In this contribution, the deposition of benzyl viologen molecules on the surface of the fabricated PdSe₂ device was achieved. The electrical properties of the device were enhanced significantly, and the transition of material from p-type to n-type was observed. As fabricated heterojunction consisted of bare PdSe₂ and doped PdSe₂ and showed an excellent rectification ratio of up to 55, evidencing the significance of surface charge transfer doping for tuning the electrical properties of PdSe₂.^[83]

PtTe₂ is considered as 1T configuration rather than 2H. 1T-PtTe₂ shows a space group of *P-3m1*, as shown in Figure 5e. In this structure, each Te-Pt-Te unit constitutes edge-connected octahedra with one representative octahedron as highlighted in pink regions of the side and top views.^[84] The crystalline structure of PdTe₂ consists of CdI₂-type trigonal (1T) structure with space group *P-3m1*, as shown in Figure 5f. Pd atoms at the basal plane are bounded by six Te atoms, forming the PdTe₆ octahedra.^[85] According to the theoretical calculations, atomically thin layers of PdTe₂, referred to as thermoelectric material, have high thermoelectric characteristics compared to other thermoelectric materials, including Bi₂Te₃. Furthermore, the presence of type-II Dirac fermions and topological superconductivity characteristics make it a favorable candidate for thermoelectric-based applications.^[86]

Emerging PtS₂ showed tunable bandgap, high mobility, and notable stability at room temperature. Most of the TMDCs have 2H-phase in thermodynamics; however, **group-10 TMDCs** have 1T phase and offer advantages over other **conventional TMDCs**, including excellent photocatalytic properties. PtS₂ has a CdI₂-type structure in which each atom of Pt acts as an octahedral hole and coordinates with six S atoms, thus leading to a PtS₆ octahedron. The layers of PtS₂ are held by vdWs forces, and construct 1T structure DFT calculations reveal that PtS₂ has a layer dependent on bandgap. Its monolayer shows an indirect bandgap of 1.6 eV,

whereas the bulk form shows 0.25 eV. The bandgap of this material strongly depends on its number of layers due to presence of pz orbital(s) of interlayer S atoms. The *d*-electron-number determined octahedral coordination structure is shown in Figure 5g.^[87]

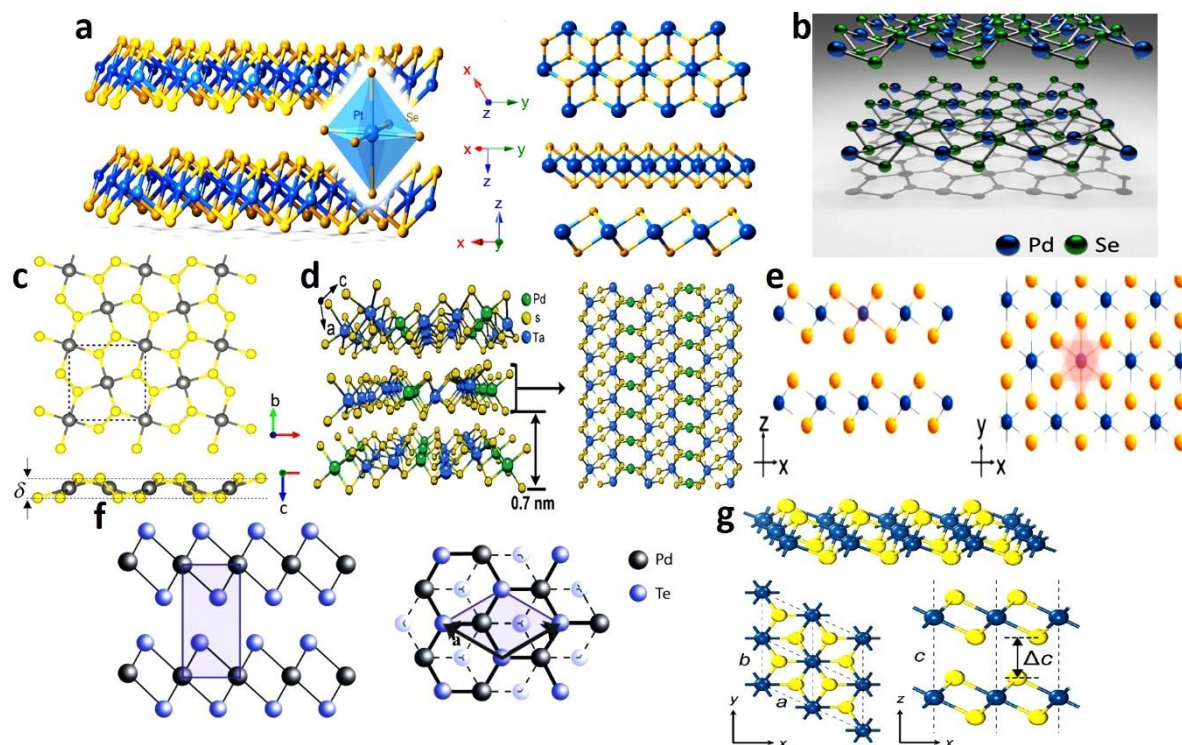


Figure 5. (a) Crystal structure of PtSe₂ (Left) with its 3D view (Right). Reprinted with the permission from Ref.^[78]. Copyright 2018 Nature Springer. (b, c) Pentagonal structure of PdSe₂ with top and side views. Reprinted with the permission from Ref.^[79b]. Copyright 2017 American Chemical Society. (d) Crystal structure of monolayer Ta₂PdS₆ which exhibits thickness of 0.7 nm (Left). Crystal structure of monolayer Ta₂PdS₆ along plane (201) (Right). Reprinted with the permission from Ref.^[80b]. Copyright 2021 Wiley-VCH. (e) Side and top views of 1T PtTe₂; orange balls represent Te atoms and blue balls represent Pt atoms. Reprinted with the permission from Ref.^[84]. Copyright 2020 American Chemical Society. (f) Side and top views (left to right, respectively) of atomic structure of PdTe₂. Reprinted with permission from Ref.^[88]. Copyright 2021 Springer Nature. (g) Schematic illustration for crystal structure of PtS₂ (3D, top and side views). Reprinted with permission from Ref.^[87]. Copyright 2016 Wiley-VCH.

4.2 Synthesis Methods

Synthesis of a high-quality monolayer, few-layer, and multilayer **group-10 TMDCs** is essential to fabricate high-performance semiconducting devices. Monolayers of **group-10 TMDCs** have received considerable attention owing to outstanding physical characteristics for both academia and commercial applications in electronics, optics, ferroelectrics, spintronics, etc. Monolayer PtSe₂ can be synthesized through a single step, direct selenization of Pt (111) substrate, as illustrated in **Figure 6a**. The Pt substrate modifies the Se chemical form (from Se⁰ to Se²⁻) in this mechanism. Following this modification, under the low temperature (270 °C), the Se⁰ peaks disappear and are dominated by Se²⁻. It leads to the complete crystallization of the PtSe₂ thin films. The as-synthesized PtSe₂ thin films are characterized through angle-resolved photoemission spectroscopy measurements. The theoretical calculations on the band structure reveal that the single layer of PtSe₂ shows semiconducting properties, and its bulk behaves as a semimetal. Owing to this simple and unique property, monolayer PtSe₂ becomes suitable for practical applications such as valleytronics and visible-light-driven photocatalysts.^[89] A monolayer crystal sheet of PtSe₂ was synthesized successfully through the CVD technique. In this technique, hexachloroplatinic acid (H₂PtCl₆) and selenium (Se) were used as source materials during the synthesis of PtSe₂ nanosheets at low temperatures (~900 °C) on the sapphire substrate. Raman, XPS, and transmission electron microscopy (TEM) measurements show excellent quality as synthesized PtSe₂ nanoflakes. Raman bands are found around 177 cm⁻¹ and 207 cm⁻¹, showing the in-plane and out-plane vibrational modes, respectively.^[90] Various techniques have emerged to synthesize the 2D layered materials, for example, CVD, liquid phase exfoliation, sonication liquid phase exfoliation, and electrochemical exfoliation methods. Among these techniques, mechanical exfoliation and CVD are adopted to obtain the few or multilayer materials at a large scale. Sonication liquid phase exfoliation can produce few layers of PtX₂ but at a small size which restricts its potentiality for realizing practical wafer

sized materials for the realization of devices. Electrochemical exfoliation is useful to obtain the micron-size layers of PtX₂ at large scale and low cost.^[91]

Researchers have synthesized PtSe₂ and PtTe₂ through chemical vapor transport (CVT), as shown in Figure 6b. An electrochemical exfoliation technique was employed to avoid unwanted defects and obtain the maximum yield, and rapid growth of solution-processable high-quality thin films of PtSe₂ and PtTe₂ was obtained. PtSe₂ bilayer was exfoliated from bulk crystal using this technique with a 44% yield. The structural quality was confirmed by their XRD and Raman spectroscopy analyses. A sharp peak (001) indicates the excellent quality of PtSe₂ and PtTe₂ thin films, as shown in Figure 6c. Furthermore, two Raman peaks at 180 cm⁻¹ and 207 cm⁻¹ within and out planes of phonon's mode evidence the excellent crystal quality of PtSe₂ and PtTe₂ thin films. Synthesized thin flakes of PtSe₂ and PtTe₂ with suitable thickness can be further employed for promising photoelectronic devices.^[92]

A report shows the direct growth of ultra-thin layers (2 to 20) of PdSe₂ on conductive Au foil through ambient pressure CVD, as shown in Figure 6d. In this deposition, PdCl₂ and Se are used as precursors, and Au is selected as a substrate for PdSe₂ flakes due to its surface catalytic activity and chemical stability at higher temperatures. As-synthesized flakes of PdSe₂ show anisotropic behavior and a large aspect ratio according to the DFT calculations. Crystal quality, atomic structure, electronic properties, and thickness depended on other properties of the PdSe₂ flakes are determined by state-of-the-art characterization approaches, including scanning transmission electron microscopy (STEM) and Raman spectroscopy. Moreover, as-grown PdSe₂ flakes on Au foil show perfect crystal lattice and offer excellent stability for a long time.^[93]

Literature on the synthesis and growth of PdSe₂ suggests that monolayer PdSe₂ has potential applications in semiconducting devices. However, it is undeniable that controllable, high quality, and large grain size synthesis of PdSe₂ is still highly challenging. Novel methodologies are being introduced to develop the techniques to solve these issues for large-area PdSe₂ flakes

synthesis. A report shows the uniform, controllable, and wafer-scale synthesis of PdSe₂ nanosheets through a facile selenization approach. The thickness (1.2 to 20 nm) of PdSe₂ nanosheets is tuned by adjusting the Pd precursor, as depicted in Figure 6e.^[94] The bandgap of the PdSe₂ strongly depended on the thickness of its layers and was verified by the optical absorption measurements of 2D PdSe₂. As the thickness of PdSe₂ nanosheets increases, the optical band edge shifts towards a lower energy state, as shown by Tacu plots in Figure 6f-I. The results confirm that with a change in the thickness of PdSe₂ nanosheets, the bandgap of PdSe₂ is changed. For instance, a 1.2 nm thick PdSe₂ layer shows a bandgap of 1.08 eV. As the thickness of PdSe₂ increases, the bandgap of PdSe₂ decreases, as shown in Figure 6f-II. As the number of layers approaches 50, the bandgap of PdSe₂ decreases to 0, suggesting that the transition of PdSe₂ from semiconductor to semimetal is achievable.^[94]

Researchers have also reported the successful preparation of single crystal bulk Ta₂PdS₆ through solid-state reaction assisted with iodine which can act as a flux agent, as shown in Figure 6g. The as-prepared bulk-Ta₂PdS₆ exhibits shiny needle-shaped structures due to smaller lattice parameters of 3.27 Å. Conventional TMDCs, such as SnSe₂ and MoS₂, show platelet shape and larger lattice parameters. This technique efficiently obtains high quality with a stoichiometric ratio of 2:1:6.^[80b] Literature also reports the one-step CVD growth of few-layer PtTe₂ on SiO₂/Si substrate. As synthesized thin films are 2 to 80 μm large and 1.8 to 20 nm thick, as confirmed by SEM and atomic force microscopy (AFM). Moreover, TEM and XRD analyses revealed that the PtTe₂ thin films offer high quality and notable crystallinity.^[95]

However, the controlled growth of 2D PtTe₂ thin films at a very large scale remains a significant challenge. A recent report demonstrates a facile technique to grow PtTe₂ thin films at a large scale for fabricating spin-orbit torque-based devices. Previously, this technique was employed to synthesize PtSe₂ thin films. It involves a two-step synthesis process.^[96] Firstly, the growth of large area Pt thin film is achieved on SiO₂/Si using a magnetron sputtering system. After that, Pt thin film is transformed into flat and uniform PtTe₂ film through annealing of Pt film at a

temperature of 460 °C, as shown in Figure 6h. This simple technique effectively grows a large area of PtTe₂ thin film with a thickness of ~5 nm. The growth of PtTe₂ thin films shows excellent spin hall conductivity of $0.2\text{-}2 \times 10^5 \hbar/2e (\Omega \text{ m})^{-1}$ that can be beneficial in spintronics applications.^[97]

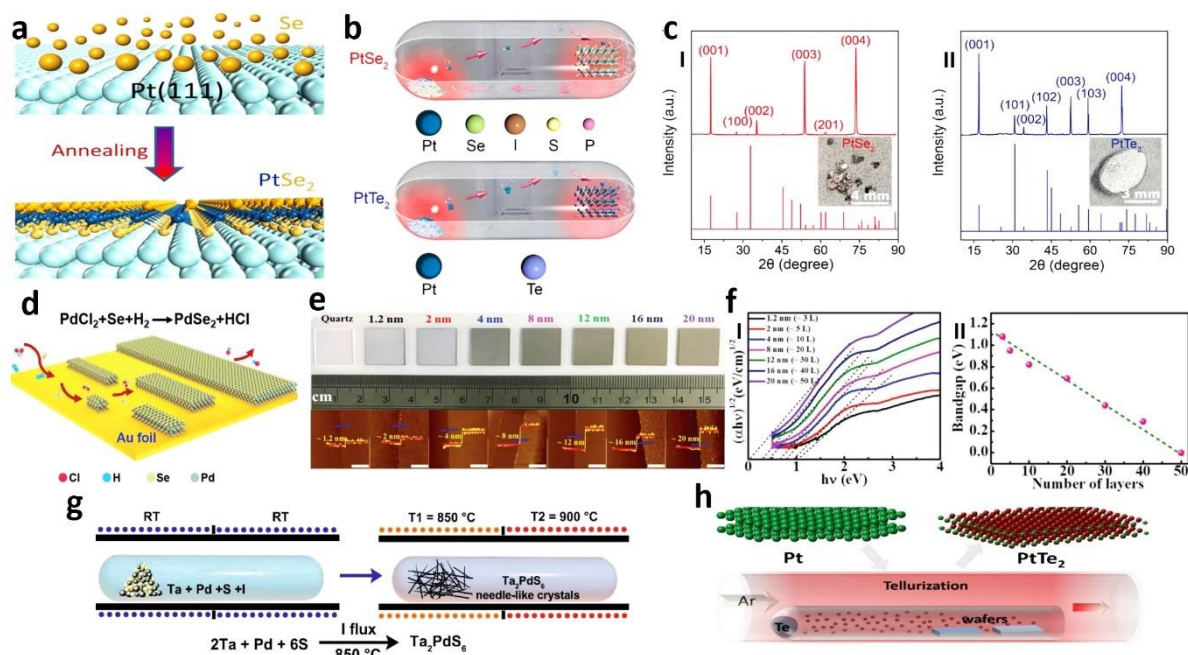


Figure 6. (a) Schematic diagram for the growth of single layer PtSe₂ through single step process (direct selenization). Reprinted with the permission from Ref.^[89]. Copyright 2015 American Chemical Society. (b) Schematic illustration of experimental setup for the synthesis of PtSe₂ and PtTe₂. (c) XRD spectra of the PtSe₂ (c)-I and PtTe₂ (c)-II. (b, c) Reprinted with the permission from Ref.^[92]. Copyright 2021 American Chemical Society. (d) Schematic diagram for controlled synthesis of PdSe₂ flakes on Au foils. Reprinted with the permission from Ref.^[93]. Copyright 2019 Wiley-VCH. (e) Digital photographs and corresponding AFM images of PdSe₂ nanosheets with varying thickness. Scale bar in each AFM image is 2 μm. (f) Tauc plots for varying thickness of PdSe₂ (I). Plot showing the dependence of bandgap on number of PdSe₂ layers determined from Tauc plots (II). (e, f) Reprinted with the permission from Ref.^[94]. Copyright 2019 Wiley-VCH. (g) Schematic diagram for synthesis of single crystal bulk Ta₂PdS₆. Reprinted with permission from Ref.^[80b]. Copyright 2021 Wiley-VCH. (h) Schematic

diagram for CVD process which can turn Pt thin film into PtTe₂ thin film. Reprinted with the permission from Ref.^[97]. Copyright 2020 Wiley-VCH.

4.3 Photodetection based on Group-10 TMDCs

During the last decade, extensive reports were published on broadband photodetectors based on 2D layered materials and TMDCs. However, most did not show notable R, D*, and photoresponse in IR and beyond, such as THz. A longer wavelength spectrum is very important to grasp a variety of applications in the field of image sensing, spectroscopy, bioimaging, and military. Commercial photodetectors based on HgCdTe and InSb alloys are normally employed to develop broadband photodetectors. However, these suffer from strict operation demand and high costs. Among 2D layered materials, group-10 TMDCs possess unique structures, narrow bandgap, interlayer transition in layers, and excellent stability, making them promising candidates for constructing high-performance broadband photodetectors. In this section, we navigate the recent progress of the group-10 TMDCs for broadband IR detection and beyond.^[5, 98]

4.3.1 PtSe₂

PtSe₂ has a great advantage in developing promising semiconducting devices because its layer depends on electronic structure, tunable bandgap, and environmental stability. Due to these properties, PtSe₂ can construct ultrathin and hybrid photodetectors along broadband IR detection. Based on this motivation, a group of researchers fabricated a few layers of PtSe₂-based photodetector. They observed that the photocurrent mechanism shifts from PCE to PGE when transfer characteristics change from OFF to ON. It is due to the Se vacancies that exist in PtSe₂ flakes. Moreover, the device exhibits an excellent R ($5 \times 10^4 \text{ AW}^{-1}$) at 405 nm.^[99] Surprisingly, negative photoconduction is found in few layers of PtSe₂ owing to the PGE at the surface of the SiO₂.^[100] The controllable thickness of the PtSe₂ flakes is highly demanded to achieve practical applications. A report shows the employment of a facile cathodic exfoliation technique for the growth of PtSe₂ to achieve a high-performance IR photodetector. The as-

obtained bilayer PtSe₂ show notable R as 0.072 AW⁻¹ for wavelength 1540 nm, respectively. Moreover, PtSe₂ bilayers show excellent D* (>10⁹), good photoresponse (370 ms/390 ms) at 1540 nm, and remarkable air stability over several months. These findings reveal that the synthesis of PtSe₂ through a solution-processed technique gives a roadmap to fabricating air-stable and high-performance IR photodetectors.^[92]

Another report shows the CVT synthesis of bilayer PtSe₂ films and their properties tuning through defect engineering. As compared to the others conventional techniques such as direct selenization and CVD, as demonstrated technique (CVT) is efficient to synthesis the nanoflakes at large scale upto several microns, control layers and high quality PtSe₂ flakes. Further, they developed the photodetector that works on the mechanism of PCE. As fabricated photodetector shows broadband spectral response from VIS (632 nm) to mid-infrared (MIR) 10000 nm wavelength along with high R (6.25 AW⁻¹ and 4.5 AW⁻¹ respectively). In addition, as fabricated device shows photoresponse (1.1 ms/1.2 ms) at 632 nm. These findings reveal that **group-10 TMDCs** such as PtSe₂ are highly promising candidate for the development of hybrid photodetectors, especially with IR photodetection regime.^[78]

Long wave infrared (LWIR) 8 μm to 15 μm spectrum regime is very important to achieve the numerous applications such as gas sensing, astronomy, deep water detection etc. Conventional 2D materials such as MoS₂, BP etc are not good enough to fabricate the LWIR photodetectors due to wide bandgap and environmental instability. Owing to the excellent properties (tunable bandgap, high optical absorption etc) of the **group-10 TMDCs** are promising candidates for LWIR photodetectors. A group of Researchers have fabricated LWIR photodetector based on 10-70 nm thick PtSe₂ multilayers.^[101] An optical cavity substrate (TiO₂/Au) is used to enhance the photodetection range up to 8350 nm, as illustrated in **Figure 7a**. As demonstrated device exhibits a markable R (54.3 mA W⁻¹), D* (2.5×10⁶ Jones) and relatively fast photoresponse of 54 ns at the wavelength of 8350 nm at ambient temperature. The results reveal that the PtSe₂ is a potential candidate for the fabrication of fast and broadband photodetectors.^[101]

4.3.2 PdSe₂

Theoretical studies show that **group-10 TMDCs** has a narrow bandgap and exhibit high carrier mobility at room temperature.^[79b, 102] In the family of **group-10 TMDCs**, PdSe₂ has superiority due to excellent characteristics such as air stability, layer dependent on bandgap, unique pentagonal structure, and decent charge carrier mobility up to 40,000 cm²V⁻¹s⁻¹. These outstanding characteristics show device-based PdSe₂ with the prospective broadening photoresponse from VIS to IR spectrum regime.^[103] Literature shows the fabrication of a broadband photodetector based on PdSe₂, which shows good photoresponse from VIS to MIR region (up to 4005 nm). It is demonstrated that the fabricated device exhibits layer **depended on bandgap**. A 2.4 nm thick layer of PdSe₂ based photodetector shows response up to VIS region and exhibits R as 3.35 AW⁻¹ for wavelength 532 nm. Whereas, 6 nm thick layer of PdSe₂ based photodetector shows response up to NIR regime and delivers R as 708 AW⁻¹ for wavelength 1064 nm as shown in Figure 7b. These values are five orders higher than that of BP-based photodetectors and two orders higher than that of commercial photodetectors. The as-fabricated devices yield a **photoconductivegain** of up to 82,700, which is mainly attributed to the photogating effect. Moreover, the thicker (50 nm) film of PdSe₂-based photodetector shows photoresponse for wavelength 4005 nm and gives R as 0.0019 AW⁻¹. R in the MIR range is lower than in VIS and NIR regions due to the energy of optical phonons, which is higher in the VIS and NIR range as compared to the MIR region. It is a common feature of 2D materials-based photodetectors. As the R in MIR is lower than the NIR range, it is proposed that D* should also be lower in this MIR region, limiting its applications in this spectral region. However, the optical characteristics of these materials can be enhanced through PdSe₂ junction with others 2D materials or through the introduction of defects or dopants.^[14] A dual-electrode photodetector was fabricated comprising a few layers of the PdSe₂. They observed the polarized sensitive photoresponse from the assembled device measured from photocurrent mapping and revealed that the device shows high sensitivity to polarized light. In addition, the device exhibits

a large ON/OFF ratio (10^2), fast photoresponse (11 ms), and high R (2.5 mA W^{-1}) at the wavelength of 532 nm. Significantly, a good ON/OFF ratio and fast photoresponse resulted from the photocurrent mechanism of PCE and indicated fast transportation and separation of photogenerated carriers. This study reveals that PdSe₂-based photodetector opens new avenues to realize polarized optoelectronic devices.^[104] PdSe₂ is an interesting material for fabricating effective, fast, and sensitive broadband photodetectors based on the photocurrent mechanism of PGE and PCE. A research study demonstrated that CVD-grown PdSe₂ flakes-based photodetector worked on the photocurrent mechanism of the PTE. The as-fabricated device shows extraordinary features, such as no Schottky barrier, and operates at zero bias. In addition, the device shows rapid photoresponse (4 μs) at the wavelength of 532 nm and air stability over nine months, as shown in Figure 7c,d. respectively. Uniquely, rapid photoresponse comes from electron temperature gradient instead of electrons-holes separation. The device shows broadband spectral response (405 nm to 940 nm) with a good R (1.3 mA W^{-1}) owing to the PTE mechanism. The PdSe₂-based photodetector can be used as a broadband photodetection and stable thermal detector.^[105]

Recently self-powered broadband photodetectors were assembled based on the multilayers of PdSe₂, as shown in Figure 7e. The fabricated device utilizes the PVE and PTE effect on a single platform. It was observed that the as-fabricated device has detection limits from VIS to terahertz (THz) regions owing to the strong carrier recombination of electrons/holes pair in the PdSe₂ channel. The as-fabricated device shows R (28 A W^{-1} and 0.4 A W^{-1}) at 405 nm and 1850 nm, respectively (Figure 7f). Moreover, the device exhibits an outstanding R at the THz frequencies, i.e., 20 mA/W at 0.10 THz and 5 mA/W at 0.24 THz. In addition, the device shows a low NEP ($900 \text{ pW}\cdot\text{Hz}^{-1/2}$) and fast photoresponse (7.5 μs). The fast photoresponse could be attributed to the built-in electric field responsible for the rapid transportation of the photogenerated charge carriers. These outstanding results indicate that PdSe₂ has the potential for developing the next generation photodetectors owing to its outstanding characteristics, such as excellent operating

speed and wideband capability, and provides a better roadmap for optoelectronic applications.^[106]

The above discussion suggests that the PdSe₂ and PtSe₂ have a broadband spectral response and exhibit ultra-high optical characteristics, including excellent air stability, and hence can be considered promising candidates for developing next-generation semiconducting devices. However, PdSe₂-based semiconducting devices have advantages over PtSe₂-based devices for the following reasons: (1) PdSe₂ possesses a pentagonal structure and offers a strong interlayer anion compared to PtSe₂, which has a hexagonal structure. (2) PdSe₂ shows strong anisotropic behavior, while PtSe₂ has low anisotropic properties due to its symmetrical hexagonal structure. (3) Photoresponse of a PdSe₂-based photodetector depends on the polarization angle of the light, while a PtSe₂-based photodetector does not show such type of response due to its hexagonal structure. (4) PdSe₂-based FETs can be modified from a p-type to an n-type through controlled light irradiation. However, this phenomenon is absent in PtSe₂-based FETs. These fascinating properties of the PdSe₂ materials make it a superior candidate among members of the **group-10 TMDCs** for developing the next generation of high-performance broadband photodetectors.^[14, 103, 107]

4.3.3 PtTe₂

PtTe₂ is a new member of **group-10 TMDCs** and shows various interesting properties, such as high electrical conductivity (10^6 S m^{-1}) and layer-dependent bandgap. It shows the transition to a gapless metallic state and can have potential applications for realizing promising photoelectronic devices.^[108] A group of researchers fabricated an IR photodetector based on the bilayer of PtTe₂. The as-fabricated device shows excellent R (1.62 AW^{-1}) and $D^* 2.11 \times 10^9$ Jones at 1540 nm. Interestingly, this device can operate at very low power, i.e., 0.16 Wcm^{-2} , and shows excellent performance stability over three months.^[92] Another report reveals that PtTe₂-based photodetector shows broadband spectrum response from 532 nm to 4000 nm. The as-fabricated device has distinct features such as quick photoresponse ($34 \mu\text{s}$), anisotropic

photocurrent response via polarization-dependent measurement, and moderate R (0.04 mA W^{-1}) at 633 nm .^[109] Photodetection at MIR spectrum is very important to tackle the applications in biological imaging, military application, optical communications and environmental monitoring.^[21c] Conventional 2D materials such as graphene, BP, and TMDCs-based photodetectors showed broadened spectral response but suffered from poor light absorption and environmental instability. Alternatively, PtTe_2 shows excellent environmental stability, low dark current, and high photoresponse, making it potentially a photoactive material for MIR photodetectors. It motivated the fabrication of a PtTe_2 -based photodetector that exhibits a broadened spectrum response from VIS (420 nm) to MIR (10700 nm). The as-assembled device exhibits high R (0.2 mA W^{-1} , 8.2 mA W^{-1}) at 10700 nm and 650 nm , respectively (Figure 7g). In addition, the measurement of power and polarization over a wide spectrum range shows an anisotropic photoresponse and a linear relationship of power photoresponse. It demonstrates that PtTe_2 is the next-generation optical material that can be employed in polarization detection sensitive devices.^[110]

TMDCs suffer from weak detection at THz band due to their large bandgap, low carrier mobility, and intrinsic defects during the preparation of the materials. Therefore, there is a great need to develop materials to address these issues. **Group-10 TMDCs** were re-discovered as topological insulators with type-II Dirac cone and weak vdWs forces between the layers. These materials can be integrated with other low-dimensional materials to enhance the optical absorption and performance of the semiconducting devices. Inspired by this, researchers fabricated the THz photodetector based on a planar metal- PtTe_2 -metal structure, as shown in Figure 7h. The as-fabricated device functions in the THz (0.12 THz) spectral range and exhibits self-powered **capability, which** can be suitable for photovoltaic devices. The as-prepared photodetector depicts an ultra-high R of 1.6 AW^{-1} 0.12 THz . It exhibits a rapid photoresponse ($17 \mu\text{s}/16 \mu\text{s}$) at 0.12 THz , as shown in Figure 7i. The fast photoresponse of the device indicates that the device can be effectively employed for the frame-rate imaging-based applications. This rapid

photoresponse is much better than other thermal-based detectors, such as bolometric or pyroelectric ones, showing photoresponse in the ms range.^[111]

Moreover, the R of the photodetector can be improved up to 1.4 kV/W by combining the PtTe₂ heterostructures with graphene, which offers fast charge transportation at the interface and boosts the performance of optoelectronic devices. This structure can be further applied to fabricate various devices for diverse applications, including imaging, biomedical and remote sensing.^[112] Another report shows that a photodetector based on the CVD-grown PtTe₂ shows a broader spectral response up to 0.3 THz. The as-fabricated device exhibits a high R, such as 30 mA W⁻¹ at 0.12 THz and 250 mA W⁻¹ at 0.3 THz. Moreover, the device shows a fast photoresponse of 7 μs/8 μs at 0.12 THz without external bias. These findings indicated that PtTe₂-based THz photodetector meets the requirement for the frame rate imaging at the THz spectrum and is a promising candidate for future THz applications.^[113]

4.3.4 PdTe₂

Emerging topological Dirac semimetals have shown strong scope to assemble modern optoelectronic devices. PdTe₂ shows notable features such as high carrier charge mobilities, anisotropic properties, and room stability. These excellent qualities of PdTe₂ suggest that PdTe₂ could be an ideal candidate for developing promising semiconductor and optoelectronic devices, especially in the terahertz spectrum range.^[114] A group of researchers fabricated PdTe₂ based photodetector that can operate in the THz spectrum range from 0.04 to 0.3 THz, as shown in Figure 7j. Surprisingly, the as-fabricated device exhibits polarization dependent on PGE, generating directional photocurrent with strong anisotropy. The device expresses excellent optical characteristics such as decent R (10 A W⁻¹) and rapid photoresponse (1 μs) that is stable in the THz regime (0.04 to 0.3 THz) as depicted in Figure 7k. In addition, the device shows low NEP (2 pW/Hz^{0.5}) for ambient temperature, excellent stability for up to one month, and good reproducibility with a rapid ON/OFF ratio at the THz spectrum. This finding opens a new

avenue for developing high-performance, stable, and fast photoelectronic devices based on topological semimetals in the THz band.^[115]

4.3.5. *PtS₂*

Very recently, *PtS₂* has shown amazing features such as tunable bandgap, high carrier mobility, and air stability. Thermodynamically, *PtS₂* has stable phase 1T that is beneficial for photocatalytic properties, while mostly 2D layered materials have a 2H stable phase.^[116] A report shows that a photodetector based on *PtS₂* flakes (10.9 nm thick) can give photoresponse in abroad spectrum range up to MIR (4100 nm), as depicted in Figure 71. The demonstrated device shows an ultra-high R (0.3 AW^{-1}) 830 nm. The response speed of the device reaches up to 74 $\mu\text{s}/101 \mu\text{s}$, as shown in Figure 7m^[117] that are the most high and faster than the previously published 2D materials-based photodetectors.^[118] As per photoresponse measurements, device works on the photocurrent mechanism of the PCE and PBE at the spectrum of NIR and MIR respectively.^[117] Usually, optoelectronic devices are constructed onto the SiO_2 substrates that sometimes cause to reduce the carrier mobility and low optical absorption due to surface roughness and surface optical phonons of SiO_2 .^[119] Apart from SiO_2 substrate, h-BN substrate provide smooth surface along free dangling bonds that are beneficial for substrates to improve the photocurrent charge transportation.^[119] Based on this motivation, a group of researchers constructed photodetector based on the few layers of *PtS₂* on the h-BN substrate. The demonstrated device exhibits the ultra-high R ($1.56 \times 10^3 \text{ AW}^{-1}$) and D^* (2.9×10^{11} Jones) and photo-gain (2×10^6) at wavelength of 500 nm which is higher values of the conventional 2D materials-based photodetector such as graphene^[2a], BP^[120] and MoS_2 .^[121] Moreover, they observed that device shows also high carrier mobility ($13 \text{ cm}^2\text{V}^{-1}\text{s}^{-1}$) making its suitable candidate for the electronic devices. Remarkably, device exhibits modified photocurrent mechanism, in which, from the PCE dominant to PGE dominant through adjusting the OFF state to ON state. These outstanding properties such as gate tuning photocurrent generation of the *PtS₂* makes its competitive candidate for optoelectronic applications.^[122]

The discovery of the **group-10 TMDCs** has great scope to develop high-performance, air-stable optoelectronic devices. To continue this stream, a group of researchers developed a broadband photodetector based on a few layers of the new variant of the **group-10 TMDCs** - Ta₂PdS₆. They found that Ta₂PdS₆ occurs semiconducting properties with a strong layer dependent on the bandgap that can be transit from 0 eV (bulk) to 1 eV (monolayer). As assembled device depicts broadband photoresponse from 450 to 1450 nm and exhibits high R as 1.42×10⁶ AW⁻¹, D* as 7.1×10¹⁰, photoresponse speed as 0.8s and photoconductive gain as 2.7×10⁶ for wavelength 633 nm. Moreover, the device shows ultra-high charge carrier mobility up to 25 cm²V⁻¹s⁻¹, an ON/OFF ratio 10⁶, and stability for more than a year. These efficiency metrics are superior to many 2D materials-based FET photodetector devices. Such excellent performance of the device based on the few-layer Ta₂PdS₆ makes it a potential candidate for designing the next generation of electronic and optoelectronic devices.^[80b] So far, **group-10 TMDCs** based photodetectors shows wide range photodetection, i.e., from VIS to THz spectrum as depicts in **Figure 8**.

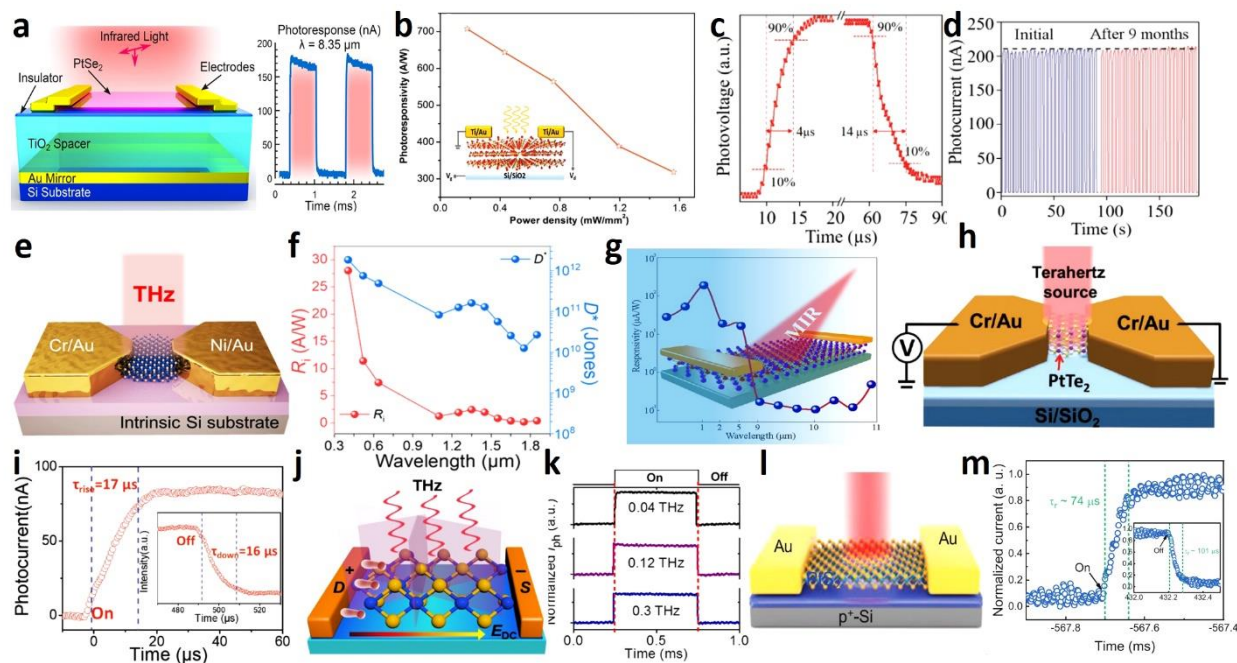


Figure 7. (a) Schematic diagram of LWIR photodetector based on PtSe₂ multilayers and graphical representation of photoresponse of the device for wavelength 8350 nm. Reprinted with permission from Ref.^[101]. Copyright 2021 American Chemical Society. (b) Graphical

representation of the power density Vs photoresponsivity of the PdSe₂ based photodetector, inset: schematic diagram of the PdSe₂ based photodetector. Reproduced with permission from Ref.^[14]. Copyright 2019 Wiley-VCH. (c) Time resolved characteristics and (d) air stability comparison of the PdSe₂ based photodetector respectively. Reprinted with permission from Ref.^[105]. Copyright 2021 Wiley-VCH. (e) Schematic illustration of PdSe₂ THz photodetector and (f) responsivity vs detectivity of PdSe₂ THz photodetector. Reprinted with permission from Ref.^[106]. Copyright 2021 American Chemical Society. (g) Graphical representation of responsivity Vs wavelength of the PtTe₂ based photodetector, inset: Schematic diagram of the PtTe₂ based photodetector. Reprinted with permission from Ref.^[110]. Copyright 2021 American Chemical Society. (h) Schematic diagram of PtTe₂ based THz photodetector and (i) photoresponse of the device. Reprinted with permission from Ref.^[112]. Copyright 2019 Wiley-VCH. (j) Schematic illustration of PdTe₂ based THz photodetector and (k) Time resolved characteristics of the device at THz spectrum. Reprinted with permission from Ref.^[115]. Copyright 2020 American Association for the Advancement of Science. (l) Schematic representation of PtS₂ based photodetector and (m) photoresponse characteristics of the PtS₂ based photodetector. Reprinted with permission from Ref.^[117]. Copyright 2019 Wiley-VCH Copyright 2020 Wiley-VCH.

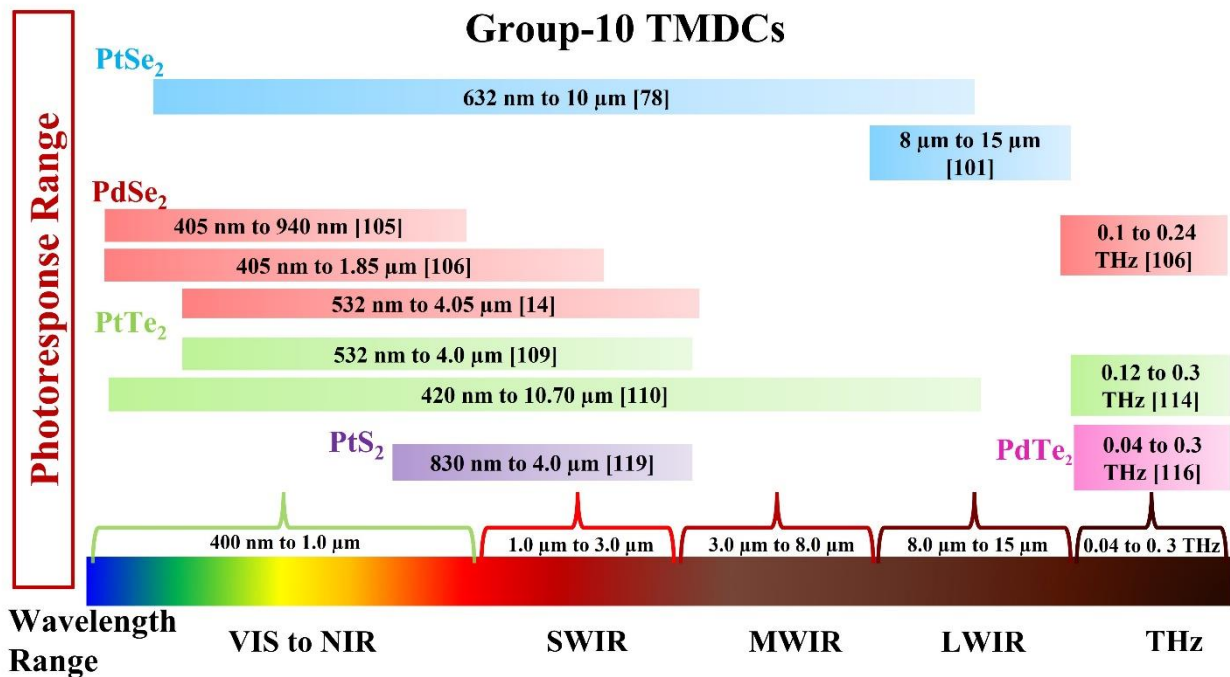


Figure 8. Schematic diagram of broadband (VIS to THz regime) photodetector based on the emerging **group-10 TMDCs**.

5. Photodetector based on **Group-10 TMDCs** Heterostructures

VdWs heterostructures offer great opportunities to achieve high-performance photodetectors. Broadband photodetectors based on single material of **group-10 TMDCs** have shown great achievements, vdWs heterostructures engineering is an effective technique for combining the different properties of different materials. VdWs heterostructure-based photodetectors possess a large degree of freedom that allows us to develop the devices with different diversity of geometries, different working mechanisms, and different bandgaps of different materials that enable the band engineering and thus effectively increase the performance of the photodetectors.^[123]

VdWs heterostructures are a promising technique to increase photoelectronic properties and thus can be employed for numerous applications such as lasers, solar cells, photodetectors, and rectifiers. **Usually, heterostructures can be categorized into three different types, (1) straddling (type I), staggered (type II), and broken gap (type III)^[123b] as shown in Figure 9.** In type-I vdWs heterostructures, band alignment is adjusted where the conduction band and valence band are

placed in the materials with narrow bandgap. In this process, electrons/holes are excited in the wide bandgap, transfer from the narrow bandgap, and realize radiative recombination. Type-I band alignment-based heterostructures are usually employed for light-emitting diode applications.^[124] Normally, 2D materials based broadband photodetectors works on the type-II band alignment Type-II vdWs heterostructures with interlaced band structure is capable to produce the interlayer excitation through the inter-face energy band engineering. It can adjust the band alignment of the materials which is responsible to modulate the interlayer transition energy and induce the charge spatial separation. This phenomenon allows vdWs heterojunction to achieve photoresponse upto the NIR spectrum by flouting the restriction of the intrinsic bandgaps of the individual materials.^[11a] Moreover, type-II band alignment in vdWs heterojunction has ability to enhance the light to electrical signal conversion efficiency because electrons and holes populate in different layers in heterojunction. Type-II band alignment based heterostructures have nonoverlapping bandgap between the two semiconductor materials and charge transport across the heterojunction through the quantum tunnelling as a result drain current enhanced.^[125] Type-III based heterostructure employed to design and developing the high speed and low cost electronic and optical devices.^[126]

Heterostructures allow us to integrate the different dimensionality of materials and the exceptional benefits of different materials, such as 2D/0D, 2D/1D, 2D/2D, and 2D/3D. Different dimensional based possess numerous advantages; for example, in 2D/0D and 2D/1D based heterostructures, the photoelectrical characteristics of 0D and 1D materials, such as increased light absorption, can help to enhance the photoelectrical performance of the 2D materials. In 2D/2D materials, different properties of different 2D materials offer a high degree of freedom to tune the band alignment that helps achieve a broad spectral response and fast charge separations/transportation at interface that can be utilized for achieving a fast photo-response. In 2D/3D heterostructures, the device structure can be optimized for enhanced light absorption.^[11a, 124] This section discusses recent advances in photodetectors based on the **group-**

10 TMDCs heterostructures with different dimensionalities, such as group-10 TMDCs/perovskite materials, group-10 TMDCs/TMDCs and group-10 TMDCs/Si.

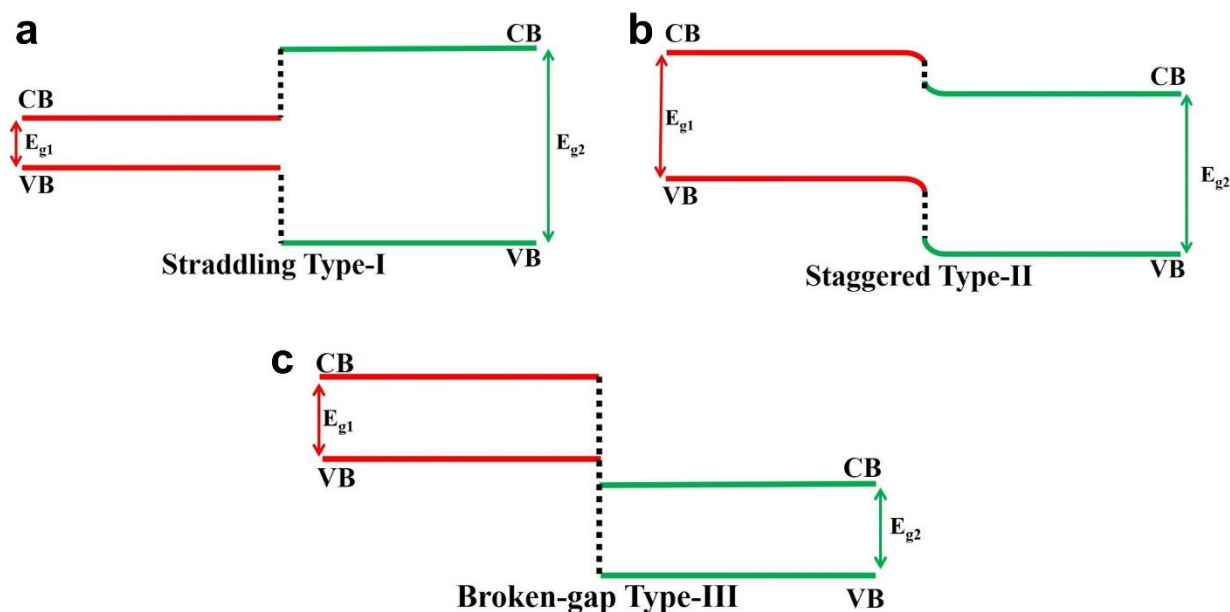


Figure 9. Schematic illustration of band alignments in the vdWs heterostructure. (a) Straddling type-I, (b) Staggered type-II, (c) Broken-gap type-III.

5.1. Group-10 TMDCs/Perovskite Materials

The emerging group-10 TMDCs materials have been proven to be interesting for developing promising electronic and optoelectronic devices. For instance, integrating these materials with other low dimensional materials such as perovskite heterostructures, is a worthy approach for assembling phototransistors and semiconductor devices. This strategy improves and enhances the R , D^* , photoconductive gain, photoresponse speed, and broadband spectral response. Literature shows that assembling these types of heterostructure depends on the preparation of materials. For instance, large-scale production of 2D materials exfoliated from their bulk is still challenging. Moreover, these suffer from several factors, such as limited photoresponse, device noise, and large dark currents. In this scenario, a detailed study is required about the fabrication of photodetectors based on group-10 TMDCs/perovskite heterostructures.^[127]

PtSe₂/perovskite materials (Cs-doped FAPbI₃) based heterojunctions exhibit a broadband spectrum response from 300 nm to 1200 nm along with photovoltaic characteristics, as shown in **Figure 10a**. The assembled device can achieve an ultra-large ON/OFF ratio (5.7×10^3), higher R (0.117 AW^{-1}), notable D* (2.91×10^{12} Jones), and relatively faster photoresponse (78/60 ns) for wavelength 808 nm. The fabricated heterojunction device shows outstanding performance compared to similar devices based on 2D/perovskite materials-based heterojunctions.^[128] However, it is important to remember that perovskite materials suffer from environmental stability, and devices from these materials degrade over time. Interestingly, the proposed geometry scheme efficiently retains the optical properties of the device for up to three months. Therefore, this strategy is efficient in developing fast, broadband, and air-stable photodetectors.^[129] Researchers fabricated the photodetector based on the multilayer of PdSe₂ and Cs-doped FAPbI₃ perovskite materials, as shown in Figure 10b. As the fabricated device is based on the photovoltaic mechanism, it has a broadband spectral response from 200 nm (UV) to 1550 nm (NIR). The wide spectral response arises from the strong built-in potential at the interface of the PdSe₂/perovskite material. The device shows excellent optical properties, for example, a high ON/OFF ratio (10^4), R (313 mAW^{-1}), and D* (10^{13} Jones) at a wavelength of 808 nm. Furthermore, the device exhibits relatively fast photoresponse $3.5 \mu\text{s}/4 \mu\text{s}$ due to the excellent properties of the PdSe₂ and built-in potential at the surface of the PdSe₂/perovskite material. The strong built-in potential at the surface is effective for the fast migration of the photogenerated electrons/holes carrier, thereby increasing the photoresponse speed and the spectral bandwidth. These results suggest perovskite materials combined with **group-10 TMDCs** may have great potential application in future optoelectronic devices.^[130]

5.2. Group-10 TMDCs/TMDCs Heterostructures

For developing promising broadband photodetectors based on **group-10 TMDCs/TMDCs** heterostructures, selection of the materials, proper design structure, and maximizing the effective area of the photodetectors are essential. Nevertheless, **group-10 TMDCs/TMDCs**

heterostructures based broadband photodetectors, along with excellent optical characteristics based on the **group-10 TMDCs**, are less in scope than conventional 2D heterostructures.

2D heterostructures exhibit unique advantages such as efficient charge carrier recombination due to a large and sharp interface, flexibility of the bandgap due to the unique band alignment in type-II heterojunctions to realize a fast charge separation, strong built-in potential, and interlayer transition.^[1b] Reports of PdSe₂ (14 nm thick) based photodetector have been fabricated that delivers R as 42.1 AW⁻¹ and D* as 8.21×10⁹ Jones and quick photoresponse as 74.5 ms for IR wavelength 1060 nm. A photodetector based on PdSe₂/MoS₂ heterostructures was also fabricated, which shows spectrum response up to the NIR regime (1060 nm), as shown in Figure 10c, left side. Current work reveals that the heterostructures reduce the noise level due to a built-in potential between the junction effectively. This feature is a highly desirable for high-performance NIR photodetectors. The D* of heterojunction-based and other reported traditional photodetectors is shown graphically in Figure. 10c, right side.^[131]

In optoelectronic devices based on vdWs heterojunction, photoresponse can rapidly be increased by enhancing numerous characteristics of the photodetectors, including fast interface, band alignment, and tunneling mechanism. However, Schottky contact barrier height, produced between the metal contact and the semiconducting material, suppresses the photoresponse. Consequently, it is necessary to address the Schottky barrier height to enhance the performance of the heterojunction. A research report shows the development of a broadband photodetector based on MoTe₂/PdSe₂ heterojunction, as depicted in Figure. 10d. Figure. 10e illustrates the optical image of the fabricated device. The as-fabricated heterojunction exhibits the spectrum response from 400 to 2000 nm along with ultra-high optical characteristics, including R as 1.24×10⁵ AW⁻¹, D* as 2.42×10¹⁴ Jones and **EQE as 3.5×10⁶ %** for VIS spectrum.

Moreover, the device shows excellent photoresponse time (rise/decay: 16.1 μs/31.1 μs), D* (> **10⁹ Jones**), and **EQE (1.3×10² %)** for the wavelength 2000 nm, which are higher values as compared to most of the TMDCs based NIR photodetectors. These results are not only from

the band-to-band transitions but also occur due to the charge transfer transition in heterojunction, as illustrated in Figure 10f. In the charge transfer mechanism, a small amount of energy is necessary ($\Delta E_{\text{MoTe}_2\text{-to-PdSe}_2}$) compared to the energy required for the intrinsic intra-TMD band-to-band optical transition for any 2D material. Therefore, MoTe₂/PdSe₂-based heterojunction provides the path for developing promising optoelectronic devices, including waveguide photodetectors and optical sensors.^[11a, 132] Another report on the assembly of type-III band alignment heterostructures consisting of PtS₂/WSe₂ reveals that the proposed unique structure offers high-performance electronic characteristics such as selective carrier contact, high reverse rectification (10⁸) and high ON/OFF ratio (10⁸) at room temperature. Moreover, the device can act as a photodetector for the VIS region (632 nm), as given in Figure 10g. The as-demonstrated device shows outstanding optical responses such as R as 1.7 AW⁻¹, D* as 3.8×10¹⁰ Jones, and a fast photoresponse at 8 μs, which is attributed to the broken gap band alignment. It is suggested that the broken gap band alignment-based heterostructures are beneficial for the realization of advanced semiconductor devices.^[133]

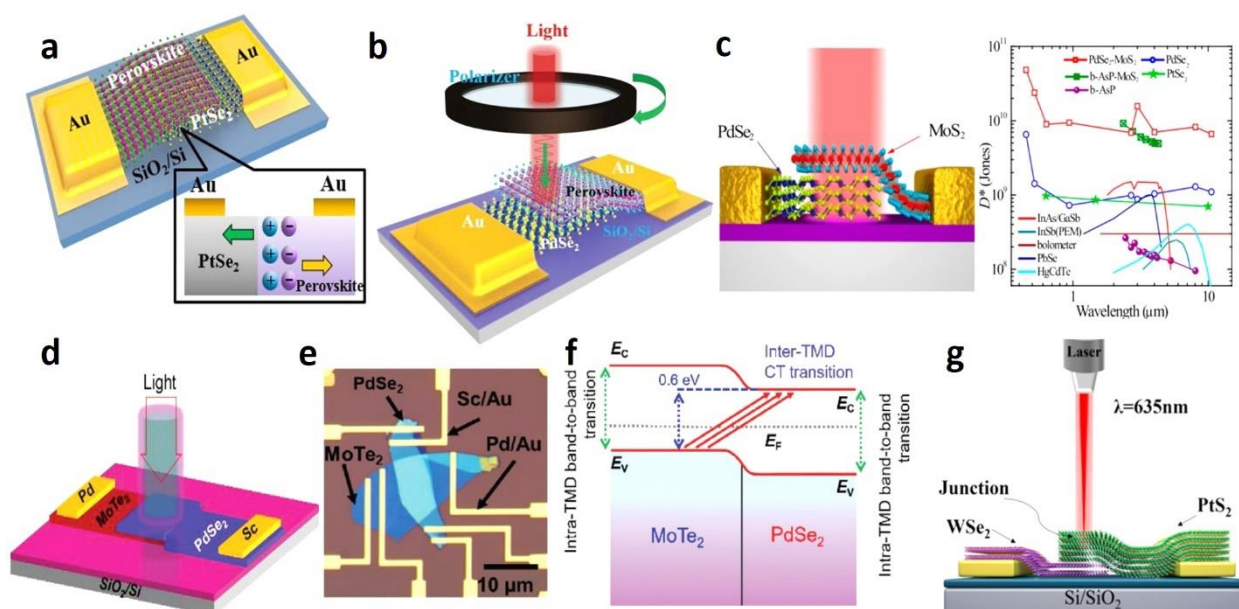


Figure 10. (a) Schematic diagram of PtSe₂/perovskite heterojunction-based photodetector; inset shows the built-in electric field at the interface that is responsible for fast separation of electron/hole pairs. Reprinted with permission from Ref.^[129]. Copyright 2018 American

Chemical Society. (b) Schematic illustration of the PdSe₂/perovskite heterojunction device. Reprinted with permission from Ref.^[130]. Copyright 2019 Wiley-VCH. (c) Schematic diagram of PdSe₂/MoS₂ based photodetector. The graph shows the comparison of D* for PdSe₂/MoS₂ based photodetector and other conventional semiconductor materials-based photodetectors. Reprinted with permission from Ref.^[131]. Copyright 2019 American Chemical Society. (d) Schematic diagram of MoTe₂/PdSe₂ heterojunction-based photodetector. (e) Optical image of fabricated photodetector. (f) Energy band-diagram of MoTe₂/PdSe₂ heterojunction-based photodetector. (d-f) Reprinted with permission from Ref.^[132]. Copyright 2021 Wiley-VCH. (g) Schematic illustration of photodetector based on WSe₂/PtS₂. Reprinted with permission from Ref.^[133]. Copyright 2021 American Chemical Society.

VdWs heterostructures enable band alignment engineering and strong interlayer coupling, generating the band to band transition as well as interlayer transition. Interlayer transition is a unique phenomenon that allows a wide bandwidth photoresponse beyond the limits of each material. Researchers fabricated the robust broadband photodetector (532 nm to 1550 nm) based on the PdSe₂/WS₂ heterostructure as visualized in **Figure 11a**. They developed the device by a simple method: first, the Pd films were deposited by direct selenization onto the CVD-grown monolayer of WS₂. The device was then transferred onto the pre-patterned electrodes via a wet transfer technique. The demonstrated device exhibits a broad spectral response along with excellent **R (3.91 mA W⁻¹) at 635 nm and R (0.019 mA W⁻¹) at 1550 nm**, which is much higher than the bare WS₂ photodetector. The outstanding performance of the heterostructure is mainly attributed to the type-I band alignment, as depicted in Figure 11b. Heterostructure based on type-I band alignment enables the photocarrier generation in band to band excitation yielding a broadband photodetection response of up to the NIR wavelength range. These findings illustrate that PdSe₂/WS₂ has potential applications in optoelectronics.^[134] In addition, type-II vdWs heterostructure based on InSe/PdSe₂ was developed, as shown in Figure 11c. The heterostructure device shows a strong interlayer transition in the NIR region (up to 1650 nm)

which is beyond the limit of the intrinsic bandgap of each component material (InSe and PdSe₂). The device shows high R (58.8 AW⁻¹), D* (1 × 10¹⁰ Jones), and EQE (4660%) as compared to the single PdSe₂ and InSe-based photodetector as shown in Figure 11d. The device exhibits relatively short photoresponse (53 ms/72 ms) at 532 nm and 160 ms/180 ms at 1650 nm owing to the type-II band alignment and interlayer charge coupling. These outstanding results illustrate that type-II vdWs heterostructure with the benefits of strong interlayer transition could help to design the next generation of infrared optoelectronic devices.^[125]

Photodetectors having unipolar barrier structure like nBn (n-type absorber, barrier layer, and n-type contact layer) or pBp (p-type absorber, barrier layer, and p-type contact layer) are effective in overcoming the dark current and allows the IR photodetectors to operate at higher temperatures. The band alignment and lattice matching must be consistently designed to reduce the dark current and enable the photocurrent unimpeded for fabricating these types of photodetectors. Previously, conventional semiconductor materials like group III-V and HgCdTe-based unipolar barrier photodetectors were fabricated. Still, these possess several issues, such as complicated synthesis, lattice mismatch, and extensive surface interface defects that limits the photodetectors performance.^[135]

Generally, 2D materials-based photodetectors work in photoconductive or photovoltaic mode. In photoconductive mode, high R can be achieved but photodetector suffers from slow photoresponse or large current. In photovoltaic mode, the selection of materials is difficult due to controlled doping limitations for 2D materials.^[136] 2D materials with layer-dependent bandgap are desirable to develop the unipolar structure photodetectors owing to their unusual features such as 2D heterostructures can be used without proper lattice mismatch, 2D materials have naturally passivated surfaces which can reduce the leakage current, and 2D structures can be assembled randomly due to absence of dangling bonds.

In the case of photodetectors with unipolar structures, there is no limitation for doping in the 2D heterostructure. Moreover, dark current can be suppressed by the designed barrier, and

photocurrent flow is not disturbed. Furthermore, careful engineering of band structure increases the band offsets in which conduction or valance band blocks the majority carriers; zero offset constructs the other side so that charge carriers in the band can move uninterruptedly. Researchers have fabricated unipolar barrier photodetectors comprising of WS₂/h-BN/PdSe₂ materials. In this work, WS₂ works as VIS wavelength n-type photon, h-BN behaves as a barrier, and PdSe₂ acts as a contact layer. The thickness of WS₂, h-BN, and PdSe₂ films is determined to be 56, 14, and 160 nm, respectively. As fabricated unipolar photodetectors suppress the current and exhibit low dark current as 15×10^{-12} A, D* as 2.5×10^{12} cm Hz^{1/2}W⁻¹), photocurrent as 20×10^{-6} A and photoresponse speed as 74 μs/26 μs for wavelength 520 nm.^[137]

5.3. Group-10 TMDCs/Si Heterostructures

2D semiconductor materials combined with 3D semiconductor materials offer a unique structure to develop the next-generation broadband photodetectors. 2D/3D heterostructures have great advantages such as enhanced light absorption, easy fabrication process, rapid transportation of charge, and a strong built-in potential that can suppress the dark current and thus enhance the D* and shorten the photoresponse. Researchers have also developed two parallel photodetectors based on two parallel PtSe₂/thin Si Schottky junctions that can respond in photodetection range from UV to NIR, as shown in Figure 11e. The parallel photodetectors deliver distinguishable spectral responses from 265 to 1050 nm under different incident intensities. The relationship between photocurrent and incident wavelength reveals that the device's working mechanism is based on a typical bijection function. Furthermore, TCAD simulation suggests that the mechanism of photodetectors depends on the photo-absorption rate and thickness of the Si wafer. Moreover, the device shows an average absolute error of <4.05 nm and an average relative error of <0.56% compared with reports published earlier. The findings reveal that the proposed unique structure may offer promising applications in sensing devices and systems.^[138]

To enhance the working spectral range and optical characteristics of photodetectors, heterostructures based on 2D/Si have emerged rapidly during the last decade. A report shows the fabrication of a broadband photodetector based on heterostructures of PdSe₂ (2D)/Si (3D). In this approach, charge carriers at the surface of junction separates rapidly due to built-in potential and reduce the Schottky barrier. In this scheme, an ionic liquid is introduced on the junction of heterojunction to enhance its electronic and optical properties. From this distinctive structure, the maximum rectification ratio (I_f/I_r) is achieved as 1×10^5 with the lowest ideality factor of 1.22 for different temperatures from 60 to 300 K. Moreover, two unique phenomena, Zener tunneling, and avalanche breakdown, are observed at the interface of heterojunction. Thus, these device shows photovoltaic behavior along with open circuit voltage (V_{oc}) as 0.6 V, notable optical characteristics such as broadband spectrum response from 400 (VIS) to 1200 nm (NIR) along quick response speed up to 9.2 μ s/17.3 μ s at 600 nm. These results demonstrate that as fabricated device provides a roadmap to develop numerous photoelectronic devices such as broadband photodetectors, solar cells, and LEDs.^[139]

Group-10 TMDCs/Si heterostructures can easily be assembled by transferring the Group-10 TMDCs materials directly on the Si surface. Conventional Si/p-n and Si/p-i-n are difficult to fabricate due to the involvement of several steps, ion diffusion at high-temperature leading to a higher device cost. It leads to a bottleneck in developing next-generation optoelectronic devices.^[5] PtTe₂ from group-10 TMDCs is a valuable material choice for various optoelectronic devices owing to its type-II Dirac-fermions. It is a material compatible with present semiconductor technology and silicon-based integrated photonics.^[140] Considering the excellent features of the noble material PtTe₂, researchers fabricated the photodetector based on PtTe₂/Si nano pillar arrays that are based on the PVE mechanism, as shown in Figure 11f. The PVE mechanism can suppress the reflection of incident light and enhance the illumination surface area of the device. The fabricated device depicts outstanding optical characteristics such as R as 0.71 AW⁻¹, D* as 2.81×10^{11} Jones, and EQE as 89.9 % for wavelength 980 nm.

Moreover, the device shows fast photoresponse (6.21 μs /26.3 μs) owing to the photoelectric conversion mechanism and its environmental stability for three months in ambient conditions. Considering these excellent features of PtTe₂/Si-nano pillar arrays, effective strategies can be introduced to achieve low-cost and facile fabrication of optoelectronic devices.^[141] Literature shows a facile, controllable, and large-scale synthesis of PtTe₂ thin films through CVD. The thickness of films ranges from 4.81 to 96.7 nm. In this process, tellurization temperature and carrier gas greatly impact the morphology and chemical crystal purity of the PtTe₂ films. The fabricated photodetector based on assembled vdWs heterostructures of PtTe₂ and Si exhibits broadband spectral response from 200 to 1650 nm and significant optical features including R as 0.406 AW⁻¹, D* as 3.62 $\times 10^{12}$ Jones and EQE as 32.1 % for wavelength 980 nm. Moreover, the as-fabricated device shows fast photoresponse (7.51 μs /36.7 μs) due to quick carrier recombination at PtTe₂/Si heterostructure interface.^[142]

Researchers synthesized multilayers of PtTe₂ at a large scale via vdWs epitaxial growth by simple tellurium vapor transformation technique. In this contribution, they obtain the high-quality of PtTe₂ layers that consist of a mosaic-like crystal structure and possess a very low rate of intrinsic defects. Using the characteristics of PtTe₂, they constructed a vertical type of Schottky junction photodetector based on the heterostructure PtTe₂ (2D)/Si (3D). In this structure, the bilayer of graphene and In-Ga alloy were also utilized as an effective carrier transporter and ohmic contact with the Si substrate, as shown in Figure 11g. The as-fabricated heterojunction shows broadband spectrum response up to MIR (10.6 μm) spectrum and attains a maximum R (5 mAW⁻¹) and D* (6.92 $\times 10^9$ Jones) at a wavelength of 3040 nm as depicted in Figure 11h. Moreover, the devices show a relatively fast photoresponse (2.4 μs /32 μs), which is attributed to the largely built-in potential at the PtTe₂/Si heterostructure. However, the photoresponse of the device can be further increased by improving the crystal quality of the PtTe₂, minimizing the device structure, and reducing the Si substrates.^[143] A report shows that the IR photodetector based on PtTe₂ flakes can be fabricated by directly synthesizing few-layer

flakes on a Si substrate. The as-fabricated device shows a broadband spectral response ranging from 1000 to 7000 nm. It can be attributed to Schottky junction characteristics, which suppress the carrier recombination and enhance the optical absorbance between the PtTe₂ and Si. Furthermore, 2D PtTe₂ can be used to fabricate flexible photodetectors. In this scheme, few-layer flakes of PtTe₂ are grown on a 50 μm Si wafer (supported on a plastic substrate). The flexible device responds to the illumination of different intensities of light, and illumination intensity depends on photocurrent. After 1000 strain cycles, about 20 to 27% reduction in photocurrent occurs, indicating the device's excellent mechanical flexibility and reliability.^[144] Usually, TMDC based electronic and optoelectronic devices suffer from contact problems as these are scaled down to a few nanometers. It may lead to low carrier mobility and poor photoresponse for longer wavelengths. Therefore, suitable strategies to increase carrier mobility and photoresponse in electronic/optical devices are strongly desired. For instance, a metal-semiconductor homojunction is an effective approach to tackling electrical contact issues. This approach can enhance the device's carrier mobility and optical absorption efficiency. However, it does not apply to all TMDCs and various 2D materials for several reasons, including the difference in structures, plasma treatment involvement, and multiple transfer steps.^[97, 145] Recently, a controllable process was reported for the deposition of PtTe₂ thin films through laser irradiation of Te. The films were used to develop a metal-semiconductor heterostructure for tunneling the 2D Te semiconductor with PtTe₂ contacts. Due to PtTe₂ contacts, 2D Te changes from p-type to metallic nature, increasing conductivity up to 500 times. Furthermore, the fabricated photodetector showed the R up to $5.8 \times 10^4 \text{ AW}^{-1}$ and $D^* 5.31 \times 10^{11} \text{ Jones}$ for wavelength 520 nm. The approach can also be applied for direct patterning of PtTe₂ on stretchable and flexible substrates, which can be beneficial for multidirectional applications in electronics, ferroelectrics and optics.^[146]

We can conclude that **group-10 TMDCs**, including their heterostructures, are most favorable for wider bandwidth, high performance, and next generations photodetectors. Furthermore, a

list of broadband photodetectors based on **group-10 TMDCs** and their heterostructures, with their notable performance parameters (R, D*, and Response time), are summarized in **Table 2**.

Group-10 TMDCs and their heterostructures-based photodetectors show relatively better performance than the conventional 2D layered materials and their heterostructures. i.e., fast photoresponse and decent R at the same time. **Figure 12** shows the graph - R Vs. response time for different technologies. This study suggests that **group-10 TMDCs** and their heterostructure are ideal for fabricating photodetectors in which broadband, fast photoresponse, and high R are needed. In addition, **group-10 TMDCs** carry unique photoelectrical properties such as tunable layer-dependent bandgap that leads to a new roadmap for the realization of high-performance and ultra-broadband photodetectors, especially for UV to THz spectrum at room temperature simultaneously high R and rapid photoresponse.

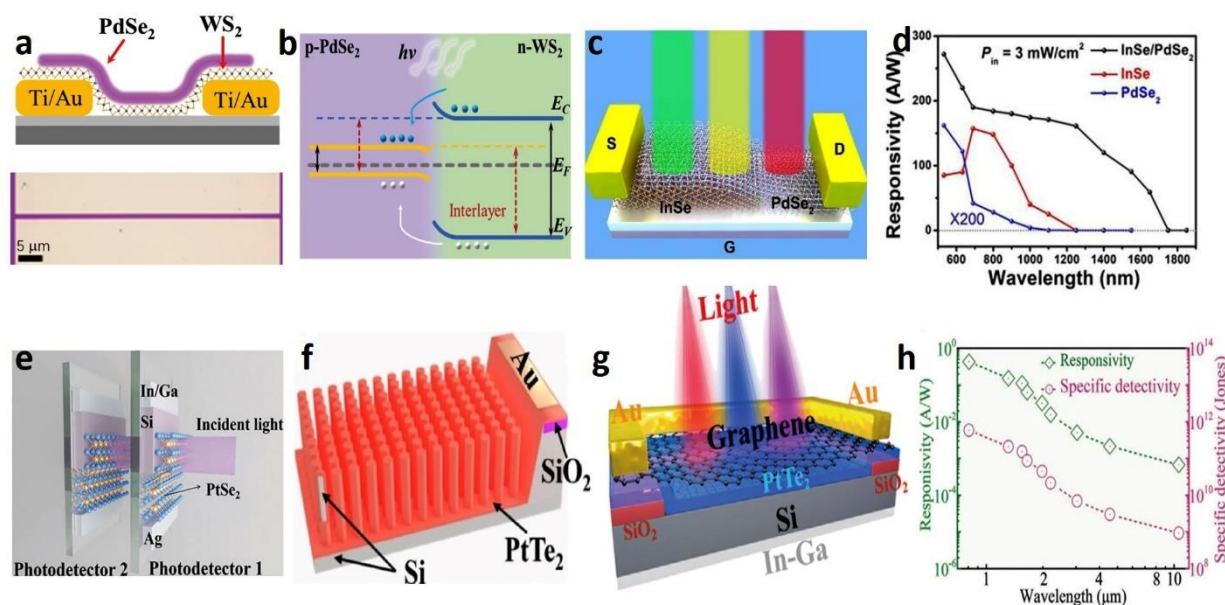


Figure 11. (a) Schematic diagram of WS₂/PdSe₂ heterostructure and optical image of top view of the device. (b) Energy band-diagram for the fabricated device. (a, b) Reprinted with permission from Ref.^[134]. Copyright 2021 Wiley-VCH. (c, d) Schematic diagram of InSe/PdSe₂ based heterostructure device. (d) Photoresponsivity of InSe/PdSe₂ that is comparable of bare InSe and PdSe₂ at V_{ds} = 1 V, P_{in} = 3 mW cm⁻². (c, d) Reprinted with the permission from Ref.^[125]. Copyright 2021 Wiley-VCH. (e) Schematic illustration of two parallel PtSe₂/Si heterojunction-

based wavelength sensors. Reprinted with permission from Ref.^[138]. Copyright 2021 Royal Society of Chemistry. (f) Schematic depiction of PtTe₂/Si-nano-pillar array heterostructure based broadband photodetector. Reprinted with the permission from Ref.^[141]. Copyright 2021 Elsevier. (g, h) Schematic diagram of vertical type of PtTe₂/Si Schottky junction photodetector and photoresponsivity and detectivity V_s/Wavelength of PtTe₂/Si Schottky junction photodetector. Reprinted with the permission from Ref.^[143]. Copyright 2020 Wiley-VCH

Table 2. List of broadband photodetectors based on **group-10 TMDCs** with their materials/device structures and performance characteristics.

Materials/ Device Structure	Wavelength Spectrum Range (nm)	Maximum R (A/W)	Maximum D* (Jones)	Rise/Fall (ms)	References
PtSe ₂ /GaAs	200-1200	0.262	10 ¹²	0.005/0.006	[147]
PtSe ₂ /CdTe	200-2000	0.506	4.2 × 10 ¹¹	0.0081/0.0436	[148]
PtSe ₂ /Ge`	1550	0.766	1.1 × 10 ¹¹	0.0549/0.0566	[149]
PtSe ₂ /Si nitride	1550	0.012	-	-	[150]
PtSe ₂ /SiNWA	200-1550	12.65	10 ¹³	0.010/0.019	[151]
PtSe ₂ /Si	808-1550	0.520	3.26 × 10 ¹³	0.013/0.020	[152]
PtSe ₂ /Si	White light	0.490	-	-	[153]
PtSe ₂ /n-GaN	265	193	3.8 × 10 ¹⁴	-	[154]
PtSe ₂ /SiO ₂	1550	0.00019	-	-	[155]
PtS ₂ /PtSe ₂	405-2200	0.188	-	66/75	[156]
PdSe ₂ /Pyramid Si	980-1650	0.456	9.97 × 10 ¹³	-	[157]
BP/PdSe ₂	532-1310	9.6 × 10 ⁵	5.8 × 10 ¹³	-	[158]
GeSe/PdSe ₂	532	1 × 10 ³	-	0.002/0.0045	[159]
PdSe ₂ /FA _{1-x} Cs _x PbI ₃	200-1550	0.313	10 ¹³	0.0035/0.004	[130]
PdSe ₂ /Ge nanococones	1350-2200	0.530	1.45 × 10 ¹¹	0.025/0.038	[160]
PdSe ₂ /Si	200-3044	0.3	10 ¹³	0.038/0.044	[94]
Gr/PdSe ₂ /Ge	200-3044	0.691	1.73 × 10 ¹³	0.0064/0.0925	[161]

PtTe ₂ /Si	625	0.213	10 ¹³	0.001	[162]
PdSe ₂ /MoS ₂	532	600	10 ¹¹	100/37	[163]
PdSe ₂ /Si	1260-1565	1.19	-	-	[164]
PtTe ₂ /Graphene	405-1850	-	4.53 × 10 ¹⁰	44/55	[165]

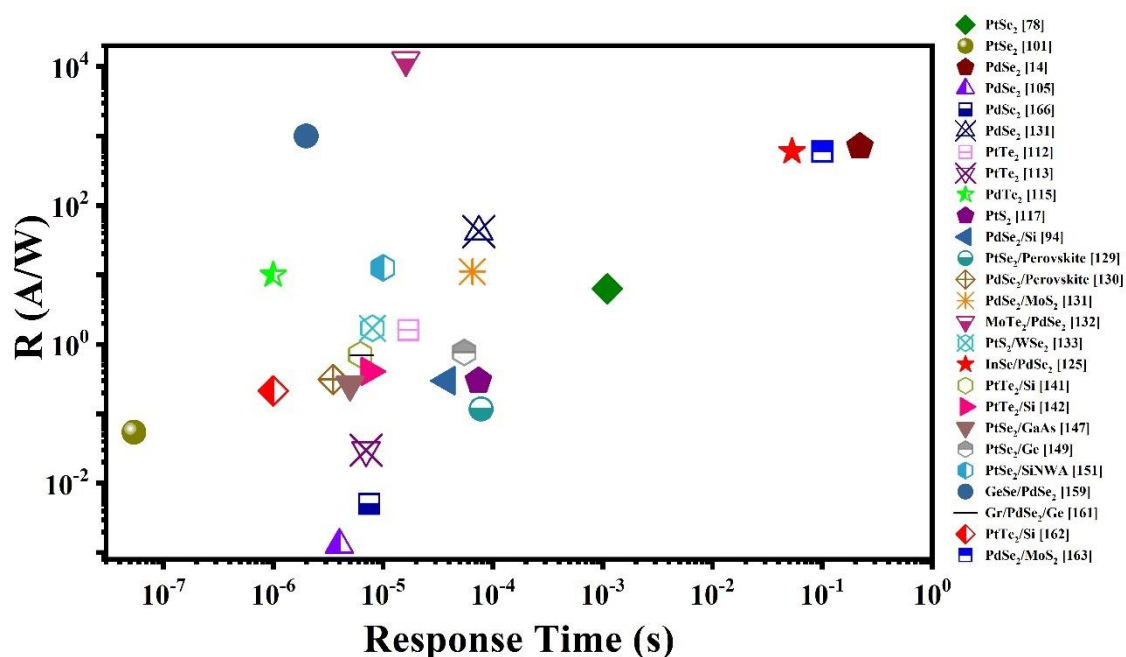


Figure 12. Comparison of R and response time of group-10 TMDCs including heterostructures based photodetectors.

6. Applications

Some of the most worthy and influential applications of photodetectors that have changed this world and human lives are briefly discussed here.

6.1. Solar Cells

A solar cell is an advanced optoelectronic device that converts sunlight into electricity. It is pollution free, pretty reliable, and shows very low photoelectric conversion efficiency. TMDCs combined with heterostructures offer two types of donors and acceptors and promise to exhibit excellent photovoltaic characteristics to develop advanced solar cells. For realizing high-performance solar cells, it is essential to have donor semiconductor materials with a bandgap

in between 1.2 to 1.6 eV, high carrier mobility, environmental stability, and a good absorption rate. Early reports reveal that 2D heterostructures such as graphene/MoS₂ and phosphorene/MoS₂ efficiently develop high-performance solar cells owing to their type-II band alignment, vdWs interaction, and strong interlayer transition.^[80a, 166]

Newly discovered tungsten telluride (WTe₂) is a member of group VIB TMDCs, having outstanding features such as the smallest bandgap (1.3 eV) and higher carrier mobility and conductivity, a potential candidate to fabricate future optoelectronic devices. Extensive reports have evidenced that the **group-10 TMDCs** possess layer-dependent narrow bandgap with excellent electronic and optoelectronics properties and enhanced environmental stability. These features motivated the researchers to develop solar cells based on WTe₂/PtXY, where X and Y are S and Se, respectively. The first principal calculations showed that the proposed structure consists of type-II band alignment, which is responsible for higher electron mobility, good air stability, and high optical absorption. It is revealed that the heterostructures such as WTe₂/PtSe₂ and WTe₂/SePtS can enhance the photoelectric conversion efficiency up to 21.43 and 19.86%, respectively. Furthermore, it is found that the solar cells based on the WTe₂/PtS₂ with ohmic contacts show the lowest power consumption and higher photoelectric performance.^[167]

Direct solar-to-hydrogen production is known as a photoelectrochemical conversion that has shown great interest in the field of renewable energy technology. Conventional materials like Si have the potential to convert direct solar energy into hydrogen owing to their suitable bandgaps (like 1.1 eV for Si) for this process. Single Si surface has relatively low-rate efficiency for hydrogen evolution reaction; therefore, such materials are highly desired that can act as a catalyst and rapidly increase the charge transfer efficiencies. Atomically thin 2D materials are realized as a potential candidate for solar-driven hydrogen evolution reactions on Si photocathodes. Numerous reports have been published in this regard. MoS₂/Si heterostructure presents the photoelectrochemical conversion for hydrogen production in which overpotential

at a solid electrolyte interface can be addressed. The thin layer of MoS₂ as a catalyst is beneficial for hydrogen evolution reaction. **Group-10 TMDCs** have superiority in electrolytic activity for hydrogen evolution reaction over group-6 TMDCs MoS₂.^[168] A group of researchers has developed PtSe₂/Si heterojunction with a suitable scheme to produce photoelectrochemical conversion for a direct solar-to-hydrogen generation. It is revealed that by managing the number of PtSe₂ layers, interfacial band alignment of heterojunction can be tuned. It is observed that three-layer (2.2 nm) thick PtSe₂ on Si delivers the best performance to generate hydrogen production at a very low intensity (-34.4 mAcm⁻²). This technique successfully develops renewable energy technology for direct solar-to-hydrogen production.^[169]

6.2. Image Sensing

An efficient photodetector can record a high-resolution image. It is a very important feature to address image-based sensing applications, including a surveillance camera that can measure the temperature. Image sensing is an important field in optoelectronic devices widely employed in various applications such as high-resolution cameras, fire determination, fax machines, and missile warning systems.^[170] Extensive reports have been published in the literature to investigate image sensing applications based on 2D materials.^[171] PtTe₂/Si-nano-pillar array heterostructure is an effective approach to constructing the homemade imaging system. The fabricated device shows excellent detection capability for wavelength 980 nm. This work uses a hollow character-based template to pattern the light. PtTe₂/Si-nano-pillar array heterostructure-based photodetector is kept onto the home-based stage with varying orbits along X and Y directions. Image system exhibits higher sensitivity and can differentiate among different wavelengths of light.^[141] Another report shows the development of a broadband photodetector based on PtSe₂/Si heterojunction that can be used for IR image sensing applications. This work presents a unique strategy to determine the imaging capability of the photodetector. A setup of a 4×4 devices array is established to evaluate their potential applications in integrated light detection systems, as shown in **Figure 13a**. It is revealed that

for wavelengths 1310, 1550, 2200, 3044 and 4550 nm, the device can be operated efficiently, and photocurrent is recorded in both light mode and dark mode from the pixel under the exposed area and under the shaded area, respectively. These findings reveal that PtSe₂/Si have great potential for broadband spectral image sensing applications.^[143] Literature shows the demonstration of PtSe₂/Ge-based photodetector that can be employed as a SWIR image sensing. In this mechanism, SWIR laser (1550 nm) incorporated with a photodetector is fixed along the stepper motor. A shadow mask with a diode pattern is placed between the stepper motor and the photodetector. As the light falls within the hollow regime of the mask, it shines the photodetector array. To efficiently record the pixel quality of the image and measurements of current values, 10 units of the device are employed, and the stepper motor is moved from its place as per desire. The procedure is sketched in Figure 13b. The results reveal the excellent image quality and evidence of the suitability of PtSe₂/Ge for the diversity of image sensing applications.^[149]

PdSe₂-based photodetector can be employed in the image-based application at THz wavelength demonstrated by Zhang's group. In this mechanism, a source of 0.24 THz was selected and fixed on the detector by an off-parabolic mirror. They choose the word "THz" and a half-filled water bottle as a target for image detection. After scanning, a 100 × 100-pixel image is attained in which each pixel has 20 ms integration time. High-resolution images of the words "THz" and the half-filled water bottle can be visualized by the bare eye (Figure 13c). Remarkably, the shape of the tube and the area of the water and air can be determined by the image detector, as depicted in Figure 13d. These outstanding results reveal that PdSe₂-based photodetector has promising applications in image detection.^[172] Broadband photodetector based on Gr/PdSe₂/Ge heterostructure can be used as an infrared image sensor. In this mechanism, a metal mask with the open letter "P" is kept between the polarizer and the device controlled by a 2D motorized stage. This system can record the voltage and current in real time through the movement of the mask. The recorded data is then used for image mapping. It also exhibits the polarized light-

dependent image for wavelength 780 nm with polarization angles 0 and 90°. It shows the excellent resolution image of the letter “P” at high contrast voltage ratio of 3.25×10^3 (angle 0°) and a small contrast voltage ratio of 2.9×10^2 (angle 90°). These results reveal that the as-fabricated device has great potential to develop infrared imaging devices.^[161] Researchers have shown that PdSe₂/Pyramid Si-based heterojunction can also be used as an infrared image sensor. In this report, the images of a house and trees are recorded using infrared wavelengths (980 nm, 1300 nm) by shining the mask with a light source. Each device is controlled by an automatic displacement platform that can sense the images in this mechanism. The heterojunction device collects each pixel's current by scanning the image and then drawing the images using current mapping software.^[157]

The PtTe₂-based photodetector can also be used as an image sensor. It can be integrated into SiO₂/Si substrate through lithography, as shown in Figure 13e-I. The as-fabricated device consists of an 8×8 array. The typical size of the device is 200×200 μm², which can be integrated onto the printed circuit board. As depicted in Figure 13e-II, the image sensing setup can draw the letter “N” when placed between the NIR-LED (light-emitting diode) and PtTe₂-based photodetector array. In this image-sensing process, LED light of wavelength 980 nm passes through the mask to directly project each word on the PtTe₂-based NIR photodetector array at 64 pixels.^[142] PdTe₂ is an ideal candidate to develop terahertz optical devices owing to its anisotropic characteristics and strong photogalvonic effect in the terahertz band. Researchers have fabricated and demonstrated PdTe₂ based terahertz optoelectronic device that works from 0.04 to 0.3 THz. The device can further be integrated with other optoelectronic devices to offer various applications, including photo-sensing, polarization, imaging and stretchable optoelectronic devices.^[170b]

Furthermore, the device can be employed as high-resolution terahertz transmission imaging owing to its excellent stability, fast response (1 μs), and broadband working spectrum. High contrast image of fresh leaf obtained using the device at 0.12 THz is shown in the inset of Figure

13f. The results certify that the device may offer potential applications in image processing devices.^[115]

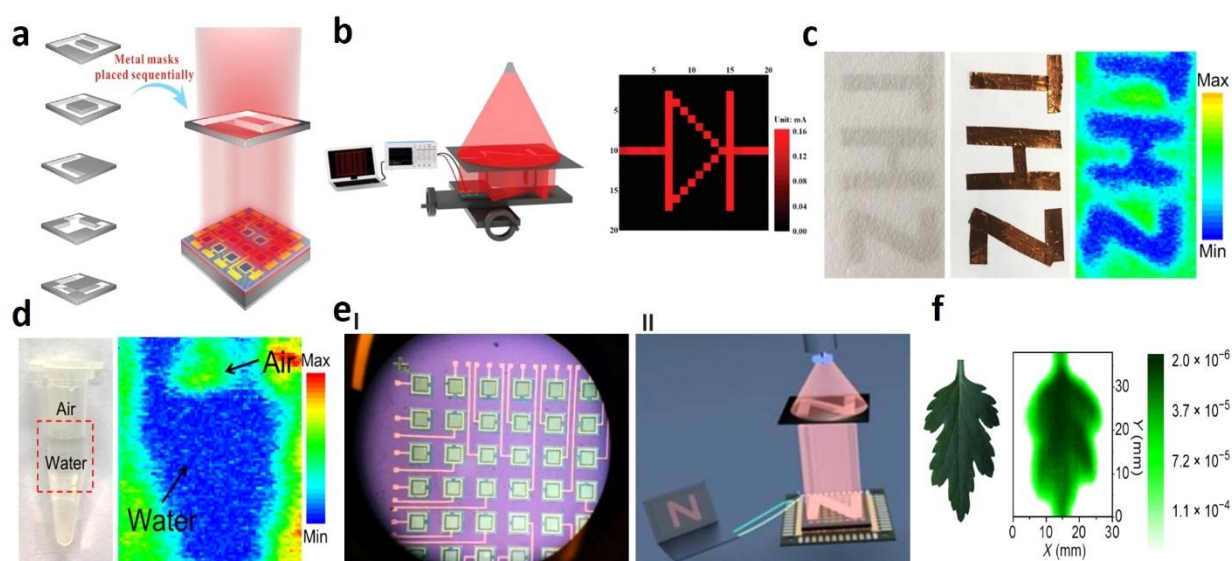


Figure 13. (a) Experimental setup for device to record IR light image sensing. Reprinted with permission from Ref.^[143]. Copyright 2020 Wiley-VCH. (b) Experimental setup for SWIR image sensing and results for 2D current map which exhibits the ability for recording the image quality of diode symbol. Reprinted with permission from Ref.^[149]. Copyright 2021 Royal Society of Chemistry. (c, d) Optical image of the copper letters “THZ” inside an envelope and high-resolution image of half water filled tube and corresponding high-resolution image respectively. Reprinted with the permission from Ref.^[172]. Copyright 2021 American Chemical Society. (e) Digital photograph of PtTe₂ based photodetector array (I), working mechanism of PtTe₂ based image sensor (II). Reprinted with permission from Ref.^[142]. Copyright 2020 American Chemical Society. (f) Schematic diagram of electrical measurement system for PdTe₂ based photodetector; inset shows the terahertz imaging of fresh leaf. Reprinted with permission from Ref.^[115]. Copyright 2020 American Association for the Advancement of Science.

6.3. Electronics

2D layered materials are ideal candidates for developing advanced semiconducting devices owing to their amazing electronic characteristics, tunable bandgap, ultra-thin nature, higher

carrier mobility, and large ON/OFF ratio.^[173] Electronic characteristics of the semiconductor electronic devices can be tuned or enhanced through modification of several factors, including structural phase transition, application of high pressure, strain engineering, and contact engineering.^[174] For instance, field effect transistors (FETs) mainly depend on controllable switching of semiconductor channel conductance investigated by charge carrier mobility and ON/OFF ratio. FET is a basic building block and main pillar in developing the next generation of electronic devices for various applications, including communication devices and high-performance switching in digital electronics. In 2D materials, MoS₂-based FET is the most extensively studied material. It usually shows one order less mobility than the theoretically calculated one ($400 \text{ cm}^2\text{V}^{-1}\text{s}^{-1}$). To get desired mobility, interfacial engineering or contact engineering are the two best options, as suggested by the reports.^[175] Group-10 TMDCs have emerged as potential candidates to gain the desired mobility, ON/OFF ratio, and stability due to their fruitful characteristics such as layer dependent on bandgap, unique structural geometry, and strong interlayer interaction. These distinct characteristics make them superior to BP and other TMDCs for the assembly of electronic devices. A report shows the fabrication of few layer (8 nm thick) PtSe₂ FET based photodetector. In demonstration, the device showed that its performance is layer (of PtSe₂) dependent rather than external effects such as pressure, strain and lithiation. It is revealed that as fabricated device shows excellent carrier mobility ($210 \text{ cm}^2\text{V}^{-1}\text{s}^{-1}$) and ON/OFF ratio (10^3) at room temperature, as depicts in Figure 14a. As demonstrated FET based photodetector exhibits photoresponse upto NIR (980 nm) with outstanding R (10 mAW^{-1}) as depicts in Figure 14b. They claimed that as fabricated device shows excellent stability as well as R which is compararvle BP based FET.^[176] These marvellous properties of PtSe₂ can have potential applications in semiconducting devices.^[116a]

TMDCs are considered an ideal candidate for developing advanced ultra-thin FETs. The ultra-thinness of TMDCs can be beneficial for extreme transistor scaling via migration of short channel effect and can further decrease the Moor's limit. Moreover, contact resistance is the

bottleneck that limits the advantages of TMDCs-based FETs. Various techniques such as the formation of Schottky barrier height, contact engineering, and Schottky Mott rule have been reported to reduce the contact resistance and boost the devices' performance. vdWs gaps in the surface of TMDCs are the main reason for the increased contact resistance. Therefore, the reduction of contact resistance and increase in the quality of metal contacts in semiconductor devices are still key challenges. One strategy is selective doping of the source and the drain contact used in a FET. However, this is not very suitable due to the ultra-thin nature of TMDCs. Moreover, conventional doping is not fully functional, and charge transfer at the interface suffers from stability issues. In the second strategy, introducing defects into the TMDCs can boost the performance of the semiconducting devices and efficiently transit the semiconductor material into a metallic state. In the third strategy, phase engineering can be employed. 2H-phase can be transferred into 1T or 1T' or vice versa. However, this technique also faces stability issues and requires high temperatures.^[177] To avoid aforesaid problems, researchers fabricated high performance all PtSe₂ based FET. In this scheme, FET consisted of few layer PtSe₂. However, in which source/drain region, it was multilayer PtSe₂. During fabrication, semiconductor PtSe₂ is transformed into metal PtSe₂ at junction due to its thickness depended on bandgap. Ultra-thin FET based on PtSe₂ along with PtSe₂ vdWs contacts, shows excellent carrier mobility ($7.5 \text{ cm}^2\text{V}^{-1}\text{s}^{-1}$), high ON/OFF ratio (10^5) and lower contact resistance as compared to conventional Ti/Au contacts in FETs. It is revealed that the demonstrated scheme can be applicable to others 2D materials in order to overcome the contact resistance issues in electronic devices.^[178] In addition, recent study shows that PtSe₂ based phototransistor demonstrated ambipolar properties that is tuned by the gate voltage as shown in Figure 14c. As fabricated device shows excellent mobility of electrons ($1496.7 \text{ cm}^2 \text{V}^{-1}\text{s}^{-1}$) and holes ($1410 \text{ cm}^2 \text{V}^{-1}\text{s}^{-1}$) at $V_{ds} = 0.16 \text{ V}$. Furthermore, as demonstrated device shows broaden spectrum response ranging 405 nm to 808 nm with R (0.086 AW^{-1}) and D^* (10^8 Jones) at wavelength of 808 nm.^[179] Research literature on group-10 TMDCs indicates that, emerging 2D PtSe₂ has great

potential to construct the next generation electronic devices. A report on phototransistor based on few layers (5-16 nm) thick PtS₂ on Al₂O₃/Si substrate as shown in Figure 14d. In this contribution, highest mobility of 62.5 cm²V⁻¹ s⁻¹ and ON/OFF ratio of 10⁶ are achieved at room temperature as depicts in Figure 14e. In addition, as fabricated phototransistor shows broaden spectrum response from VIS to NIR as well as decent photoresponse such as 175 μs at wavelength of 830 nm.^[117]

Surprisingly, 2D materials-based junction field-effect transistors (JFET) gained tremendous attraction owing to their excellent electronic properties, for example, near ideal subthreshold swing (SS) that is beneficial tuning of the photodetection performance at small voltage, high carrier mobility that has a function to transports carrier generation resulting to high R and photoresponse speed. Owing to these advantages, JFET based on 2D materials has attracted great interest in developing high-performance optoelectronic devices. Recently, X. Zhou group fabricated the JFET based on PdSe₂/MoS₂ vdWs heterostructures in which PdSe₂ act as a gate and MoS₂ realize as a channel, as shown in Figure 14f. The device shows excellent electrical characteristics such as decent carrier mobility 213 cm²V⁻¹ s⁻¹ and near SS value, i.e., 150 mVdec⁻¹, which is much higher than the conventional MoS₂ MOSFET. This small value of SS results from the large capacitance due to the dielectric layer's absence. The back gate voltage can effectively modulate the JFET's carrier mobility. By applying a back gate voltage, the mobility can be tuned from 1 to 213 cm²V⁻¹ s⁻¹ as shown in Figure 14g. It can be attributed to the variation of the series resistance of the MoS₂ channel by the back gate. In this mechanism, the channel of the device was not covered by the PdSe₂ layer, which acts as the top gate layer causing a large series resistance and reducing the carrier mobility in the channel. While applying SiO₂ back gate voltage, the conductance of the channel enhanced and thus increased the n-type polarity carrier transport and the charge carrier mobility. In this way, the charge carrier mobility of the PdSe₂/MoS₂ device can be tunable and have significant advantages over the traditional MOSFET. They claimed that owing to JFET characteristics, as fabricated device shows

outstanding optical properties such as R (600 AW^{-1}) D^* (10^{11} Jones) and reasonable photoresponse (100 ms) at wavelength of 532 nm as shown in Figure 14h.^[163]

Group-10 TMDCs not only beneficial for developing the phototransistor but also have shown interest for constructing the next generation electronic devices such as memristor.

A memristor is an electronic device with numerous applications in the fabrication of next-generation digital memory, biological devices, neuromorphic computing, and logic circuits owing to their beneficial properties, such as non-volatility and fast switching. The basic function of the memristor involves the filamentary switching behavior in which operating voltage and resistance states show unwanted variations due to random formation and rupture of conductive filaments. Numerous attempts have been made to boost the performance of memristors based on TMDCs, including confining the formation of filaments by adding thin layers, introducing defects, and engineering graphene nanopores. However, memristors based on TMDCs still require further modifications to offer flexibility and integration density.^[180] Researchers have fabricated PdSe₂ based memristor, as shown in Figure 14i. This memristor has a unique switching behavior driven by hetero-phase grain boundaries. The local phase transition phenomenon is observed in PdSe₂-based memristor owing to the electron beam irradiation that induces the hetero-phase grain boundaries without producing interface states or traps. Such behavior enables vital interchangeable total/quasi-rest phenomena in the device, which is absent in typical TMDCs-based memristors. Compared to TMDC-based memristors, the fabricated device shows high switching uniformity under quasi-reset mode along with a decrease in voltage, longer retention, and re-generatable resistive switching. Moreover, at low voltage (0.6 V), the device can achieve a 6-fold improvement in switching uniformity. This unique phenomenon is mainly attributed to residual filaments and grain boundaries that can lead to the construction of conductive filaments. Furthermore, as the fabricated device can imitate both short-term and long-term plasticity, multi-patterning of memristors can be employed via cross-bar array architectures.^[181]

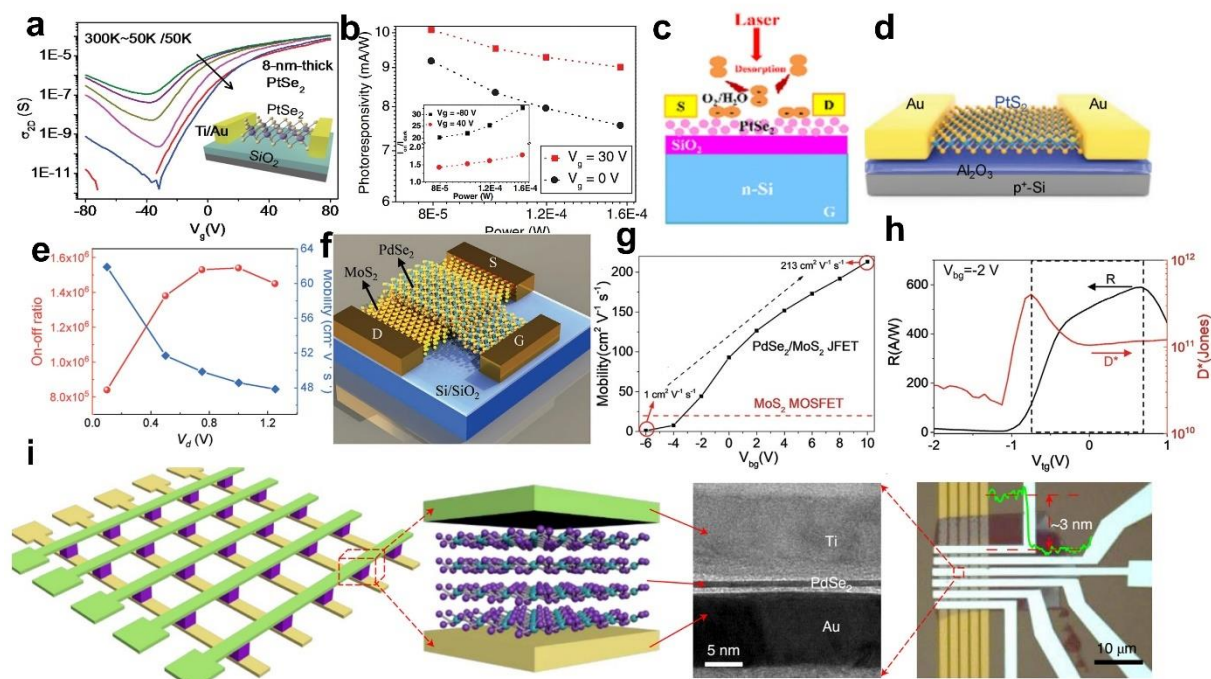


Figure 14. (a) Transfer characteristics of few layer PtSe₂ based phototransistor. Inset shows the schematic diagram of fabricated phototransistor. (b) Depiction of Power/Responsivity of the PtSe₂ based phototransistor. (a, b) Reprinted with permission from Ref.^[116a]. Copyright 2016 Wiley-VCH. (c) Schematic diagram of PtSe₂ based phototransistor with negative and positive conductivity. Reprinted with permission from Ref.^[179]. Copyright 2022 American Chemical Society. (d) Schematic diagram of PtS₂ based phototransistor. (e) Schematic illustration of charge carrier mobility and ON/OFF ratio of PtS₂ based phototransistor. (d, e) Reprinted with permission from Ref.^[117]. Copyright 2020 Wiley-VCH. (f, g) Schematic diagram of JFET device based on PdSe₂/MoS₂ heterostructure and carrier mobility of PdSe₂/MoS₂ with comparison of bare MoS₂ MOSFET. (h) depiction of R and D* under tunable voltage. (f-h) Reprinted with permission from Ref.^[163]. Copyright 2021 Wiley-VCH. (i) Schematic illustration of PdSe₂ based memristor, PdSe₂ based memristor in vertical configuration, TEM image of PdSe₂ based memristor and typical optical image of PdSe₂ based memristor (from left to right). Reprinted with permission from Ref.^[181]. Copyright 2021 Springer Nature.

6.4. Miscellaneous Applications

Photocatalytic water splitting is an effective strategy to produce hydrogen from water. It is a pollution-free renewable energy technology that can help us resolve energy shortages and environmental pollution problems. Numerous semiconductor materials have been employed to produce hydrogen via photocatalytic water splitting. Compared to conventional materials such as bulk counterparts, 2D materials have offered great potential for designing advanced photocatalysts for water-splitting applications owing to their beneficial properties, including higher optical absorption, broadband photoresponse, tunable bandgap, and a large active surface-to-volume ratio.^[182]

For an ideal photocatalyst, the desired material should attain these criteria: it should have a tunable and suitable bandgap for energy harvesting-based applications, ideal band edge energy, and low recombination rate of electrons/holes to achieve the higher photocatalytic efficiency.^[183] Among 2D layered materials, very few materials are suitable for photocatalytic applications due to their strict requirements. DFT calculations reveal that PdSe₂ is a suitable material for energy harvesting based applications owing to its unusual characteristics. Due to the low degree of lattice symmetry and anisotropic behaviour, PdSe₂ has a suitable band edge position, tunable bandgap, and low electrons/holes recombination process. These advantages make it a potential candidate for solar-to-hydrogen (where efficiency up to 12.59% is achieved) and future water-splitting applications.^[184]

Among members of **group-10 TMDCs**, platinum (Pt) is a very stable material due to its catalytic characteristics, considerable corrosion resistance, and biocompatibility. Compared to other TMDCs, Pt-based TMDCs show ambient stability, require low temperatures for the synthesis of materials, and offer layers depending on bandgap, which can lead to its transition from metal to semiconductor. These excellent characteristics of the group-10 TMDCs allow us to develop wearable bio-electronic devices.^[185] **A group of researchers reveals that few layers of PtSe₂ can induce fast photocurrent with outstanding efficiency by the technique of photon drag effect.**

Owing to this technique, anisotropic current observed at the THz spectrum which can be controlled by directly helicity of pump beam. In addition, they proposed a new model named as THz emission by the circular ac Hall effect to determine the charge carrier efficient at the THz spectrum. They claimed that, as proposed technique could be efficient to determine the carrier transport as well as efficient to investigate photon drag current in telecommunication devices.^[186]

A report demonstrates the ultra-thin flakes of Pt-TMDC-based electronic imprints for next-generation wearable electronics. In this contribution, large-scale synthesis of PtSe₂ and PtTe₂ is achieved through CVD at low temperatures (400 °C). The electronic imprints based on PtSe₂ and PtTe₂ are used to monitor various medical anxieties, such as vital physiological signs, the electrical activity of the heart and brain, muscle contractions, eye movements, and body temperature, as shown in **Figure 15a**. It is revealed that both materials (PtSe₂ and PtTe₂) are suitable for these wearable applications. However, PtTe₂ is superior to PtSe₂ and other 2D materials (graphene and TMDCs) due to its metallic structure, four times lower impedance, and 100 times lower sheet resistance.

Moreover, electronic imprints based on the Pt-TMDCs can identify eye movement and direction of individual sight and can be integrated with advanced human-machine interfaces.^[187] Literature shows the investigations on chemical and thermal properties of PdTe₂ through DFT calculations and experiments using state-of-the-art equipment, including high-resolution electron energy loss spectroscopy, XPS, and AFM. The results revealed that Te atoms turn into TeO₂ skin in oxygen and air. The thickness of TeO₂ remains unchanged at sub nanometric scale for one year. Due to its excellent stability, researchers fabricated a millimeter wave receiver, as shown in Figure 15b,c. PdTe₂-based millimeter receiver exhibits electromagnetic radiation with an output power of 30 mW at 40 GHz carrier frequency which can be used for future interconnected communication systems. Moreover, the device shows a high R of 6.4 AW⁻¹, which is the highest value among for other similar devices (it is 21 and 13 times higher than that of graphene and BP, respectively). The device shows excellent air stability for up to one

month, less than 4% degradation, and fast photoresponse, as shown in Figure 15d. These results reveal that a PdTe₂-based device could be an ideal choice for developing engineering devices for promising communications and optoelectronic applications.^[85]

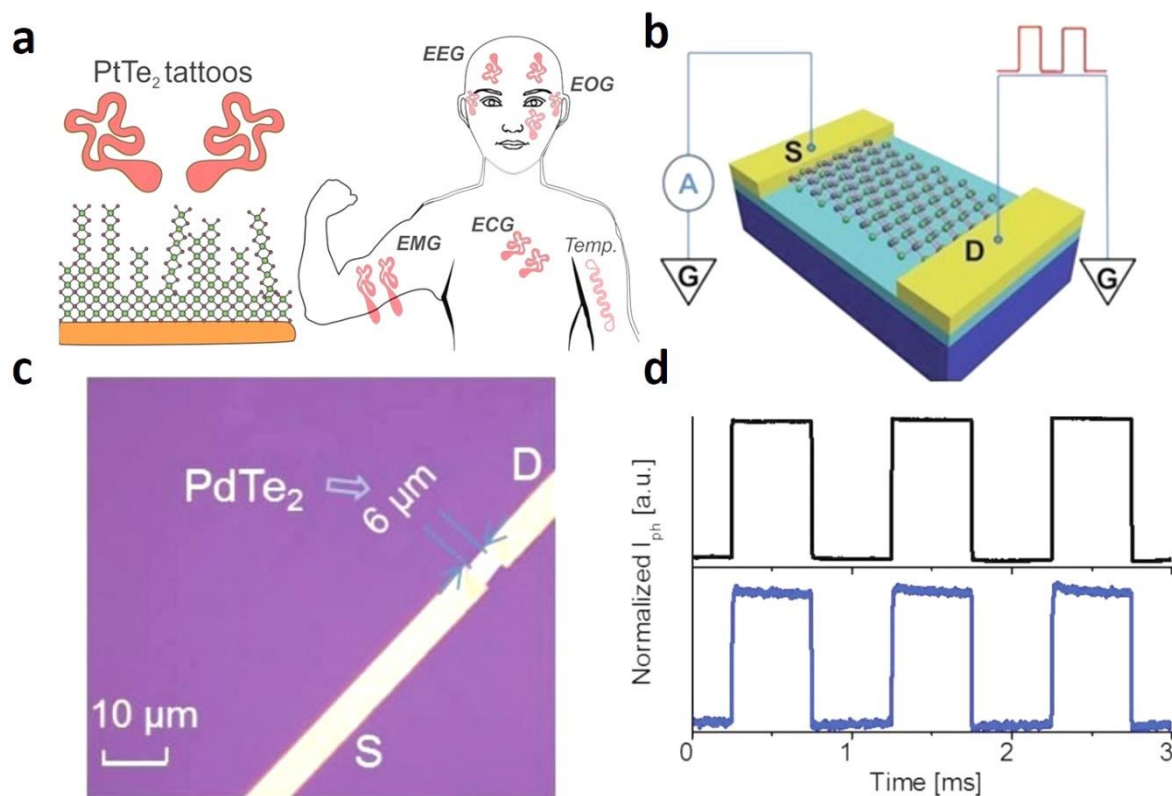


Figure 15. (a) Schematic diagram of PdTe₂ electronic tattoos and their application for monitoring of various physiological human vital signs. Reprinted with permission from Ref. ^[187]. Copyright 2021 American Chemical Society. (b) Schematic diagram and (c) optical image of PdTe₂ based millimeter receiver. (d) Time resolved characteristics of PdTe₂ based millimeter receiver: as prepared (black curve) and after 30 days (blue curve). (b-d) Reprinted with permission from Ref. ^[85]. Copyright 2020 Wiley-VCH.

7. Conclusions and Future Outlook

The emerging **group-10 TMDCs** possess unique electrical, electronic, and optical properties not found in conventional 2D materials, including BP and graphene. **Group-10 TMDCs** exhibit diverse electronic phases such as metallic, semiconducting, and superconducting that depend on the strong layers of bandgaps, making them a promising candidate for next-generation

optoelectronic applications at the nanoscale. Firstly, this review sheds light recent progress on broadband photodetectors based on conventional 2D TMDCs. After that, this review focused entirely on **group-10 TMDCs** in terms of their lattice structure, synthesis techniques, and photodetectors based on their single materials of **group-10 TMDCs** and their heterostructures. Lastly, the recent advances of **group-10 TMDCs** in optoelectronics device applications have been summarized.

Group-10 TMDCs materials have unique electronic structures, anisotropic behavior, and tunable layers dependent on the bandgap and strong interlayer transition in layers, which makes them promising candidates for the fabrication of broadband photodetectors, especially IR photodetectors. Despite its great progress, photodetectors with a broad spectrum still suffer many challenges. The following points should be addressed to enhance the photodetection performance and compete with conventional semiconductor devices.

1. **Continued development of **group-10 TMDCs** family.** The present family of **group-10 TMDCs** is limited and restricted to several binary compounds.^[188] High throughput computing (a theoretical calculation) can predict new members of **group-10 TMDCs** as thousands of 2D materials exist theoretically.^[189] In the future, there is the possibility to discover more members, such as semiconductors, insulators, and topological materials, that could have potential applications in multidisciplinary applications.
2. **Large-area and high-quality synthesis.** Among the synthesis strategies, CVD is the most promising method for preparing large-area of **Group-10 TMDCs** nanoflakes. Although CVD method has been studied for several decades and large-area CVD growth of 2D materials (such as grapheme, h-BN and MoS₂) has been realized, large-area and high-quality CVD growth of **group-10 TMDCs** materials are still challenging mainly because of uncontrollable grain size and lattice defects.
3. **Phase transition engineering.** **Group-10 TMDCs** possess multiple binary phases, rich **electronic phases such as metallic, semiconducting, and superconducting and different**

polymorphism phases (2H, 1T and pyrite) depends on its bandgap variations. The phase transition engineering enables multifaceted control factors and thus can be realize more phases of group-10 TMDCs and thus new groom of research in multiple areas.

4. **Characteristic investigations.** Outstanding properties of group-10 TMDCs such as physical, mechanical, structural, thermodynamics and chemical properties needs to be well explored. New state of art characterizations equipment's should be developed to investigate the inherent characteristics of the group-10 TMDCs. Furthermore, manipulating the properties of the group-10 TMDCs such as defect engineering, interface with substrates and other materials could be effective strategies to enhance their applications in next generation optoelectronic devices.
5. **Light harvesting.** Even though the light absorption of monolayer group-10 TMDCs is considerable, the total light absorption is quite low because of the ultrathin thickness of group-10 TMDCs materials. Optical techniques such as plasmonic structure in the form of Au nanoparticles and microcavities enhance light absorption and thus increase the photoresponse to overcome these drawbacks.
6. **Schottky barrier at contacts.** For an ideal 2D/metal interface reaching the Mott-Schottky limit, the high Schottky barrier can be eliminated using metals with proper work function. However, because of the Fermi-level pinning effect, the Fermi level of the metal is strongly pinned around a certain position inside the band gap of the 2D semiconductor regardless of the intrinsic work functions of the metal, making the Schottky barrier difficult to eliminate. The Schottky barrier suppresses charge carrier injection at the contact, resulting in poor and slow photoresponse. In addition, the Schottky junction at the contact may present photoresponse, which sometimes is even higher than that of the 2D/2D junction, introducing a great interference in studying the latter. Several interface engineering such as electrical contact engineering (asymmetric contacts) strategies have been reported to reduce the Schottky barrier, including vdWs

contact, edge contact, and phase engineering. However, the strategies introduce additional complex fabrication processes, and very few can realize true ohmic contact.

7. **Stability.** Although **group-10 TMDCs** exhibit much higher stability than other TMDCs (such as MoS₂, MoSe₂, and MoTe₂), long-and stable operation under strong light irradiation is still challenging for the materials, especially in ambient conditions. The common solution is encapsulating devices with h-BN or ALD-Al₂O₃, but these strategies may involve additional complex processes or potential doping-effect.
8. **Large-scale and high-quality assembly of vdWs heterostructures.** Numerous 2D/2D vdWs heterostructures have been realized in previous studies, but most were manually stacked via targeted transfer under a microscope, which is low yield. Automatic vertical integration equipment is necessary for industrial fabrication. On the other hand, realizing ideal interfaces without involving polymer, solvent and gas bubbles requires a damage-free, residual-free transfer strategy in a vacuum/inert atmosphere.

In conclusion, numerous attainments of group-10 TMDCs and their heterostructures have the potential to yield the next generation of high-performance broadband photodetectors. Simultaneously, commercial applications of these materials are still facing many challenges, which are highly desired to be tackled in future research. These novel materials are research hotspot for the developments of advanced optoelectronic devices More research should be made in the rational device design, fabrication techniques and device performance.

Acknowledgements

Z. M. Wang acknowledges the National Key Research and Development Program of China (2019YFB 2203400) and the “111 project” (B20030).

Conflict of Interest

The authors declare no conflict of interest.

References

- [1] a) F. Wang, Y. Zhang, Y. Gao, P. Luo, J. Su, W. Han, K. Liu, H. Li, T. Zhai, *Small* **2019**, 15, 1901347; b) M. Long, P. Wang, H. Fang, W. Hu, *Advanced Functional Materials* **2019**, 29, 1803807.
- [2] a) F. Xia, T. Mueller, Y.-m. Lin, A. Valdes-Garcia, P. Avouris, *Nature nanotechnology* **2009**, 4, 839; b) M.-B. Lien, C.-H. Liu, I. Y. Chun, S. Ravishankar, H. Nien, M. Zhou, J. A. Fessler, Z. Zhong, T. B. Norris, *Nature Photonics* **2020**, 14, 143; c) A. Zada, P. Muhammad, W. Ahmad, Z. Hussain, S. Ali, M. Khan, Q. Khan, M. Maqbool, *Advanced Functional Materials* **2020**, 30, 1906744.
- [3] a) F. Yan, Z. Wei, X. Wei, Q. Lv, W. Zhu, K. Wang, *Small Methods* **2018**, 2, 1700349; b) Z. Yang, J. Hao, *Advanced Materials Technologies* **2019**, 4, 1900108; c) L. Pi, L. Li, K. Liu, Q. Zhang, H. Li, T. Zhai, *Advanced Functional Materials* **2019**, 29, 1904932; d) J. Gusakova, X. Wang, L. L. Shiau, A. Krivosheeva, V. Shaposhnikov, V. Borisenko, V. Gusakov, B. K. Tay, *physica status solidi (a)* **2017**, 214, 1700218; e) W. Choi, N. Choudhary, G. H. Han, J. Park, D. Akinwande, Y. H. Lee, *Materials Today* **2017**, 20, 116.
- [4] a) X. Guan, X. Yu, D. Periyanaounder, M. R. Benzigar, J. K. Huang, C. H. Lin, J. Kim, S. Singh, L. Hu, G. Liu, *Advanced Optical Materials* **2021**, 9, 2001708; b) K. Khan, A. K. Tareen, M. Iqbal, L. Wang, C. Ma, Z. Shi, Z. Ye, W. Ahmad, R. U. R. Sagar, S. S. Shams, *Progress in Solid State Chemistry* **2021**, 63, 100326.
- [5] Q. Qiu, Z. Huang, *Advanced Materials* **2021**, 33, 2008126.
- [6] a) R. G. Dickinson, L. Pauling, *Journal of the American Chemical Society* **1923**, 45, 1466; b) J. A. Wilson, A. Yoffe, *Advances in Physics* **1969**, 18, 193; c) R. Frindt, A. Yoffe, *Proceedings of the Royal Society of London. Series A. Mathematical and Physical Sciences* **1963**, 273, 69; d) P. Joensen, R. Frindt, S. R. Morrison, *Materials research bulletin* **1986**, 21, 457.

- [7] A. Weston, Y. Zou, V. Enaldiev, A. Summerfield, N. Clark, V. Zólyomi, A. Graham, C. Yelgel, S. Magorrian, M. Zhou, *Nature Nanotechnology* **2020**, 15, 592.
- [8] a) S. Manzeli, D. Ovchinnikov, D. Pasquier, O. V. Yazyev, A. Kis, *Nature Reviews Materials* **2017**, 2, 1; b) D. Jariwala, V. K. Sangwan, L. J. Lauhon, T. J. Marks, M. C. Hersam, *ACS nano* **2014**, 8, 1102.
- [9] Z. Huang, J. Liu, T. Zhang, Y. Jin, J. Wang, S. Fan, Q. Li, *ACS Applied Materials & Interfaces* **2021**, 13, 22796.
- [10] X. Guo, L. Zhang, J. Chen, X. Zheng, L. Zhang, *Physical Chemistry Chemical Physics* **2021**, 23, 399.
- [11] a) J. Jiang, Y. Wen, H. Wang, L. Yin, R. Cheng, C. Liu, L. Feng, J. He, *Advanced Electronic Materials* **2021**, 2001125; b) W. Gao, S. Zhang, F. Zhang, P. Wen, L. Zhang, Y. Sun, H. Chen, Z. Zheng, M. Yang, D. Luo, *Advanced Electronic Materials* **2021**, 7, 2000964; c) F. Zhong, J. Ye, T. He, L. Zhang, Z. Wang, Q. Li, B. Han, P. Wang, P. Wu, Y. Yu, *Small* **2021**, 17, 2102855; d) M. Zhang, X. Liu, X. Duan, S. Zhang, C. Liu, D. Wan, G. Li, Z. Xia, Z. Fan, L. Liao, *ACS Photonics* **2022**, 9, 132.
- [12] W. Wang, J. Lu, Z. Ni, *Nano Research* **2020**, 14, 1889.
- [13] a) Z. Lin, B. Xiao, Z. Wang, W. Tao, S. Shen, L. Huang, J. Zhang, F. Meng, Q. Zhang, L. Gu, *Advanced Functional Materials* **2021**, 2102321; b) A. Grillo, E. Faella, A. Pelella, F. Giubileo, L. Ansari, F. Gity, P. K. Hurley, N. McEvoy, A. DiBartolomeo, *Advanced Functional Materials* **2021**, 2105722; c) J. Lu, X. Zhang, G. Su, W. Yang, K. Han, X. Yu, Y. Wan, X. Wang, P. Yang, *Materials Today Physics* **2021**, 18, 100376.
- [14] Q. Liang, Q. Wang, Q. Zhang, J. Wei, S. X. Lim, R. Zhu, J. Hu, W. Wei, C. Lee, C. Sow, *Advanced Materials* **2019**, 31, 1807609.
- [15] a) C. Yin, C. Gong, J. Chu, X. Wang, C. Yan, S. Qian, Y. Wang, G. Rao, H. Wang, Y. Liu, *Advanced Materials* **2020**, 32, 2002237; b) W. Guo, Z. Dong, Y. Xu, C. Liu, D. Wei, L. Zhang, X. Shi, C. Guo, H. Xu, G. Chen, *Advanced Science* **2020**, 7, 1902699;

- c) M. M. Furchi, A. Pospischil, F. Libisch, J. Burgdörfer, T. Mueller, *Nano letters* **2014**, 14, 4785.
- [16] F. Wang, Z. Wang, L. Yin, R. Cheng, J. Wang, Y. Wen, T. A. Shifa, F. Wang, Y. Zhang, X. Zhan, *Chemical Society Reviews* **2018**, 47, 6296.
- [17] C. Xie, C. Mak, X. Tao, F. Yan, *Advanced Functional Materials* **2017**, 27, 1603886.
- [18] a) S. Brichkin, V. Y. Gak, M. Spirin, A. Gadomska, S. Bocharova, V. Razumov, *High Energy Chemistry* **2020**, 54, 36; b) W. Wu, Y. Wang, Y. Niu, P. Wang, M. Chen, J. Sun, N. Wang, D. Wu, Z. Zhao, *ACS Applied Materials & Interfaces* **2020**, 12, 14165; c) L. Wang, Y. Xue, M. Cui, Y. Huang, H. Xu, C. Qin, J. Yang, H. Dai, M. Yuan, *Angewandte Chemie* **2020**, 132, 6504.
- [19] a) Q. H. Wang, K. Kalantar-Zadeh, A. Kis, J. N. Coleman, M. S. Strano, *Nature nanotechnology* **2012**, 7, 699; b) Q. Liang, Q. Zhang, X. Zhao, M. Liu, A. T. Wee, *ACS nano* **2021**, 15, 2165; c) C. Trovatiello, A. Marini, X. Xu, C. Lee, F. Liu, N. Curreli, C. Manzoni, S. Dal Conte, K. Yao, A. Ciattoni, *Nature Photonics* **2021**, 15, 6; d) A. K. Tareen, K. Khan, W. Ahmad, M. F. Khan, Q. U. Khan, X. Liu, *RSC Advances* **2021**, 11, 19316.
- [20] a) Y. Zhang, Y. Xu, J. Guo, X. Zhang, X. Liu, Y. Fu, F. Zhang, C. Ma, Z. Shi, R. Cao, *Chemical Engineering Journal* **2021**, 129556; b) W. Ahmad, M. U. Ali, V. Laxmi, A. S. Syed, *Asian Journal of Nanosciences and Materials* **2018**, 1, 122.
- [21] a) S. Cao, B. Shen, T. Tong, J. Fu, J. Yu, *Advanced Functional Materials* **2018**, 28, 1800136; b) Q. Li, J. Lin, T.-Y. Liu, X.-Y. Zhu, W.-H. Yao, J. Liu, *npj 2D Materials and Applications* **2021**, 5, 1; c) X. Hu, X. Li, G. Li, T. Ji, F. Ai, J. Wu, E. Ha, J. Hu, *Advanced Functional Materials* **2021**, 2011284.
- [22] H. S. Ra, M. H. Jeong, T. Yoon, S. Kim, Y. J. Song, J. S. Lee, *Advanced Science* **2020**, 7, 2001475.

- [23] M. Hussain, S. H. A. Jaffery, A. Ali, C. D. Nguyen, S. Aftab, M. Riaz, S. Abbas, S. Hussain, Y. Seo, J. Jung, *Scientific reports* **2021**, 11, 1.
- [24] a) S. Gbadamasi, M. Mohiuddin, V. Krishnamurthi, R. Verma, M. W. Khan, S. Pathak, K. Kalantar-Zadeh, N. Mahmood, *Chemical Society Reviews* **2021**, 50, 4684; b) X. Gan, D. Lei, R. Ye, H. Zhao, K.-Y. Wong, *Nano Research* **2020**, 14, 2003.
- [25] D. Zhao, Y. Chen, W. Jiang, X. Wang, J. Liu, X. Huang, S. Han, T. Lin, H. Shen, X. Wang, *Advanced Electronic Materials* **2021**, 2001066.
- [26] P. Luo, F. Wang, J. Qu, K. Liu, X. Hu, K. Liu, T. Zhai, *Advanced Functional Materials* **2021**, 31, 2008351.
- [27] C. K. Kanade, H. Seok, V. K. Kanade, K. Aydin, H.-U. Kim, S. B. Mitta, W. J. Yoo, T. Kim, *ACS Applied Materials & Interfaces* **2021**, 13, 8710.
- [28] Z. Huang, T. Zhang, J. Liu, L. Zhang, Y. Jin, J. Wang, K. Jiang, S. Fan, Q. Li, *ACS Applied Electronic Materials* **2019**, 1, 1314.
- [29] Y. Xie, F. Liang, D. Wang, S. Chi, H. Yu, Z. Lin, H. Zhang, Y. Chen, J. Wang, Y. Wu, *Advanced Materials* **2018**, 30, 1804858.
- [30] S. Ki, M. Chen, X. Liang, *Journal of Vacuum Science & Technology B, Nanotechnology and Microelectronics: Materials, Processing, Measurement, and Phenomena* **2021**, 39, 062201.
- [31] Z. Zheng, T. Zhang, J. Yao, Y. Zhang, J. Xu, G. Yang, *Nanotechnology* **2016**, 27, 225501.
- [32] J. Tai, B. Wang, D. Hu, P. Xu, Z. Zhang, *Materials Letters* **2021**, 287, 129247.
- [33] A. Sharma, A. Srivastava, T. Senguttuvan, S. Husale, *Scientific reports* **2017**, 7, 1.
- [34] F. Wang, L. Li, W. Huang, L. Li, B. Jin, H. Li, T. Zhai, *Advanced Functional Materials* **2018**, 28, 1802707.
- [35] E. P. Mukhokosi, S. B. Krupanidhi, K. K. Nanda, *Scientific reports* **2017**, 7, 1.

- [36] Z. Yang, W. Jie, C.-H. Mak, S. Lin, H. Lin, X. Yang, F. Yan, S. P. Lau, J. Hao, *ACS nano* **2017**, 11, 4225.
- [37] L. Fu, F. Wang, B. Wu, N. Wu, W. Huang, H. Wang, C. Jin, L. Zhuang, J. He, L. Fu, *Advanced Materials* **2017**, 29, 1700439.
- [38] H. Huang, J. Wang, W. Hu, L. Liao, P. Wang, X. Wang, F. Gong, Y. Chen, G. Wu, W. Luo, *Nanotechnology* **2016**, 27, 445201.
- [39] J. Y. Wu, Y. T. Chun, S. Li, T. Zhang, J. Wang, P. K. Shrestha, D. Chu, *Advanced Materials* **2018**, 30, 1705880.
- [40] L.-C. Tien, Y.-C. Shih, C.-Y. Chen, Y.-T. Huang, R.-S. Chen, *Journal of Alloys and Compounds* **2021**, 870, 160195.
- [41] D. Kufer, G. Konstantatos, *Nano letters* **2015**, 15, 7307.
- [42] Y. Wang, X. Huang, D. Wu, R. Zhuo, E. Wu, C. Jia, Z. Shi, T. Xu, Y. Tian, X. Li, *Journal of Materials Chemistry C* **2018**, 6, 4861.
- [43] Y. Zhang, Y. Yu, L. Mi, H. Wang, Z. Zhu, Q. Wu, Y. Zhang, Y. Jiang, *Small* **2016**, 12, 1062.
- [44] X. Liu, S. Hu, Z. Lin, X. Li, L. Song, W. Yu, Q. Wang, W. He, *ACS Applied Materials & Interfaces* **2021**, 13, 15820.
- [45] D. K. Singh, R. K. Pant, K. Nanda, S. Krupanidhi, *Applied Physics Letters* **2021**, 119, 121102.
- [46] L. Ye, P. Wang, W. Luo, F. Gong, L. Liao, T. Liu, L. Tong, J. Zang, J. Xu, W. Hu, *Nano Energy* **2017**, 37, 53.
- [47] A. Pezeshki, S. H. H. Shokouh, T. Nazari, K. Oh, S. Im, *Advanced Materials* **2016**, 28, 3216.
- [48] H. Xue, Y. Dai, W. Kim, Y. Wang, X. Bai, M. Qi, K. Halonen, H. Lipsanen, Z. Sun, *Nanoscale* **2019**, 11, 3240.

- [49] K. Zhang, X. Fang, Y. Wang, Y. Wan, Q. Song, W. Zhai, Y. Li, G. Ran, Y. Ye, L. Dai, *ACS applied materials & interfaces* **2017**, 9, 5392.
- [50] H. Qiao, J. Yuan, Z. Xu, C. Chen, S. Lin, Y. Wang, J. Song, Y. Liu, Q. Khan, H. Y. Hoh, *Acs Nano* **2015**, 9, 1886.
- [51] R. Xiao, C. Lan, Y. Li, C. Zeng, T. He, S. Wang, C. Li, Y. Yin, Y. Liu, *Advanced Materials Interfaces* **2019**, 6, 1901304.
- [52] F. Yang, H. Cong, K. Yu, L. Zhou, N. Wang, Z. Liu, C. Li, Q. Wang, B. Cheng, *ACS applied materials & interfaces* **2017**, 9, 13422.
- [53] M. Sun, Q. Fang, D. Xie, Y. Sun, J. Xu, C. Teng, R. Dai, P. Yang, Z. Li, W. Li, *Advanced Electronic Materials* **2017**, 3, 1600502.
- [54] Z. Wang, P. Zeng, S. Hu, X. Wu, J. He, Z. Wu, W. Wang, P. Zheng, H. Zheng, L. Zheng, *Nanotechnology* **2021**, 32, 465201.
- [55] S. Yuan, C. Shen, B. Deng, X. Chen, Q. Guo, Y. Ma, A. Abbas, B. Liu, R. Haiges, C. Ott, *Nano letters* **2018**, 18, 3172.
- [56] Y. F. Xiong, J. H. Chen, Y. Q. Lu, F. Xu, *Advanced Electronic Materials* **2019**, 5, 1800562.
- [57] V. Dhyani, P. Dwivedi, S. Dhanekar, S. Das, *Applied Physics Letters* **2017**, 111, 191107.
- [58] J. Ye, K. Liao, X. Ge, Z. Wang, Y. Wang, M. Peng, T. He, P. Wu, H. Wang, Y. Chen, *Advanced Optical Materials* **2021**, 2002248.
- [59] Y. Guo, L. Kang, P. Song, Q. Zeng, B. Tang, J. Yang, Y. Wu, D. Tian, M. Xu, W. Zhao, *2D Materials* **2021**, 8, 035036
- [60] A. M. Afzal, S. Mumtaz, M. Z. Iqbal, M. W. Iqbal, A. Manzoor, G. Dastgeer, M. J. Iqbal, M. Y. Javeed, R. Khan, N. A. Shad, *Journal of Materials Chemistry C* **2021**, 9, 7110.
- [61] Z. Zou, J. Liang, X. Zhang, C. Ma, P. Xu, X. Yang, Z. Zeng, X. Sun, C. Zhu, D. Liang, *ACS nano* **2021**, 15, 10039.

- [62] A. Abderrahmane, C. Woo, P. J. Ko, *Journal of Electronic Materials* **2021**, 50, 5713
- [63] J. Tan, H. Nan, Q. Fu, X. Zhang, X. Liu, Z. Ni, K. Ostrikov, S. Xiao, X. Gu, *Advanced Electronic Materials* 2100673.
- [64] J. Yao, Z. Zheng, J. Shao, G. Yang, *ACS applied materials & interfaces* **2015**, 7, 26701.
- [65] X. Gong, M. Tong, Y. Xia, W. Cai, J. S. Moon, Y. Cao, G. Yu, C.-L. Shieh, B. Nilsson, A. J. Heeger, *Science* **2009**, 325, 1665.
- [66] D. Liu, H.-J. Li, J. Gao, S. Zhao, Y. Zhu, P. Wang, D. Wang, A. Chen, X. Wang, J. Yang, *Nanoscale research letters* **2018**, 13, 1.
- [67] W. Feng, Z. Jin, J. Yuan, J. Zhang, S. Jia, L. Dong, J. Yoon, L. Zhou, R. Vajtai, J. M. Tour, *2D Materials* **2018**, 5, 025008.
- [68] R. K. Chowdhury, R. Maiti, A. Ghorai, A. Midya, S. K. Ray, *Nanoscale* **2016**, 8, 13429.
- [69] J. Yao, Z. Zheng, G. Yang, *Journal of Materials chemistry C* **2016**, 4, 7831.
- [70] S. Zhao, J. Wu, K. Jin, H. Ding, T. Li, C. Wu, N. Pan, X. Wang, *Advanced Functional Materials* **2018**, 28, 1802011.
- [71] X. Zhou, X. Hu, S. Zhou, H. Song, Q. Zhang, L. Pi, L. Li, H. Li, J. Lü, T. Zhai, *Advanced Materials* **2018**, 30, 1703286.
- [72] Y. Chen, X. Wang, G. Wu, Z. Wang, H. Fang, T. Lin, S. Sun, H. Shen, W. Hu, J. Wang, *Small* **2018**, 14, 1703293.
- [73] B. Y. Zhang, T. Liu, B. Meng, X. Li, G. Liang, X. Hu, Q. J. Wang, *Nature communications* **2013**, 4, 1.
- [74] L. Ye, H. Li, Z. Chen, J. Xu, *Acs Photonics* **2016**, 3, 692.
- [75] R. Cao, H. D. Wang, Z. N. Guo, D. K. Sang, L. Y. Zhang, Q. L. Xiao, Y. P. Zhang, D. Y. Fan, J. Q. Li, H. Zhang, *Advanced Optical Materials* **2019**, 7, 1900020.
- [76] W. Luo, Y. Cao, P. Hu, K. Cai, Q. Feng, F. Yan, T. Yan, X. Zhang, K. Wang, *Advanced Optical Materials* **2015**, 3, 1418.

- [77] T. Qi, Y. Gong, A. Li, X. Ma, P. Wang, R. Huang, C. Liu, R. Sakidja, J. Z. Wu, R. Chen, *Advanced Functional Materials* **2020**, 30, 1905687.
- [78] X. Yu, P. Yu, D. Wu, B. Singh, Q. Zeng, H. Lin, W. Zhou, J. Lin, K. Suenaga, Z. Liu, *Nature communications* **2018**, 9, 1.
- [79] a) V. Shautsova, S. Sinha, L. Hou, Q. Zhang, M. Tweedie, Y. Lu, Y. Sheng, B. F. Porter, H. Bhaskaran, J. H. Warner, *ACS nano* **2019**, 13, 14162; b) A. D. Oyedele, S. Yang, L. Liang, A. A. Puretzky, K. Wang, J. Zhang, P. Yu, P. R. Pudasaini, A. W. Ghosh, Z. Liu, *Journal of the American Chemical Society* **2017**, 139, 14090.
- [80] a) M. Jakhar, J. Singh, A. Kumar, R. Pandey, *The Journal of Physical Chemistry C* **2020**, 124, 26565; b) P. Yu, Q. Zeng, C. Zhu, L. Zhou, W. Zhao, J. Tong, Z. Liu, G. Yang, *Advanced Materials* **2021**, 33, 2005607.
- [81] Q. Liang, Q. Zhang, J. Gou, T. Song, Arramel, H. Chen, M. Yang, S. X. Lim, Q. Wang, R. Zhu, *ACS nano* **2020**, 14, 5668.
- [82] X. Liu, P. Gao, W. Hu, J. Yang, *The journal of physical chemistry letters* **2020**, 11, 4070.
- [83] S. S. Withanage, B. Chamlagain, A. C. Johnston, S. I. Khondaker, *Advanced Electronic Materials* **2021**, 7, 2001057.
- [84] M. Wang, T.-J. Ko, M. S. Shawkat, S. S. Han, E. Okogbue, H.-S. Chung, T.-S. Bae, S. Sattar, J. Gil, C. Noh, *ACS applied materials & interfaces* **2020**, 12, 10839.
- [85] G. D'Olimpio, C. Guo, C. N. Kuo, R. Edla, C. S. Lue, L. Ottaviano, P. Torelli, L. Wang, D. W. Boukhvalov, A. Politano, *Advanced Functional Materials* **2020**, 30, 1906556.
- [86] H. J. Goldsmid, *Materials* **2014**, 7, 2577.
- [87] Y. Zhao, J. Qiao, P. Yu, Z. Hu, Z. Lin, S. P. Lau, Z. Liu, W. Ji, Y. Chai, *Advanced materials* **2016**, 28, 2399.
- [88] G. Anemone, P. C. Aguilar, M. Garnica, F. Calleja, A. Al Taleb, C.-N. Kuo, C. S. Lue, A. Politano, A. L. V. de Parga, G. Benedek, *npj 2D Materials and Applications* **2021**, 5, 1.

- [89] Y. Wang, L. Li, W. Yao, S. Song, J. Sun, J. Pan, X. Ren, C. Li, E. Okunishi, Y.-Q. Wang, *Nano letters* **2015**, 15, 4013.
- [90] Z. Wang, Q. Li, F. Besenbacher, M. Dong, *Advanced Materials* **2016**, 28, 10224.
- [91] a) B. M. Szydłowska, O. Hartwig, B. Tywoniuk, T. Hartman, T. Stimpel-Lindner, Z. Sofer, N. McEvoy, G. S. Duesberg, C. Backes, *2D Materials* **2020**, 7, 045027; b) S. S. Han, J. H. Kim, C. Noh, J. H. Kim, E. Ji, J. Kwon, S. M. Yu, T.-J. Ko, E. Okogbue, K. H. Oh, *ACS applied materials & interfaces* **2019**, 11, 13598; c) R. Kempt, A. Kuc, T. Heine, *Angewandte Chemie International Edition* **2020**, 59, 9242.
- [92] Y. Ma, X. Shao, J. Li, B. Dong, Z. Hu, Q. Zhou, H. Xu, X. Zhao, H. Fang, X. Li, *ACS Applied Materials & Interfaces* **2021**, 13, 8518.
- [93] S. Jiang, C. Xie, Y. Gu, Q. Zhang, X. Wu, Y. Sun, W. Li, Y. Shi, L. Zhao, S. Pan, *Small* **2019**, 15, 1902789.
- [94] L. H. Zeng, D. Wu, S. H. Lin, C. Xie, H. Y. Yuan, W. Lu, S. P. Lau, Y. Chai, L. B. Luo, Z. J. Li, *Advanced Functional Materials* **2019**, 29, 1806878.
- [95] H. Ma, P. Chen, B. Li, J. Li, R. Ai, Z. Zhang, G. Sun, K. Yao, Z. Lin, B. Zhao, *Nano letters* **2018**, 18, 3523.
- [96] a) J. He, W. Jiang, X. Zhu, R. Zhang, J. Wang, M. Zhu, S. Wang, Y. Zheng, L. Chen, *Physical Chemistry Chemical Physics* **2020**, 22, 26383; b) Y. Zhou, H. Jang, J. M. Woods, Y. Xie, P. Kumaravadivel, G. A. Pan, J. Liu, Y. Liu, D. G. Cahill, J. J. Cha, *Advanced Functional Materials* **2017**, 27, 1605928.
- [97] H. Xu, J. Wei, H. Zhou, J. Feng, T. Xu, H. Du, C. He, Y. Huang, J. Zhang, Y. Liu, *Advanced Materials* **2020**, 32, 2000513.
- [98] Y. Xiong, Q. Liao, Z. Huang, X. Huang, C. Ke, H. Zhu, C. Dong, H. Wang, K. Xi, P. Zhan, *Advanced Materials* **2020**, 32, 1907242.
- [99] Y. Yang, J. Li, S. Choi, S. Jeon, J. H. Cho, B. H. Lee, S. Lee, *Applied Physics Letters* **2021**, 118, 013103.

- [100] F. Urban, F. Gity, P. K. Hurley, N. McEvoy, A. Di Bartolomeo, *Applied Physics Letters* **2020**, 117, 193102.
- [101] N. Sefidmooye Azar, J. Bullock, V. R. Shrestha, S. Balendhran, W. Yan, H. Kim, A. Javey, K. B. Crozier, *ACS nano* **2021**, 15, 6573.
- [102] J. Sun, H. Shi, T. Siegrist, D. J. Singh, *Applied Physics Letters* **2015**, 107, 153902.
- [103] G. D. Nguyen, A. D. Oyedele, A. Haglund, W. Ko, L. Liang, A. A. Puretzky, D. Mandrus, K. Xiao, A.-P. Li, *ACS nano* **2020**, 14, 1951.
- [104] J. Zhong, J. Yu, L. Cao, C. Zeng, J. Ding, C. Cong, Z. Liu, Y. Liu, *Nano Research* **2020**, 13, 1780.
- [105] G. Li, S. Yin, C. Tan, L. Chen, M. Yu, L. Li, F. Yan, *Advanced Functional Materials* **2021**, 31, 2104787.
- [106] Z. Dong, W. Yu, L. Zhang, H. Mu, L. Xie, J. Li, Y. Zhang, L. Huang, X. He, L. Wang, S. Lin, K. Zhang, *ACS Nano* **2021**, 15, 20403.
- [107] L. Jia, J. Wu, T. Yang, B. Jia, D. J. Moss, *ACS Applied Nano Materials* **2020**, 3, 6876.
- [108] a) M.-K. Lin, R. A. B. Villaos, J. A. Hlevyack, P. Chen, R.-Y. Liu, C.-H. Hsu, J. Avila, S.-K. Mo, F.-C. Chuang, T.-C. Chiang, *Physical review letters* **2020**, 124, 036402; b) E. Okogbue, T.-J. Ko, S. S. Han, M. S. Shawkat, M. Wang, H.-S. Chung, K. H. Oh, Y. Jung, *Nanoscale* **2020**, 12, 10647.
- [109] J. Lai, J. Ma, Y. Liu, K. Zhang, X. Zhuo, J. Chen, S. Zhou, D. Sun, *2D Materials* **2020**, 7, 034003.
- [110] T. Wei, X. Wang, Q. Yang, Z. He, P. Yu, Z. Xie, H. Chen, S. Li, S. Wu, *ACS Applied Materials & Interfaces* **2021**, 13, 22757.
- [111] a) Y. Hui, J. S. Gomez-Diaz, Z. Qian, A. Alu, M. Rinaldi, *Nature communications* **2016**, 7, 1; b) H. Fang, W. Hu, *Advanced science* **2017**, 4, 1700323.
- [112] H. Xu, C. Guo, J. Zhang, W. Guo, C. N. Kuo, C. S. Lue, W. Hu, L. Wang, G. Chen, A. Politano, *Small* **2019**, 15, 1903362.

- [113] Y. Yang, K. Zhang, L. Zhang, G. Hong, C. Chen, H. Jing, J. Lu, P. Wang, X. Chen, L. Wang, *InfoMat* **2021**, 3, 705.
- [114] Y. Liang, C. Xie, C.-y. Dong, X.-w. Tong, W.-h. Yang, C.-y. Wu, L.-b. Luo, *Journal of Materials Chemistry C* **2021**, 9, 14897.
- [115] C. Guo, Y. Hu, G. Chen, D. Wei, L. Zhang, Z. Chen, W. Guo, H. Xu, C.-N. Kuo, C. S. Lue, *Science advances* **2020**, 6, eabb6500.
- [116] a) Y. Zhao, J. Qiao, Z. Yu, P. Yu, K. Xu, S. P. Lau, W. Zhou, Z. Liu, X. Wang, W. Ji, *Advanced Materials* **2017**, 29, 1604230; b) P. Miró, M. Ghorbani-Asl, T. Heine, *Angewandte Chemie International Edition* **2014**, 53, 3015.
- [117] Z. Wang, P. Wang, F. Wang, J. Ye, T. He, F. Wu, M. Peng, P. Wu, Y. Chen, F. Zhong, *Advanced Functional Materials* **2020**, 30, 1907945.
- [118] a) M. Buscema, D. J. Groenendijk, S. I. Blanter, G. A. Steele, H. S. Van Der Zant, A. Castellanos-Gomez, *Nano letters* **2014**, 14, 3347; b) N. Huo, S. Yang, Z. Wei, S.-S. Li, J.-B. Xia, J. Li, *Scientific reports* **2014**, 4, 1; c) E. Zhang, Y. Jin, X. Yuan, W. Wang, C. Zhang, L. Tang, S. Liu, P. Zhou, W. Hu, F. Xiu, *Advanced Functional Materials* **2015**, 25, 4076.
- [119] C. R. Dean, A. F. Young, I. Meric, C. Lee, L. Wang, S. Sorgenfrei, K. Watanabe, T. Taniguchi, P. Kim, K. L. Shepard, *Nature nanotechnology* **2010**, 5, 722.
- [120] N. Youngblood, C. Chen, S. J. Koester, M. Li, *Nature Photonics* **2015**, 9, 247.
- [121] M. M. Furchi, D. K. Polyushkin, A. Pospischil, T. Mueller, *Nano letters* **2014**, 14, 6165.
- [122] L. Li, W. Wang, Y. Chai, H. Li, M. Tian, T. Zhai, *Advanced Functional Materials* **2017**, 27, 1701011.
- [123] a) A. K. Geim, I. V. Grigorieva, *Nature* **2013**, 499, 419; b) Y. Liu, N. O. Weiss, X. Duan, H.-C. Cheng, Y. Huang, X. Duan, *Nature Reviews Materials* **2016**, 1, 1.
- [124] H. Wang, Z. Li, D. Li, P. Chen, L. Pi, X. Zhou, T. Zhai, *Advanced Functional Materials* **2021**, 2103106.

- [125] W. Ahmad, J. Liu, J. Jiang, Q. Hao, D. Wu, Y. Ke, H. Gan, V. Laxmi, Z. Ouyang, F. Ouyang, *Advanced Functional Materials* **2021**, 31, 2104143.
- [126] C. Lei, Y. Ma, X. Xu, T. Zhang, B. Huang, Y. Dai, *The Journal of Physical Chemistry C* **2019**, 123, 23089.
- [127] a) J. An, X. Zhao, Y. Zhang, M. Liu, J. Yuan, X. Sun, Z. Zhang, B. Wang, S. Li, D. Li, *Advanced Functional Materials* **2021**, 2110119; b) F. Bai, J. Qi, F. Li, Y. Fang, W. Han, H. Wu, Y. Zhang, *Advanced Materials Interfaces* **2018**, 5, 1701275.
- [128] a) C. Ma, Y. Shi, W. Hu, M. H. Chiu, Z. Liu, A. Bera, F. Li, H. Wang, L. J. Li, T. Wu, *Advanced Materials* **2016**, 28, 3683; b) A. A. Bessonov, M. Allen, Y. Liu, S. Malik, J. Bottomley, A. Rushton, I. Medina-Salazar, M. Voutilainen, S. Kallioinen, A. Colli, *ACS nano* **2017**, 11, 5547.
- [129] Z.-X. Zhang, L.-H. Zeng, X.-W. Tong, Y. Gao, C. Xie, Y. H. Tsang, L.-B. Luo, Y.-C. Wu, *The journal of physical chemistry letters* **2018**, 9, 1185.
- [130] L. H. Zeng, Q. M. Chen, Z. X. Zhang, D. Wu, H. Yuan, Y. Y. Li, W. Qarony, S. P. Lau, L. B. Luo, Y. H. Tsang, *Advanced Science* **2019**, 6, 1901134.
- [131] M. Long, Y. Wang, P. Wang, X. Zhou, H. Xia, C. Luo, S. Huang, G. Zhang, H. Yan, Z. Fan, *ACS nano* **2019**, 13, 2511.
- [132] A. M. Afzal, M. Z. Iqbal, G. Dastgeer, A. u. Ahmad, B. Park, *Advanced Science* **2021**, 8, 2003713.
- [133] C. Tan, S. Yin, J. Chen, Y. Lu, W. Wei, H. Du, K. Liu, F. Wang, T. Zhai, L. Li, *ACS nano* **2021**, 15, 8328.
- [134] X. Kang, C. Lan, F. Li, W. Wang, S. Yip, Y. Meng, F. Wang, Z. Lai, C. Liu, J. C. Ho, *Advanced Optical Materials* **2021**, 9, 2001991.
- [135] a) V. M. More, Y. Kim, J. Jeon, J. C. Shin, S. J. Lee, *Journal of Alloys and Compounds* **2021**, 868, 159195; b) K. Arora, D. P. Singh, P. Fischer, M. Kumar, *Advanced Optical Materials* **2020**, 8, 2000212.

- [136] a) V. Selamneni, S. K. Ganeshan, P. Sahatiya, *Journal of Materials Chemistry C* **2020**, 8, 11593; b) J. Wei, C. Xu, B. Dong, C.-W. Qiu, C. Lee, *Nature Photonics* **2021**, 15, 614.
- [137] Y. Chen, Y. Wang, Z. Wang, Y. Gu, Y. Ye, X. Chai, J. Ye, Y. Chen, R. Xie, Y. Zhou, *Nature Electronics* **2021**, 4, 357.
- [138] W.-H. Yang, X.-Y. Jiang, Y.-T. Xiao, C. Fu, J.-K. Wan, X. Yin, X.-W. Tong, D. Wu, L.-M. Chen, L.-B. Luo, *Materials Horizons* **2021**, 8, 1976.
- [139] S. Aftab, M. Samiya, W. Liao, M. W. Iqbal, M. Ishfaq, K. Ramachandraiah, H. M. S. Ajmal, H. M. U. Haque, S. Yousuf, Z. Ahmed, *Journal of Materials Chemistry C* **2021**, 9, 3998.
- [140] Á. Coogan, Y. K. Gun'ko, *Materials Advances* **2021**, 2, 146.
- [141] X.-W. Tong, J.-J. Wang, J.-X. Li, X.-F. Hu, D. Wu, L.-B. Luo, *Sensors and Actuators A: Physical* **2021**, 322, 112625.
- [142] X.-W. Tong, Y.-N. Lin, R. Huang, Z.-X. Zhang, C. Fu, D. Wu, L.-B. Luo, Z.-J. Li, F.-X. Liang, W. Zhang, *ACS Applied Materials & Interfaces* **2020**, 12, 53921.
- [143] L. Zeng, D. Wu, J. Jie, X. Ren, X. Hu, S. P. Lau, Y. Chai, Y. H. Tsang, *Advanced Materials* **2020**, 32, 2004412.
- [144] M. S. Shawkat, S. B. Hafiz, M. M. Islam, S. A. Mofid, M. M. Al Mahfuz, A. Biswas, H.-S. Chung, E. Okogbue, T.-J. Ko, D. Chanda, *ACS applied materials & interfaces* **2021**, 13, 15542.
- [145] G. Qiu, C. Niu, Y. Wang, M. Si, Z. Zhang, W. Wu, D. Y. Peide, *Nature Nanotechnology* **2020**, 15, 585.
- [146] D. A. Nguyen, D. Y. Park, J. Lee, N. T. Duong, C. Park, D. H. Nguyen, T. S. Le, D. Suh, H. Yang, M. S. Jeong, *Nano Energy* **2021**, 106049.
- [147] L. H. Zeng, S. H. Lin, Z. J. Li, Z. X. Zhang, T. F. Zhang, C. Xie, C. H. Mak, Y. Chai, S. P. Lau, L. B. Luo, *Advanced Functional Materials* **2018**, 28, 1705970.

- [148] D. Wu, Y. Wang, L. Zeng, C. Jia, E. Wu, T. Xu, Z. Shi, Y. Tian, X. Li, Y. H. Tsang, *Acs Photonics* **2018**, 5, 3820.
- [149] Y. Lu, Y. Wang, C. Xu, C. Xie, W. Li, J. Ding, W. Zhou, Z. Qin, X. Shen, L.-B. Luo, *Nanoscale* **2021**, 13, 7606.
- [150] Y. Wang, Z. Yu, Z. Zhang, B. Sun, Y. Tong, J.-B. Xu, X. Sun, H. K. Tsang, *ACS Photonics* **2020**, 7, 2643.
- [151] L. Zeng, S. Lin, Z. Lou, H. Yuan, H. Long, Y. Li, W. Lu, S. P. Lau, D. Wu, Y. H. Tsang, *NPG Asia Materials* **2018**, 10, 352.
- [152] C. Xie, L. Zeng, Z. Zhang, Y.-H. Tsang, L. Luo, J.-H. Lee, *Nanoscale* **2018**, 10, 15285.
- [153] C. Yim, N. McEvoy, S. Riazimehr, D. S. Schneider, F. Gity, S. Monaghan, P. K. Hurley, M. C. Lemme, G. S. Duesberg, *Nano letters* **2018**, 18, 1794.
- [154] R. Zhuo, L. Zeng, H. Yuan, D. Wu, Y. Wang, Z. Shi, T. Xu, Y. Tian, X. Li, Y. H. Tsang, *Nano Research* **2019**, 12, 183.
- [155] Y. Wang, Z. Yu, Y. Tong, B. Sun, Z. Zhang, J.-B. Xu, X. Sun, H. K. Tsang, *Applied Physics Letters* **2020**, 116, 211101.
- [156] J. Yuan, T. Sun, Z. Hu, W. Yu, W. Ma, K. Zhang, B. Sun, S. P. Lau, Q. Bao, S. Lin, *ACS applied materials & interfaces* **2018**, 10, 40614.
- [157] F. X. Liang, X. Y. Zhao, J. J. Jiang, J. G. Hu, W. Q. Xie, J. Lv, Z. X. Zhang, D. Wu, L. B. Luo, *Small* **2019**, 15, 1903831.
- [158] A. M. Afzal, G. Dastgeer, M. Z. Iqbal, P. Gautam, M. M. Faisal, *ACS applied materials & interfaces* **2020**, 12, 19625.
- [159] A. M. Afzal, M. Z. Iqbal, S. Mumtaz, I. Akhtar, *Journal of Materials Chemistry C* **2020**, 8, 4743.
- [160] L. B. Luo, D. Wang, C. Xie, J. G. Hu, X. Y. Zhao, F. X. Liang, *Advanced Functional Materials* **2019**, 29, 1900849.

- [161] D. Wu, J. Guo, J. Du, C. Xia, L. Zeng, Y. Tian, Z. Shi, Y. Tian, X. J. Li, Y. H. Tsang, *ACS nano* **2019**, 13, 9907.
- [162] M. S. Shawkat, T. A. Chowdhury, H.-S. Chung, S. Sattar, T.-J. Ko, J. A. Larsson, Y. Jung, *Nanoscale* **2020**, 12, 23116.
- [163] H. Wang, Z. Li, D. Li, X. Xu, P. Chen, L. Pi, X. Zhou, T. Zhai, *Advanced Functional Materials* **2021**, 31, 2106105.
- [164] J. Wu, H. Ma, C. Zhong, M. Wei, C. Sun, Y. Ye, Y. Xu, B. Tang, Y. Luo, B. Sun, *Nano Letters* **2022**, 22, 6816.
- [165] W. Yu, Z. Dong, H. Mu, G. Ren, X. He, X. Li, S. Lin, K. Zhang, Q. Bao, S. Mokkalpati, *ACS nano* **2022**, 16, 12922.
- [166] F. Ceballos, M. Z. Bellus, H.-Y. Chiu, H. Zhao, *ACS nano* **2014**, 8, 12717.
- [167] D. Zhang, S. Hu, X. Liu, Y. Chen, Y. Xia, H. Wang, H. Wang, Y. Ni, *ACS Applied Energy Materials* **2020**, 4, 357.
- [168] a) K. C. Kwon, S. Choi, K. Hong, C. W. Moon, Y.-S. Shim, T. Kim, W. Sohn, J.-M. Jeon, C.-H. Lee, K. T. Nam, *Energy & Environmental Science* **2016**, 9, 2240; b) Q. Ding, F. Meng, C. R. English, M. Cabán-Acevedo, M. J. Shearer, D. Liang, A. S. Daniel, R. J. Hamers, S. Jin, *Journal of the American Chemical Society* **2014**, 136, 8504.
- [169] C.-C. Chung, H. Yeh, P.-H. Wu, C.-C. Lin, C.-S. Li, T.-T. Yeh, Y. Chou, C.-Y. Wei, C.-Y. Wen, Y.-C. Chou, *ACS nano* **2021**, 15, 4627.
- [170] a) W. Ahmad, A. K. Tareen, K. Khan, M. Khan, Q. Khan, Z. Wang, M. Maqbool, *Applied Materials Today* **2023**, 30, 101717; b) W. Ahmad, Z. Ullah, K. Khan, *FlatChem* **2022**, 100452.
- [171] a) S. Goossens, G. Navickaite, C. Monasterio, S. Gupta, J. J. Piqueras, R. Pérez, G. Burwell, I. Nikitskiy, T. Lasanta, T. Galán, *Nature Photonics* **2017**, 11, 366; b) Y. T. Lee, J.-H. Kang, K. Kwak, J. Ahn, H. T. Choi, B.-K. Ju, S. H. Shokouh, S. Im, M.-C. Park, D. K. Hwang, *ACS Photonics* **2018**, 5, 4745.

- [172] Z. Dong, W. Yu, L. Zhang, H. Mu, L. Xie, J. Li, Y. Zhang, L. Huang, X. He, L. Wang, *ACS nano* **2021**, 15, 20403.
- [173] a) C.-C. Huang, H. Medina, Y.-Z. Chen, T.-Y. Su, J.-G. Li, C.-W. Chen, Y.-T. Yen, Z. M. Wang, Y.-L. Chueh, *Nano letters* **2016**, 16, 2463; b) W. Du, P. Yu, J. Zhu, C. Li, H. Xu, J. Zou, C. Wu, Q. Wen, H. Ji, T. Liu, *Nanotechnology* **2020**, 31, 225201; c) W. Ahmad, Y. Gong, G. Abbas, K. Khan, M. Khan, G. Ali, A. Shuja, A. K. Tareen, Q. Khan, D. Li, *Nanoscale* **2021**, 13, 5162.
- [174] a) Z. Wang, A. Hemmetter, B. Uzlu, M. Saeed, A. Hamed, S. Kataria, R. Negra, D. Neumaier, M. C. Lemme, *Advanced Electronic Materials* **2021**, 2001210; b) Z. D. Luo, M. M. Yang, Y. Liu, M. Alexe, *Advanced Materials* **2021**, 33, 2005620; c) W. Ahmad, S. Ahmed, M. Amjad, S. Akhtar, M. Ali, *Optik* **2018**, 155, 297.
- [175] a) S. G. Noyce, J. L. Doherty, S. Zauscher, A. D. Franklin, *ACS nano* **2020**, 14, 11637; b) H. Cho, D. Kang, Y. Lee, H. Bae, S. Hong, Y. Cho, K. Kim, Y. Yi, J. H. Park, S. Im, *Nano letters* **2021**, 21, 3503.
- [176] M. Engel, M. Steiner, P. Avouris, *Nano letters* **2014**, 14, 6414.
- [177] a) M. S. Shawkat, J. Gil, S. S. Han, T.-J. Ko, M. Wang, D. Dev, J. Kwon, G.-H. Lee, K. H. Oh, H.-S. Chung, *ACS applied materials & interfaces* **2020**, 12, 14341; b) S. S. Chee, D. Seo, H. Kim, H. Jang, S. Lee, S. P. Moon, K. H. Lee, S. W. Kim, H. Choi, M. H. Ham, *Advanced Materials* **2019**, 31, 1804422; c) W. Ahmad, Z. Ullah, N. I. Sonil, K. Khan, *Journal of Materials Science: Materials in Electronics* **2021**, 32, 19991.
- [178] T. Das, E. Yang, J. E. Seo, J. H. Kim, E. Park, M. Kim, D. Seo, J. Y. Kwak, J. Chang, *ACS Applied Materials & Interfaces* **2021**, 13, 1861.
- [179] H. Zhang, H. Li, F. Wang, X. Song, Z. Xu, D. Wei, J. Zhang, Z. Dai, Y. Ren, Y. Ye, *ACS Applied Electronic Materials* **2022**, 4, 5177.
- [180] a) Q. Xia, J. J. Yang, *Nature materials* **2019**, 18, 309; b) C. Y. Wang, C. Wang, F. Meng, P. Wang, S. Wang, S. J. Liang, F. Miao, *Advanced Electronic Materials* **2020**, 6,

- 1901107; c) S. Choi, S. H. Tan, Z. Li, Y. Kim, C. Choi, P.-Y. Chen, H. Yeon, S. Yu, J. Kim, *Nature materials* **2018**, 17, 335.
- [181] Y. Li, L. Loh, S. Li, L. Chen, B. Li, M. Bosman, K.-W. Ang, *Nature Electronics* **2021**, 4, 348.
- [182] a) H. Boumeriame, E. S. Da Silva, A. S. Cherevan, T. Chafik, J. L. Faria, D. Eder, *Journal of Energy Chemistry* **2022**, 64, 406; b) Y. Luo, M. Sun, J. Yu, U. Schwingenschlogl, *Chemistry of Materials* **2021**, 33, 4128.
- [183] a) K. Maeda, K. Domen, *The Journal of Physical Chemistry Letters* **2010**, 1, 2655; b) M. E. Kilic, K.-R. Lee, *Carbon* **2021**, 174, 368.
- [184] a) X. Wang, K. Maeda, A. Thomas, K. Takanahe, G. Xin, J. M. Carlsson, K. Domen, M. Antonietti, *Nature materials* **2009**, 8, 76; b) C. Long, Y. Liang, H. Jin, B. Huang, Y. Dai, *ACS Applied Energy Materials* **2018**, 2, 513.
- [185] a) E. Okogbue, S. S. Han, T.-J. Ko, H.-S. Chung, J. Ma, M. S. Shawkat, J. H. Kim, J. H. Kim, E. Ji, K. H. Oh, *Nano letters* **2019**, 19, 7598; b) A. Ciarrocchi, A. Avsar, D. Ovchinnikov, A. Kis, *Nature communications* **2018**, 9, 1.
- [186] L. Zhang, D. Zhang, F. Hu, X. Xu, Q. Zhao, X. Sun, H. Wu, Z. Lü, X. Wang, Z. Zhao, *Advanced Optical Materials* **2022**, 2201881.
- [187] D. Kireev, E. Okogbue, R. Jayanth, T.-J. Ko, Y. Jung, D. Akinwande, *ACS nano* **2021**, 15, 2800.
- [188] Q. Liang, Z. Chen, Q. Zhang, A. T. S. Wee, *Advanced Functional Materials* **2022**, 2203555.
- [189] a) N. Mounet, M. Gibertini, P. Schwaller, D. Campi, A. Merkys, A. Marrazzo, T. Sohier, I. E. Castelli, A. Cepellotti, G. Pizzi, *Nature nanotechnology* **2018**, 13, 246; b) L. Liu, H. L. Zhuang, *Computational Materials Science* **2019**, 166, 105; c) X. Liu, X. Shao, Y. Zheng, S. Qi, M. Zhang, H. Li, C. Li, M. Tan, D. Zheng, M. Zhao, *Applied Surface*

Science **2020**, 518, 146197; d) M. Sharma, R. Singh, *Canadian Journal of Physics* **2021**, 99, 788.



Waqas Ahmad is a postdoctoral research associate in the institute of fundamental and frontier sciences at University of Electronic Science and Technology of China. He received his PhD in Optical Engineering from Shenzhen University, Shenzhen, China. His current research focuses on the development of the next generation optoelectronic devices based on group-10 TMDCs and their heterostructures.



Zhiming Wang is a Professor of National Distinguished Experts at University of Electronic Science and Technology of China (UESTC). He is a Fellow of the Royal Society of Chemistry (RSC) and the Optical Society of America (OSA). His research interests lie primarily in Nanomaterials and Microstructures for applications including Optical Manipulation, Integrated Photonics, Renewable Energy, Flexible Electronics, and Quantum Technology.

This review presents a detailed summary of the current progress of broadband photodetectors based on group-10 TMDCs. It is followed by an overview of the structural characteristics and synthesis of group-10 TMDCs used in realizing their heterostructures aimed at broadband photodetectors. Subsequently, this review describes the potential applications of group-10 TMDCs in electronics and optoelectronics

Waqas Ahmad, Jiang Wu, Qiangdong Zhuang, Arup Neogi, Zhiming Wang*

Research Process on Photodetectors Based on Group-10 Transition Metal Dichalcogenides

